THE PREPARATION AND CHARACTERIZATION OF ZEOLITE
FRAMEWORK STABILIZED RUTHENIUM(0) NANOCLUSTERS; A SUPERB
CATALYST FOR THE HYDROLYSIS OF SODIUM BOROHYDRIDE AND THE
HYDROGENATION OF AROMATICS UNDER MILD CONDITIONS


A THESIS SUBMITTED TO
THE GRADUATE SCHOOL OF NATURAL AND APPLIED SCIENCES
OF
MIDDLE EAST TECHNICAL UNIVERSITY


BY


MEHMET ZAHMAKIRAN


IN PARTIAL FULFILLMENT OF THE REQUIREMENTS
FOR
THE DEGREE OF DOCTOR OF PHILOSOPHY
IN
CHEMISTRY


APRIL 2010

Approval of the thesis:

**THE PREPARATION AND CHARACTERIZATION OF ZEOLITE FRAMEWORK STABILIZED RUTHENIUM(0) NANOCLUSTERS; A SUPERB CATALYST FOR THE HYDROLYSIS OF SODIUM BOROHYDRIDE AND THE HYDROGENATION OF AROMATICS UNDER MILD CONDITIONS**

submitted by **MEHMET ZAHMAKIRAN** in partial fulfillment of the requirements for the degree of **Doctor of Philosophy in Chemistry Department, Middle East Technical University** by,

Prof. Dr. Canan Özgen          **_____**
Dean, Graduate School of **Natural and Applied Sciences**

Prof. Dr. İlker Özkan          _____
Head of Department, **Chemistry**

Prof. Dr. Saim Özkar
Supervisor, **Chemistry Dept., METU**          _____

**Examining Committee Members:**

Prof. Dr. Ceyhan Kayran          _____
Chemistry Dept., METU

Prof. Dr. Saim Özkar          _____
Chemistry Dept., METU

Prof. Dr. Ömer Dağ          _____
Chemistry Dept., Bilkent University

Assist. Prof. Dr. Emrah Özensoy          _____
Chemistry Dept., Bilkent University

Assoc. Prof. Dr. Ayşen Yılmaz          _____
Chemistry Dept., Bilkent University

         **Date:**    16/04/2010

I hereby declare that all information in this document has been obtained and presented in accordance with academic rules and ethical conduct. I also declare that, as required by these rules and conduct, I have fully cited and referenced all material and results that are not original to this work.

Name, Last name: Mehmet Zahmakıran

Signature

# ABSTRACT

## THE PREPARATION AND CHARACTERIZATION ZEOLITE FRAMEWORK STABILIZED RUTHENIUM(0) NANOCLUSTERS; A SUPERB CATALYST FOR THE HYDROLYSIS OF SODIUM BOROHYDRIDE AND THE HYDROGENATION OF AROMATICS UNDER MILD CONDITIONS

Zahmakıran, Mehmet

Ph.D., Department of Chemistry

Supervisor: Prof. Dr. Saim Özkar

April 2010, 136 pages

The use of microporous materials with ordered porous structures as the hosts to stabilize metal nanoclusters has attracted particular interest in the catalysis because the pore size restriction could confine the growth of nanoclusters and lead to an increase in the percentage of catalytically active surface atoms. In this dissertation we report the preparation, characterization and the investigation of the catalytic performance of zeolite framework stabilized ruthenium(0) nanoclusters in the hydrolysis of sodium borohydride and the hydrogenation of aromatics. The zeolite framework stabilized ruthenium(0) nanoclusters were prepared by borohydride reduction of ruthenium(III)-exchanged zeolite-Y in aqueous solution at room temperature and isolated as black powders. Their characterization by using ICP-OES, XRD, TEM, ZC-TEM, HR-TEM, TEM-EDX, SEM, XPS, DR-UV-vis, far-IR, mid-IR, Raman spectroscopy, $N_2$ adsorption-desorption technique and $(P(C_6H_{11})_3)/(PC_6H_{11}O_3)$ poisoning experiments reveal the formation of ruthenium(0) nanoclusters within the zeolite cages as well as on the external surface of zeolite without causing alteration in the framework lattice or loss in the crystallinity.

The catalytic performance of zeolite framework stabilized ruthenium(0) nanoclusters depending on the various parameters was tested in the hydrolysis of sodium borohydride and the hydrogenation of aromatics. The important results

obtained from these experiments can be listed as follows: (*i*) the zeolite framework stabilized ruthenium(0) nanoclusters provide a record total turnover number (103200 mol $H_2$/mol Ru) and turnover frequency (33000 mol $H_2$/mol Ru·h) in the hydrolysis of sodium borohydride at room temperature, (*ii*) they also catalyze the same reaction in the basic medium (in 5 wt % NaOH solution) at room temperature with the unprecedented catalytic activity (4000 mol $H_2$/mol Ru·h) and lifetime (27200 mol $H_2$/mol Ru), (*iii*) the isolated and vacuum dried samples of zeolite framework stabilized ruthenium(0) nanoclusters are active catalysts in the hydrogenation of cyclohexene, benzene, toluene and *o*-xylene in cyclohexane, they provide TOF values of 6150, 5660, 3200, and 1550 mol $H_2$/mol Ru·h, respectively under mild conditions (at 22.0 ± 0.1 °C, and 40 ± 1 psig of initial $H_2$ pressure), (*iv*) more importantly, the zeolite framework stabilized ruthenium(0) nanoclusters are the lowest temperature, most active, most selective (100 % selectivity with complete conversion) and longest lifetime catalyst hitherto known for the hydrogenation of benzene to cyclohexane in the *solvent-free* system (TTON of 2420 and TOF of 1040 mol benzene/mol Ru·h) under mild conditions (at 22.0 ± 0.1 °C, and 40 ± 1 psig of initial $H_2$ pressure), (*v*) moreover, the resultant ruthenium(0) nanoclusters exhibit high durability throughout their catalytic use against agglomeration and leaching. This significant property makes them reusable catalyst without appreciable loss of their inherent activity.

Keywords: Nanoclusters, Ruthenium, Zeolite, Catalyst, Hydrolysis of Sodium Borohydride, Hydrogenation of Aromatics.

# ÖZ

## ILIMLI KOŞULLAR ALTINDA SODYUM BORHİDRÜRÜN HİDROLİZİ VE AROMATİKLERİN HİDROJENLENMESİ İÇİN SÜPER BİR KATALİZÖR OLAN ZEOLİT YAPISIYLA KARARLAŞTIRILMIŞ RUTENYUM(0) NANOKÜMELERİNİN HAZIRLANMASI VE TANIMLANMASI

Zahmakıran, Mehmet

Doktora, Kimya Bölümü

Tez Yöneticisi: Prof. Dr. Saim Özkar

Nisan 2010, 136 sayfa

Düzenli gözenek yapısına sahip mikro gözenekli malzemelerin metal nanokümelerinin kararlaştırılması için taşıyıcı olarak kullanılması, bu malzemelerin gözenek büyüklüklerinin nanokümelerin büyümesini sınırlandırması ve böylece katalitikçe etkin yüzey atomlarının yüzdesini arttırmasından dolayı kataliz alanında özel bir ilgi görmektedir. Bu tezde zeolit yapısıyla kararlaştırılmış rutenyum(0) nanokümelerinin hazırlanması, tanımlanması ve sodyum borhidrürün hidrolizi ile aromatiklerin hidrojenlenmesindeki katalitik performanslarının incelenmesini sunuyoruz. Zeolit yapısıyla kararlaştırılmış rutenyum(0) nanokümeleri, rutenyum(III)-değiştirilmiş zeolit-Y'nin sulu çözelti içerisinde oda sıcaklığında sodyum borhidrür ile indirgenmesiyle hazırlandı ve siyah toz halinde izole edildi. Bunların ICP-OES, XRD, TEM, HR-TEM, TEM-EDX, SEM, XPS, DR-UV-vis, far-IR, mid-IR, Raman spectroskopisi, $N_2$ adsorpsiyon-desorpsiyon yöntemi ve $(P(C_6H_{11})_3)/(PC_6H_{11}O_3)$ zehirlenme deneyleri kullanılarak tanımlanması rutenyum(0) nanokümelerinin zeolitin gözenek içlerinin yanısıra yüzeyinde zeolitin örgü yapısını değiştirmeden ve kristalliğini kaybettirmeden oluştuğunu göstermektedir.

Zeolit yapısıyla kararlaştırılmış rutenyum(0) nanokümelerinin katalitik performansları farklı parametrelere bağlı olarak sodyum borhidrürün hidrolizinde ve

aromatiklerin hidrojenlenmesinde test edildi. Bu deneylerden şu önemli sonuçlar gözlenmiştir (*i*) zeolit yapısıyla kararlı rutenyum(0) nanokümeleri oda sıcaklığında sodyum borhidrürün hidrolizinde rekor toplam çevrim sayısı (103200 mol $H_2$/mol Ru) ve çevrim frekansı (33000 mol $H_2$/mol Ru·h) sağlamaktadır, (*ii*) bunlar aynı zamanda oda sıcaklığında aynı tepkimeyi bazik ortamdada (%5'lik NaOH çözeltisi içerisinde) daha önceden görülmemiş yükseklikte katalitik etkinlik (4000 mol $H_2$/mol *toplam* Ru·h) ve katalitik ömür (27200 mol $H_2$/mol Ru) sağlayarak katalizlemektedir, (*iii*) izole edilip vakumda kurutulan zeolit yapısıyla kararlaştırılmış rutenyum(0) nanokümeleri ılımlı koşullar altında (22.0 ± 0.1 °C'de ve 40 ± 1 psig başlangıç $H_2$ basıncında) siklohekzen, benzen, toluen ve *o*-ksilenin siklohekzan içerisindeki hidrojenlenmesinde sırasıyla 6150, 5660, 3200 ve 1550 mol $H_2$/mol Ru·h çevrim frekansı sağlayan yüksek etkinlikte bir katalizördür, (*iv*) dahada önemlisi zeolit yapısıyla kararlaştırılmış rutenyum(0) nanokümeleri ılımlı koşullar altında (22.0 ± 0.1 °C'de ve 40 ± 1 psig başlangıç $H_2$ basıncında) çözücüsüz ortamda benzenin siklohekzana hidrojenlenmesinde şimdiye kadar bilinen en etkin, en seçici (tüm çevrimde 100% seçicilik) ve en uzun ömürlü katalizördür, (*v*) dahası oluşan rutenyum(0) nanokümeleri katalitik uygulamaları sırasında külçelenmeye ve sızmaya karşı yüksek dayanıklılık göstermektedir, bu önemli özellik bunları sahip oldukları katalitik etkinlikte önemli bir kayba uğramadan tekrar kullanılabilir bir katalizör yapar.

Anahtar Kelimeler: Nanokümeler, Rutenyum, Zeolit, Katalizör, Sodyum Borhidrürün Hidrolizi, Aromatiklerin Hidrojenlenmesi.

*To my mom and dad*

# ACKNOWLEDGEMENT

# TABLE OF CONTENTS

# LIST OF FIGURES

FIGURES

xvii

**LIST OF TABLES**

TABLES

# LIST OF ABBREVIATIONS

| | |
|---|---|
| NP | : Nanoparticles |
| NC | : Nanoclusters |
| DLVO | : Derjaugin-Landau-Verwey-Overbeek |
| Ea | : Activation Energy |
| HOMO | : Highest Occupied Molecular Orbital |
| LUMO | : Lowest Unoccupied Molecular Orbital |
| TOF | : Turnover Frequency |
| TTON | : Total Turnover Number |
| $v$ | : Rate of Reaction |
| $\Delta G$ | : Change in Gibbs Free Energy |
| $\Delta H^{\#}$ | : Enthalpy of Activation |
| $\Delta S^{\#}$ | : Entropy of Activation |
| Hz | : Hertz |
| $P(C_6H_{11}O_3)$ | : 4-ethyl-2,6,7-trioxa-1-phosphabicyclo[2.2.2]octane |
| $P(C_6H_{11})_3$ | : Tricyclohexylphosphine |
| J | : Coupling constant |
| $k$ | : Rate constant |
| FP | : Fischer-Porter |
| ZC-TEM | : Zero Contrast Transmission Electron Microsocopy |
| BET | : Brunauer-Emmett-Teller |
| BJH | : Barrett-Joyner-Halenda |
| ppm | : Parts per Million |
| DR | : Diffuse Reflectance |
| FAU | : Faujasite |
| MTL | : Mass Transfer Limitation |

# CHAPTER 1

# INTRODUCTION

## 1.1. Transition Metal Nanoclusters: General Introduction and Key Definitions

Transition metal nanoclusters are those "strange morsels of matter" [1] about 1–10 nm (10–100Å) in size and distinguished from traditional colloidal metals by several important factors [2]. Specifically, transition metal nanoclusters are expected to be smaller (1–10 nm) with near-monodisperse size distributions (≤15%), while colloidal metals are often >10 nm with much broader size distributions. Additionally, transition metal nanoclusters should have reproducible syntheses leading to compositionally well-defined, isolable, and redissolvable nanoclusters. In respect to these characteristics, classic colloids traditionally have less well-defined compositions (frequently, their surfaces are contaminated with oxide/hydroxide, water, and halides) along with less reproducible syntheses [3].

Transition metal nanoclusters have unique properties, derived in part from the fact that these particles and their properties lie somewhere between those of bulk and single-particle species [4,5]. They have many fascinating potential uses, including quantum dots [6], quantum computers [7], quantum devices [8], chemical sensors [9], light-emitting diodes [10], ferrofluids for cell separations [11], photochemical pattern applications such as flat-panel displays [12], highly active and selective catalysis [13].

Two reasons chemists believe that nanoclusters have unique physical and chemical properties are that a large percentage of a nanoclusters' metal atoms lie on the surface, and that surface atoms do not necessarily order themselves in the same way that those in the bulk do [14]. Furthermore, the electrons in nanoclusters are confined to spaces that can be as small as a few atom-widths across, giving rise to quantum size effects [15]. The transition from a bulk to a nanosized material is best explained by the sketch in Figure 1 where the electronic situation in three different particles of metal atoms is illustrated. When a metal particle with bulk properties are reduced to the nanometer size scale, the density of states in the valence and the conduction band decreases to such an extent that the quasi-continous density of states is replaced by a discrete energy level structure and the electronic properties change dramatically.



| Bulk Metal | Nanoclusters | Molecule |
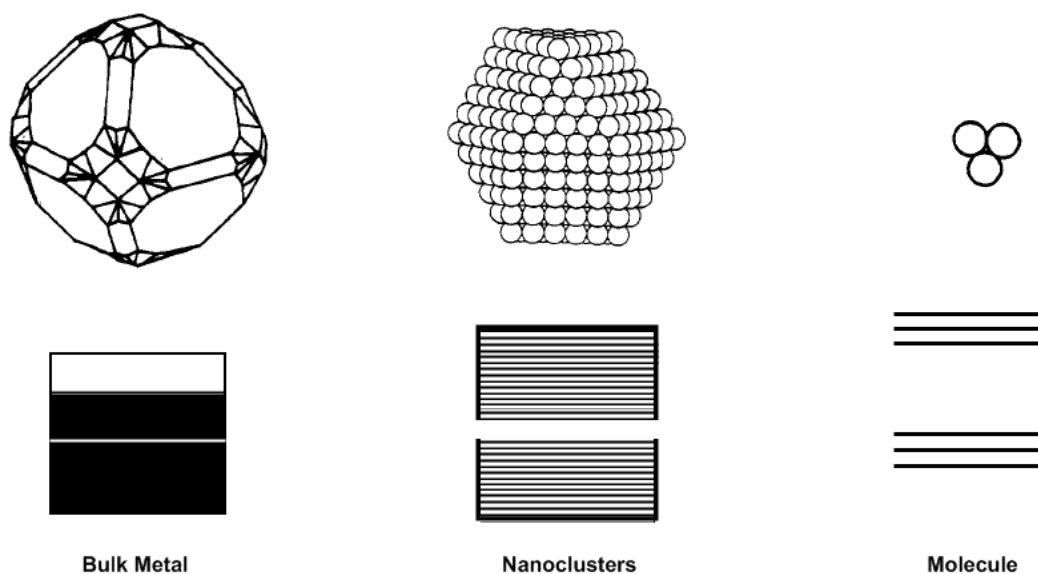
**Figure 1.** The illustration of the the electronic states in (a) a metal particle with bulk properties and its typical band structure, (b) a large cluster of cubic close packed atoms with a small band gap, and (c) a simple triatomic cluster with completely separated bonding and antibonding molecular orbitals [15].

To investigate the quantum size behavior as well as other physical and chemical properties of nanoclusters, the preparation of them in a great degree of control over size, structure, and surface composition is essentially required. However, transition-metal nanoclusters remain only kinetically stable, the thermodynamic minimum being bulk metal in all cases to date.

Consequently, substantial effort has been centered on the stabilization of transition-metal nanoclusters, as long-term solution and solid-state (e.g., storage) stability is crucial if practical applications of metal nanoclusters are to be realized. Therefore, before beginning a description of synthetic methods for the preparation of metal nanoclusters, this general and critical aspect should be considered.

### 1.1.1. DLVO Theory and Stabilization of Transition Metal Nanoclusters

DLVO (Derjaugin-Landau-Verwey-Overbeek) theory [16] was developed in the 1940's to describe how colloids are stabilized [17]. DLVO theory relies on anions adsorbed to the coordinatively unsaturated, electrophilic surface of nanocolloids to achieve Columbic repulsion between particles. The electrostatic repulsion opposes van der Waals attractions that would otherwise lead to particle agglomeration and precipitation. Hence, DLVO-type stabilization is also commonly referred to as *electrostatic* stabilization (Figure 2).
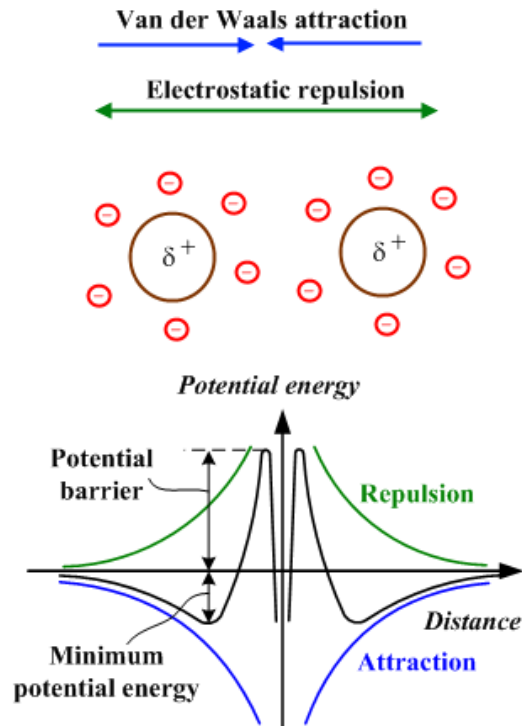
**Figure 2.** Plot of energy versus interparticular distance for electrostatic stabilization and the schematic representation of the electrostatic stabilization of transition metal nanoclusters.

The other general sources of colloidal stabilization include the followings:

(*i*) *steric stabilization*; it is achieved by surrounding the metal nanoclusters by layers of protecting groups that are sterically bulky such as polymers or oligomers [18]. These large adsorbates provide a steric barrier which prevents close contact of metal nanoclusters to each other as demonstrated in Figure 3.
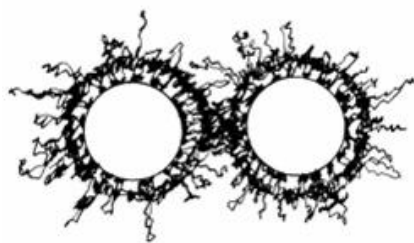
**Figure 3.** The schematic representation of the steric stabilization of transition metal nanoclusters.

(*ii*) *electrosteric stabilization*; the electrostatic and steric stabilization can be combined to maintain stable metal nanoclusters [19]. This kind of stabilization is generally provided by means of ionic surfactants. These compounds bear a polar head group able to generate an electrical double layer and a lypophilic side chain able to provide steric repulsion (Figure 4).
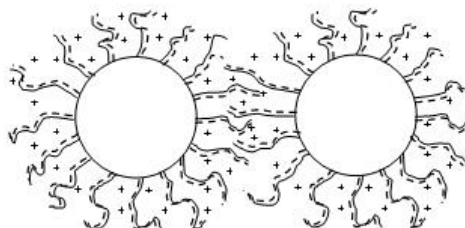


**Figure 4.** The schematic representation of the electosteric stabilization of transition metal nanoclusters.

(*iii*) *solvent stabilization*; it has also reported that metal nanoclusters can be stabilized only by donating solvents such as rhodium(0) [20] and ruthenium(0) [21] nanoclusters have been synthesized in THF without adding steric or electrostatic stabilizers.

### 1.1.2. Preparation of Transition Metal Nanoclusters

The preparation of transition metal nanoclusters can be obtained by two main methods: (*i*) *top-down approach*; mechanic subdivision of metallic aggregates (also called as physical method) or (*ii*) *bottom-up approach*; nucleation and growth of metallic atoms (also called as chemical method). The top-down approach yields dispersions where the particle size distribution is very broad typically larger (>10 nm) and not reproducibly prepared giving irreproducible catalytic activity [22]. At this concern, bottom-up approach provides more convenient ways to control the size of the particles and it includes five general synthetic methods: (1) chemical reduction of transition metal complexes [23], (2) thermal, photochemical or sonochemical decomposition [24], (3) decomposition of organometallics [25], (4) metal vapor synthesis [26], and (5) electrochemical reduction [27].

Today, the key goal in the transition metal nanoclusters area is the development of reproducible modern nanoclusters syntheses in opposition to traditional colloids. As previously reported nanoclusters should be or have at least (*i*) specific size (1-10 nm), (*ii*) well defined surface composition, (*iii*) reproducible synthesis and properties, and (*iv*) isolable and redissolvable "Bottleable" [3].

### 1.2. Transition Metal Nanoclusters in Catalysis

### 1.2.1. Introductory Concepts of Catalysis

It has long been known that the rates of many chemical reactions can be affected by traces of an alien material which may be adventitiously present in the system or may be added deliberately. The word 'alien' is used to imply that the material it describes does not appear in stoichiometric equation for the reaction. Such a material is termed as a *catalyst* and it is defined as a substance which increases the rate at which a chemical reaction approaches equilibrium, without being consumed in the process. The phenomenon occurring when a catalyst acts is termed *catalysis*.

Catalysts fall into three main groups as *heterogeneous*, *homogeneous*, and *biological* given in Figure 5.
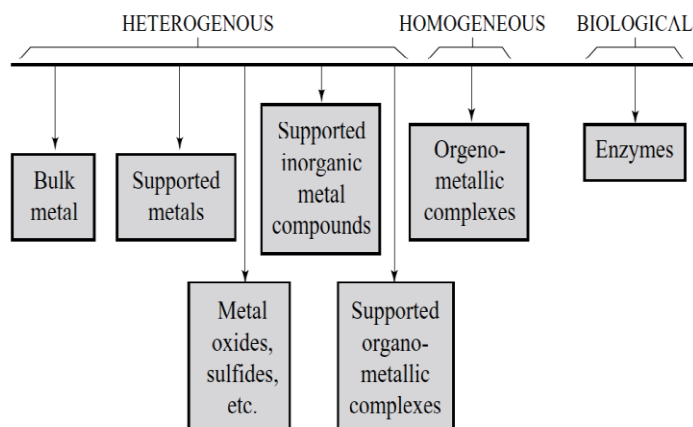


**Figure 5.** The classification of catalysts [28].

Homogeneous and heterogeneous classification is depending on whether it exists in the same phase as the substrate. Homogeneous catalyst acts in the same phase with the substrates. Heterogeneous catalysts are those that act in a different phase than the substrates. Heterogeneous catalysis is crucial for chemical technology. Most catalytic processes are heterogeneous in nature, typically involving a solid catalyst and gas- or liquid-phase reactants. Today, the majority of the industrial processes involve heterogeneous catalysis [29], because of their advantages such as easy separation of reaction products, reusability, stability, low-cost and low-toxicity [30]. However, heterogeneous catalysts often tend to require high temperatures and pressures and they have low selectivity compared to homogeneous catalysts. There also exist another group of catalysts those cannot be categorized according to phase difference: biocatalysts which are also called enzymes. Enzymes possess the highest level of complexity among the three types of catalysts. Enzymes are nature's own catalysts and fundamental for life, as they catalyze essentially all biological processes [31].

The primary effect of a catalyst on a chemical reaction is, as stated in the above definition of catalysis, to increase its rate: this means therefore to increase its rate constant. The consequent effects may be analyzed in terms of transition-state theory. In the transition state theory, the effect of catalyst must be a decrease in the free energy of activation of the reaction. This, in turn, is composed of changes in entropy and enthalpy of activation. The entropy of activation in a catalyzed reaction will usually be less than in corresponding uncatalyzed reaction because the transition state is immobilized on the catalyst surface with consequent loss of translational freedom. There must therefore be a corresponding decrease in the enthalpy of activation to compensate for this, or to overcompensate for efficient catalysis. Thus, according to the theory the activation energy for a catalyzed reaction ought to be less than for the same uncatalyzed reaction.

A catalyst changes the activation energy of a reaction in two ways. In the first way, it forms bonds with one or more of the reactants and so reduces the energy needed by the reactant molecules in order to complete the reaction. In the second way, it brings the reactants together and holds them in a way that makes reaction more likely. When molecules come together in the appropriate orientation for reaction there is a big reduction in entropy. If a catalyst already holds the molecules next to each other then the entropy change for the reaction step will be far less negative than it would be without the catalyst, and the reaction is more likely. An example is the reaction of diene with dienophile in the presence of $AlCl_3$ catalyst. The catalyst lowers the energy of LUMO and the interaction between the LUMO of the dienophile and the HOMO of the diene increases. As a result; the reaction becomes faster than the uncatalyzed one. Note that the catalyst does not affect the overall entropy change for the reaction. Catalysts increase the rate of approach to equilibrium but not the thermodynamic equilibrium value itself. In other words a catalyst provides a new reaction pathway with a low barrier of activation, which may involve many intermediates and many steps. The sequence of steps we call the mechanism of the reaction. The uncatalyzed reaction has higher activation energy

than that of any catalyzed reaction. The differences in activation energies between catalyzed and uncatalyzed reactions are shown in Figure 6.
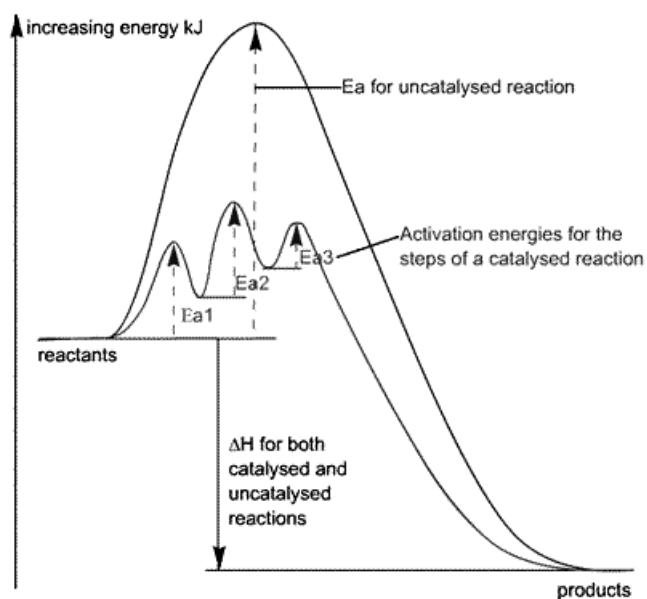


**Figure 6.** Schematic representation of the energetics (increasing energy vs extent of reaction) in a catalytic cycle.

### 1.2.2. Definition of the Catalytic Activity, Lifetime and Selectivity

The catalytic turnover frequency (TOF) is the catalytic turnover number per unit time (the number of moles of product per mole of catalyst per unit time) and is often used to express the efficiency of a catalyst, for the conversion of A to B catalyzed by Q and with a rate v, Eq.1; TOF is given by Eq. 2, where |Q| is the mole of the catalyst.

$$A \xrightarrow{\text{catalyst}} B \qquad v = \frac{d\,[B]}{d\,t} \quad (1)$$

$$TOF = \frac{v}{[\text{catalyst}]} \quad (2)$$

9
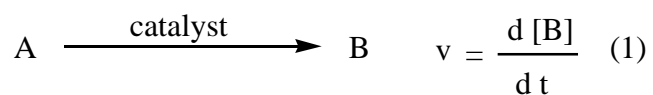
The determination of the number of active sites in a heterogeneous catalyst is particularly challenging, and often the denominator [catalyst] in Eq.2 should be replaced by the concentration of active atoms. The catalytic lifetime of any catalyst is usually expressed by total turnover number (TTON), Eq. 3, which equals to the

number of moles of product per mole of catalyst; this number indicates the number of total catalytic cycles before deactivation of the active catalyst in a given process.

$$\text{TTON} = (\text{TOF}) \times (\text{time}) = \frac{\text{mol of product}}{\text{mol of catalyst}} \quad (3)$$

Selectivity is also another important parameter that should be considered in the evaluation of the performance of any catalyst. Selectivity in catalysis can be defined as accelerating one of the competing reactions and or selecting one reagent out of a complex mixture. The selective catalyst yields a high proportion of the desired product with minimum amount of the side products. High selectivity plays a key role in industry to reduce waste, to reduce the work-up equipment of a plant, and to ensure a more effective use of the feedstocks.

**1.2.3. Transition Metal Nanoclusters are More Active Catalysts than Their Bulk-Counterparts**

Surface processes are of key importance in multifarious processes, including corrosion, adsorption, oxidation-reduction and catalysis. Understanding the surface properties and surface chemistry of metal nanoclusters is essential if their behavior is to be fully understood [32]. As mentioned earlier, from macroscale to nanoscale there exists a considerable change in the intrinsic properties of materials; moreover the properties of nanoclusters also change with size. Of particular interest, metal nanoclusters exhibit unusual surface morphologies and possess more reactive surfaces, hereby open a new perspective in the surface chemistry. They show a great potential in catalysis because of the large surface area of these particles. The

resultant huge surface areas of them dictate that many of the atoms lie on the surface, thus allowing a good 'atom economy' in surface-gas, surface-liquid, or even surface-solid reactions [33].

Transition metal nanoclusters have a high percentage of surface atoms and they do not necessarily order themselves in the same way that those in bulk do. As an illustrative example Klabunde and co-workers calculated the percentage of surface iron atoms on spherical iron(0) nanoclusters depending on their size (Figure 7).
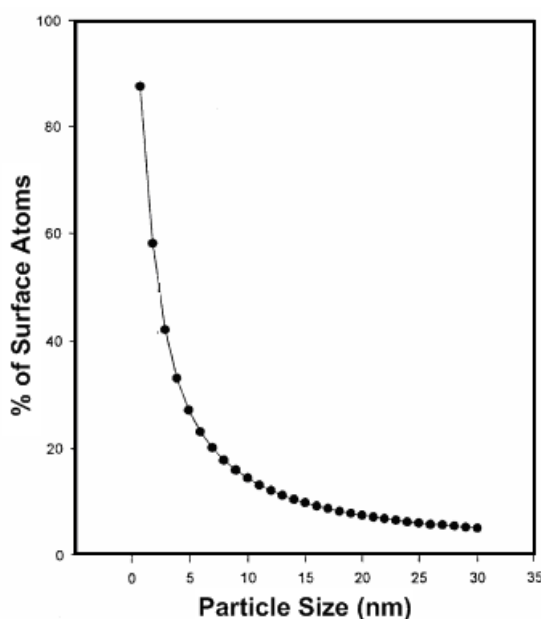


**Figure 7.** The change in percentage of surface iron atoms depending on the size of iron(0) nanoclusters [34].

The increasing proportion of surface atoms with decreasing particle size, compared with bulk metals, makes metal nanoclusters more active catalysts than their bulk counterparts, as surface atoms are the active centers for catalytic elementary processes. Among the surface atoms, those sitting on the edges and corners are more active than those in planes. Metal clusters which have a complete, regular outer geometry are designated full-shell, or 'magic number', clusters. Many

11

nanocluster distributions center around one of these full-shell geometries. Each metal atom has the maximum number of nearest neighbors, which imparts some degree of extra stability to full-shell clusters. Note that as the number of atoms increases, the percentage of surface atoms decreases as illustrated in Figure 8.

| Full-shell Clusters | | Total Number of Atoms | Surface Atoms (%) |
|---|---|---|---|
| 1 Shell | | 13 | 92 |
| 2 Shells | | 55 | 76 |
| 3 Shells | | 147 | 63 |
| 4 Shells | | 309 | 52 |
| 5 Shells | | 561 | 45 |
| 7 Shells | | 1415 | 35 |

**Figure 8.** Idealized representation of hexagonal close-packed full-shell 'magic number' clusters and the relation between the total number of atoms in full shell clusters and the percentage of surface atoms [35].

Expectedly, the studies reported in the literature show that transition metal nanoclusters are more active catalyst than their bulk-counterparts in various reactions such as catalytic reforming reaction [36], hydrocracking and aromitization processes [37], hydrogenations [38], hydrosilylations [39], oxidation of alcohols [40], McMurry couplings [41], Suzuki couplings [42], Heck-type couplings [43] and cycloaddition reactions [44].

**1.3. Can the Employment of Zeolite as the Host Material for the Stabilization of the Guest Naked Transition Metal Nanoclusters Enhance Their Stability in the Catalytic Applications?**

**1.3.1. The Composition and the Structure of Zeolite**

In general, zeolites are crystalline aluminosilicates with microporous channels and/or cages in their structures. The first zeolitic minerals were discovered in 1756 by the Swedish mineralogist Cronstedt [45]. Upon heating of the minerals, he observed the release of steam from the crystals and called this new class of minerals zeolites (Greek: zeos = to boil, lithos = stone). Currently, about 160 different zeolite structure topologies are known [46] and many of them are found in nature. However, for catalytic applications only a small number of synthetic zeolites are used. Natural zeolites typically have many impurities and are therefore of limited use for catalytic applications. Synthetic zeolites can be obtained with exactly defined compositions, and desired particle sizes and shapes can be obtained by controlling the crystallization process. The frameworks of zeolites are formed by fully connected $SiO_4$ and $AlO_4$ tetrahedra linked by shared oxygen atoms as shown in Figure 9 (top) for a Faujasite-type zeolite. Faujasite is a zeolitic mineral, which can be found in nature.

The silicon and aluminum atoms are located on the centers of the tetrahedra and are frequently denoted as T-atoms (T for tetrahedra). A $TO_4$ unit could thus represent both $SiO_4$ and $AlO_4$ tetrahedra. The Faujasite structure, as shown in Figure 9, can be considered as being formed by double rings consisting of six $TO_4$ units. Larger cages are formed by the connection of them, which build up cavities and open pore windows with a window diameter of about 0.7 nm. Obviously, the structure representation showing all atoms present in a structure is rather confusing and details of the structure are hardly visible. Therefore, a simplified representation is often chosen as shown in Figure 9 (middle). The oxygen atoms are omitted and straight lines directly connect the silicon and aluminium atoms in the center of $SiO_4$ and

AlO$_4$ tetrahedra. As a result, substructures such as cages and channels are much easier recognized. Polyhedra representations as shown in Figure 9 (bottom), allow an even easier perception of the zeolite cages and pore openings. The large cages of the Faujasite structure are formed by smaller β-cages. Similar cages are found in many zeolite structures as can be seen in Figure 10.
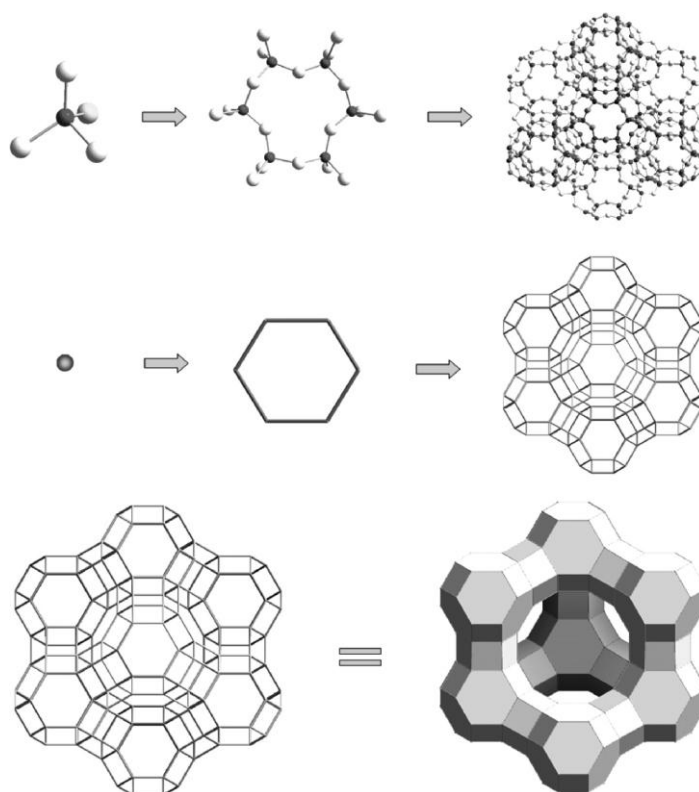


**Figure 9.** The framework structure of a Faujasite-type zeolite and simplified structure representations thereof (top: ball and stick model, middle: simplified stick model, and bottom: comparison stick model and polyhedra model).

The connectivity (topology) of the zeolite framework is characteristic for a given zeolite type, whereas the composition of the framework and the type of extra-framework species can vary. Each zeolite structure type is denoted by a three-letter code [46]. As an example, Faujasite-type zeolites have the structure type FAU. The

pores and cages of the different zeolites are thus formed by modifications of the $TO_4$ connectivity of the zeolite framework. Similar cages are found in many zeolite structures as can be seen in Figure 10.



$\beta$ - cage

$\alpha$ - cage

Faujasite - cage

SOD

LTA

FAU
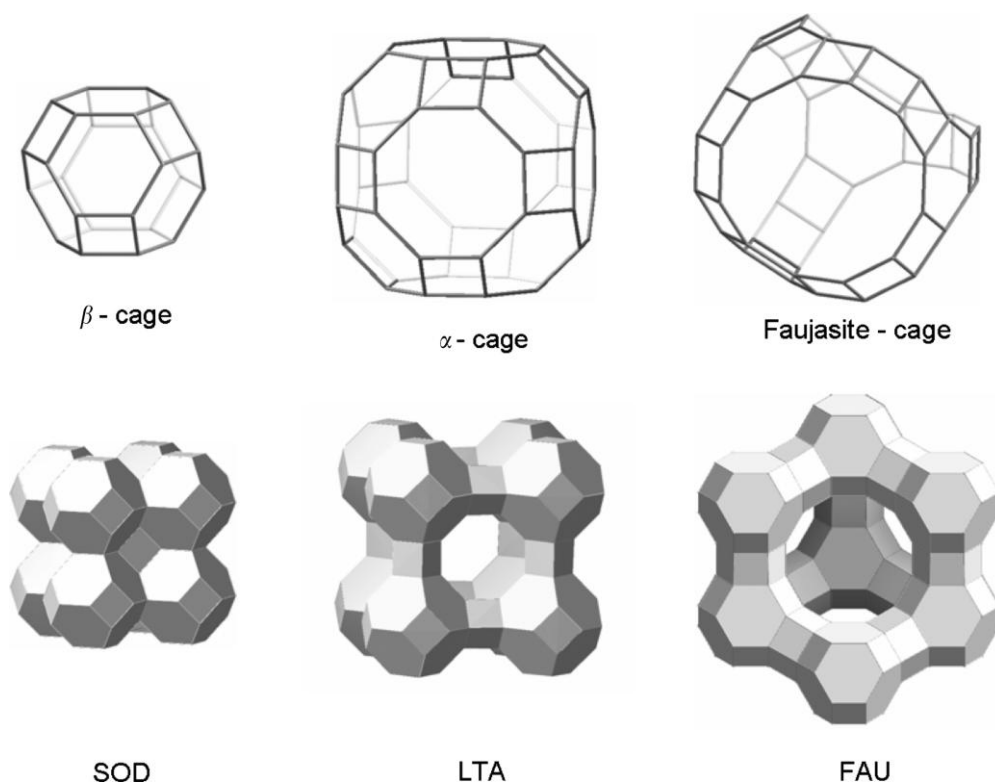
**Figure 10.** Zeolite cages as found in Sodalite (SOD), Zeolite A (LTA), and Faujasites (FAU) [47].

Besides the more or less stable framework, extra-framework cations, and inorganic or organic guest molecules may be found in the zeolite pores. What is the reason for the presence of extraframework cations? We know that the zeolite framework is formed by $SiO_4$ and $TiO_4$ tetrahedra. Each $O^{2-}$ anion is connected to two $Si^{4+}$ cations, thus each $O^{2-}$ anion provides one negative charge per $Si^{4+}$ cation. Therefore, the four positive charges of a given $Si^{4+}$ cation are compensated by four negative charges of the surrounding oxygen atoms. In the same way, the three

positive charges of an $Al^{3+}$ cation are balanced by four negative charges from the four surrounding oxygen atoms, resulting in one negative excess charge. Thus, each $Al^{3+}$ cation in the zeolite framework causes a negative framework charge. These negative charges are balanced by extra-framework cations located in the zeolite pores, as shown schematically in Figure 11. Typically, synthetic zeolites are crystallized in alkaline reaction mixtures containing $Na^+$ cations and the charge compensating extra-framework cations are then $Na^+$ cations. The composition of such a zeolite can be written as:

$$Na_x(AlO_2)_x(SiO_2)_y \cdot nH_2O \text{ or } Na_x[Al_x Si_{y-x}O_{2y}]nH_2O$$
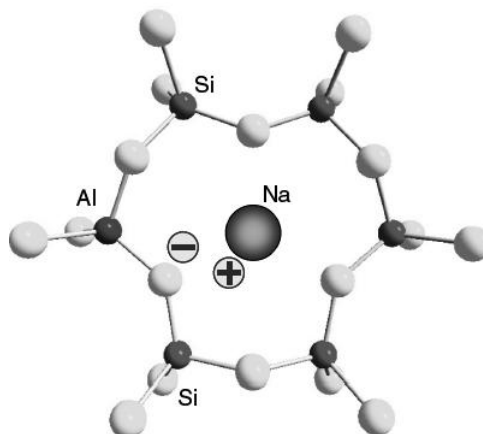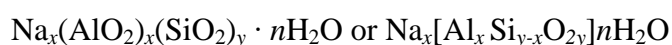


**Figure 11.** Compensation of a negative framework charge by a $Na^+$ cation.

The negative framework charges can also be balanced by many other cations, e.g., by most alkaline and earth alkaline cations as well as by transition metal cations. The extra-framework cations are usually easy to exchange by other ones, e.g., from aqueous solutions, provided the ions are small enough to fit into the pores. For this reason they are widely used as water softeners in detergents.

The chemical composition is often given as the composition of a unit cell of the respective zeolite structure. An important feature of a given zeolite material is its

16

silicon to aluminum (Si/Al) ratio. Zeolites with a Si/Al ratio up to ten are called low silica zeolites, those with higher Si/Al ratios high silica zeolites. The framework structures of low silica zeolites contain a large number of aluminum cations. Since all these framework aluminum cations cause negative framework charges, balanced by extra-framework cations, such low silica zeolites have a very high ion exchange capacity. However, the lower limit for the Si/Al ratio is one. This implies that the framework of a normal zeolite never contains more aluminum than silicon. The pore size of a zeolite depends on its structure, but in general, the pore openings are enclosed by a certain number of $TO_4$ units, forming circular or elliptic rings. Figure 12 shows the width of some circular pore openings with respect to the number of $TO_4$ units. Depending on the shape of the pore window, the width of the pores can vary in the range 0.3 to 0.8 nm for pores formed by rings consisting of six (6MR) to twelve (12MR) $TO_4$ units. Furthermore, the type and position of specific extraframework cations can affect the pore opening, since these cations may partially block the pore windows. The diameters of the windows in zeolites determine the size of molecules being able to pass through these windows, making them very efficient as molecular sieves and as selective catalysts [48].
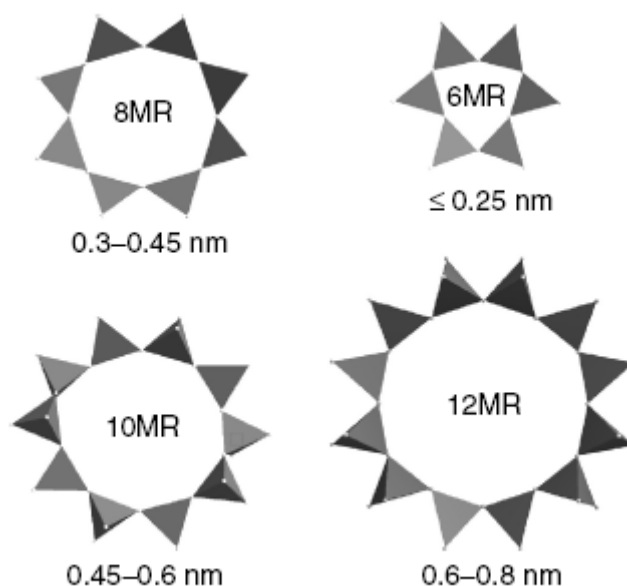


**Figure 12.** Typical pore diameters as observed in zeolites [48].

### 1.3.2. The Motivation of Thesis

As mentioned in the previous sections the preparation of transition metal(0) nanoclusters with controllable size and size distribution are of great importance because of their potential applications in many fields, including catalysis. However, the aggregation of nanoclusters ultimately to the bulk metal despite of using the best stabilizer [49,50] is still the most important problem that should be overcome in their catalytic application as their agglomeration into bulk metal leads to a momentous decrease in their catalytic activity and lifetime. At this concern, the use of nanocluster catalysts in systems with confined void spaces such as inside mesoporous and microporous represents an especially promising direction of preventing aggregation [51]. Additionally, the pore size restriction of these host materials could limit the growth of guest metal nanoclusters and lead to an increase in the percentage of the catalytically active surface atoms. Moreover, metal nanoclusters catalyst encapsulated within the cavities of zeolite or between the zeolite-supported layers (i.e., zeolite films, powders or membranes supported on the surface of solid materials) [52] may provide kinetic control for the catalytic reactions.

Among a vast number of microporous and mesoporous materials, zeolite-Y (with FAU framework) is considered to be a suitable host material because of the following advantages; (*i*) it provides highly ordered large cavities with diameters of 1.3 nm for supercage (α-cage) and 0.7 nm for sodalite cage (β-cage), Figure 13, (*ii*) this framework structure is the most open to any zeolite and is about 51 % void volume, including the sodalite cages; the supercage volume represents 45 % of the unit cell volume, (*iii*) in this framework, each cavitiy is connected to four other cavities, which in turn are themselves connected to three-dimensional cavities to form three-dimensonal pore structure and it enables transferring of substrates or products throughout the framework eventhough one of the channels is blocked, (*iv*) the main pore structure is large enough to admit large molecules.
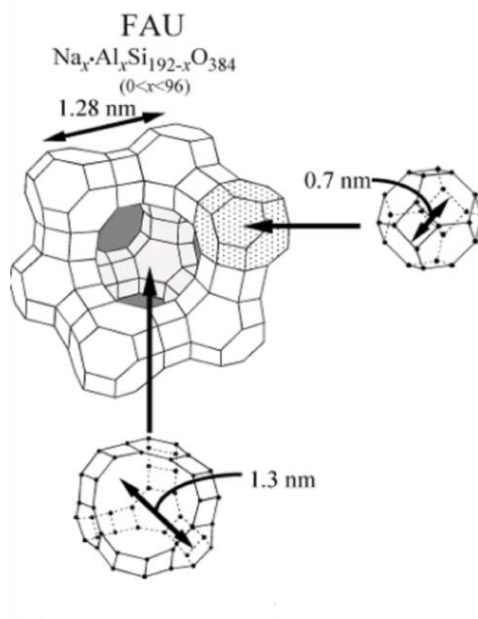
**Figure 13.** The framework structure and the cavities of zeolite-Y.

Thus far, the preparation of nanoparticles or clusters of different metals within Faujasite zeolites have been intensively studied [53, 54, 55]. Commonly, the convenient procedure for generating metal nanoparticles inside the zeolite pores comprises the introduction of metal species (cations or complexes) into the zeolite by ion-exchange or vapor deposition and then reduction by $H_2$ at temperatures higher than 300 °C and calcination up to 400-500 °C. However, this high temperature treatment may cause alteration in the zeolite framework due to the formation of an unstable acid form and may lead to the migration of a large part of the guest metal atoms out of cavities of the zeolite [54, 55, 55, 56, 57]. Therefore, the improvement of the existing method for the preparation of zeolite confined metal nanoclusters in a way that prevents sintering of nanoclusters and migration of them from the zeolite framework is the important and challenging issue in this research field.

## 1.4. The Catalytic Reactions Investigated in the Scope of Thesis

### 1.4.1. The Hydrolysis of Sodium Borohydride

Because of increasing concern about environmental problems, including global warming caused by the emission gases from the combustion of fossil fuels, there has been a growing interest for the "hydrogen-economy" as a long-term solution toward a sustainable energy future [58]. The effective storage of hydrogen is one of the key elements of the hydrogen economy, and the chemical hydrides have been tested as hydrogen-storage materials [59]. Among these chemical hydrides, sodium borohydride, $NaBH_4$, has been considered as the most attractive hydrogen storage material, as it provides a safe and a practical mean of producing hydrogen and has high hydrogen content (10.7% wt) [60]. Although a cost-effective process for the recyclability of thr hydrolysis product, the conversion of metaborate to borohydride, is still lacking, the hydrolysis of sodium borohydride, Eq. 4, is a convenient method of hydrogen generation for portable fuel cell applications [61].

$$NaBH_4 + 2H_2O \xrightarrow{\text{catalyst}} NaBO_2 + 4H_2 \qquad (4)$$
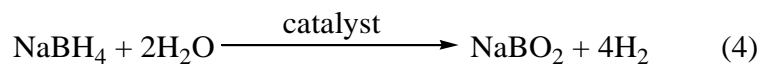
Since the hydrolysis occurs only in the presence of a suitable catalyst [62], many transition metals or their compounds have been tested as catalyst for this industrially important reaction [63]. However, the development of highly stable long-lived heterogeneous catalysts is still needed for this important reaction.

### 1.4.2. The Hydrogenation of Aromatics

The complete hydrogenation of aromatics is one of the most important and challenging transformations in the synthesis of fine chemicals and intermediates [64] and, traditionally, has been carried out at high temperature (>100 °C) and/or high pressure (50 atm $H_2$) [65]. Literature review reveals that a range of homogeneous and

heterogeneous catalysts have been used to hydrogenate benzene, which is well-know test reaction in the hydrogenation of aromatics, Eq. 5.

$$\text{benzene} \xrightarrow[\text{H}_2]{\text{catalyst}} \text{cyclohexane} \qquad (5)$$
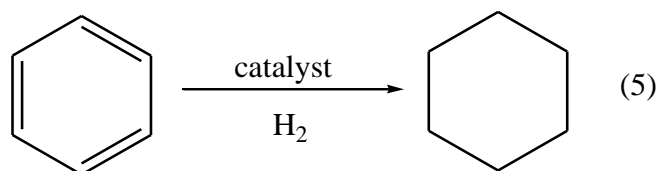
Among these, the catalysts [66] that achieve the complete hydrogenation of benzene without any side products under mild conditons ($\leq 25°C$, and $\leq 3$ atm $H_2$) are the hydroxyalkylammonium halide-stabilized rhodium(0) [67] and iridium(0) nanoclusters [68], cyclodextrins-stabilized rhodium(0) nanoclusters [69], rhodium(0) nanoclusters immobilized on silica [70], Rh(COD) moiety anchored to polymers [71], rhodium(0) nanoclusters entrapped in boehmite nanofibers [72], ruthenium(0) nanoclusters immobilized into SBA-15 [73], $[(Cp^*)_2Zr(CH_3)_2]^+$ activated via super acidic sulfated alumina or sulfated zirconia [74], rhodium(0) nanoclusters stabilized by polyhydroxylated ammonium chloride [75] and CNT-supported rhodium(0) nanoclusters [76]. Although, these catalysts [67-76] can hydrogenate benzene to cyclohexane at 100 % conversion, a relatively few of them operates at significant rate. Therefore, the development of an easily prepared, highly active, long-lived and reusable catalyst that operates under mild conditions is still a paramount challenge.

**1.5. Scope of the Thesis**

The aim of this thesis is to prepare and characterize zeolite framework stabilized ruthenium(0) nanoclusters as well as to test their catalytic performance in terms of activity, lifetime, isolability, bottlability and reusability throughout their catalytic use in the hydrolysis of sodium borohydirde in aqueous solution and the hyrogenation of aromatics in organic medium.

The scope of the research includes:

(a) The preparation of zeolite framework stabilized ruthenium(0) nanoclusters under mild conditions in a simple and reproducible way; zeolite framework stabilized ruthenium(0) nanoclusters were reproducibly prepared by the method comprising of the ion-exchange of $Ru^{3+}$ ions with the extra framework $Na^+$ ions in zeolite-Y, followed by the reduction of the $Ru^{3+}$ ions within the framework of zeolite-Y with sodium borohydride in aqueous solution at room temperature. The resultant ruthenium(0) nanoclusters were found to be stable enough for being isolated as solid material.

(b) The characterization of zeolite framework stabilized ruthenium(0) nanoclusters; zeolite framework stabilized ruthenium(0) nanoclusters were characterized by a combination of advanced analytical techniques including ICP-OES, XRD, TEM, ZC-TEM, HR-TEM, TEM-EDX, SEM, XPS, DR-UV-vis, far-IR, mid-IR, Raman spectroscopy and $N_2$ adsorption-desorption technique.

(c) Testing the catalytic performance of zeolite framework stabilized ruthenium(0) nanoclusters: Zeolite framework stabilized ruthenium(0) nanoclusters were tested as catalysts in two important catalytic reactions: the hydrolysis of sodium borohydride in aqueous medium, which has been considered as a promising hydrogen storage material, and the hydrogenation of aromatics in organic medium, usually known as a difficult industrial reaction that requires vigorous conditions. In addition to their catalytic activity depending on catalyst concentration and temperature, the other important parameters such as catalytic lifetime, isolability, bottlability and reusability of them were also investigated in these reactions.

# CHAPTER 2

# EXPERIMENTAL

## 2.1. Materials

Ruthenium(III) chloride trihydrate ($RuCl_3 \cdot x H_2O$), sodium borohydride ($NaBH_4$, purity > 98 %), borontrifluoride etherate ($BF_3 \cdot (C_2H_5)_2O$), deuterated water ($D_2O$), deuterated chloroform ($CDCl_3$), cyclohexane (purity > 99.9 %), benzene (purity > 99.9 %), and filter papers (Whatman-1) were purchased from Aldrich[®]. Cyclohexene (purity > 98 %), toluene (purity > 99.9), mesitylene (purity > 99.5), *o*-xylene (purity > 99.5), tricyclohexylphosphine ($P(C_6H_{11})_3$), sodium chloride (NaCl), acetone (purity > 99) were purchased from Fluka[®]. 4-ethyl-2,6,7-trioxa-1-phosphabicyclo[2.2.2]octane ($P(C_6H_{11}O_3)$) was purchased from Ventron [®]. Sodium zeolite-Y ($Na_{56}Y$ with Si/Al = 2.5) was purchased from Zeolyst[®]. [1]H standard and ^{11}B natural quartz NMR tubes were purchased from Norell[®].

Ruthenium(III) chloride was recrystallized from water and the water content of $RuCl_3 \cdot x H_2O$ was determined by TGA and found to be $x = 3$. Cyclohexane, cyclohexene, benzene, toluene, mesitylene and *o*-xylene were distilled over sodium under argon and stored in the drybox (Labsconco, $0_2 < 5$ ppm, $H_2O < 1$ ppm). Sodium zeolite-Y was slurried with 0.1 M NaCl to remove sodium defect sites, washed until free of chloride and calcined in dry oxygen at 500 °C for 12 h before to use.

Deionized water was distilled by water purification system (Milli-Q System). All glassware and Teflon coated magnetic stir bars were cleaned with acetone, followed by copious rinsing with distilled water before drying in an oven at 150 °C. The manipulations that require to inert atmosphere were carried out in a drybox (Labsconco drybox, $0_2 < 5$ ppm, $H_2O < 1$ ppm) or by using Schlenk technique. H2, N2, and H2/N2 (10 % : 90 % mixture) gases were purchased from Linda and for all the purity > 99 %. The oxygen and moisture traps were purchased from Startedk Inc.

## 2.2.    Characterization

The ruthenium and sodium content of the zeolite were determined by ICP-OES (inductively coupled plasma optical emission spectroscopy) using Leeman, Direct Reading Echelle after each sample was completely dissolved in a mixture of $HNO_3$/HCl (1/3 ratio). Powder X-ray diffraction (XRD) patterns were recorded with a MAC Science MXP 3TZ diffractometer using Cu Kα radiation (wavelength 1.5406 Å, 40 kV, 55 mA). Scanning electron microscope (SEM) images were measured using a JEOL JSM-5310LV at 15 kV and 33 Pa in a low-vacuum mode without metal coating by sticking the powder samples on SEM sample holder. Transmission electron microscopy (TEM) and high resolution transmission electron microscopy (HRTEM) analyses were performed on a JEM-2010F microscope (JEOL) operating at 200 kV. A small amount of powder sample was placed on the copper grid of the transmission electron microscope. Samples were examined at magnification between 100 and 400K. The elemental analyses of the powder samples were recorded during the TEM analyses with an energy dispersive X-ray (EDX) analyzer (KEVEX Delta series) mounted on the Hitachi S-800 modulated to JEM-2010F microscope The XPS analyses of the samples were performed on a Physical Electronics 5800 spectrometer equipped with a hemispherical analyzer and using monochromatic Al Kα radiation (1486.6 eV, the X-ray tube working at 15 kV, 350 W and pass energy of 23.5 eV). Diffuse reflectance UV-Vis spectra were recorded on a Cary 5000 (Varian) UV-Vis-NIR spectrophotometer, the background correction was done by using KBr as a

reference sample with zero reflectance. The Raman spectra of the powder samples were recorded on Bruker RFS-100/S series Raman spectrometer equipped with Nd-YAG laser at 1064 nm using the FT-Raman technique. The nitrogen adsorption-desorption experiments were carried out at 77 K using a NOVA 3000 series instrument (Quantachrome Instruments). The powder samples were outgassed under vacuum at 573 K for 3 h before the adsorption of nitrogen. NMR spectra were recorded on Bruker Avance DPX 400 MHz spectrometer (400.1 MHz for ^{1}HNMR and 128.2 MHz for ^{11}B NMR). Tetramethylsilane was used as the internal reference for [1]H. ($BF_3 \cdot (C_2H_5)_2O$) was used as the external reference for ^{11}B NMR chemical shifts.

## 2.2.1. The Pretreatment of Samples and Measurement Conditions for Far-IR Studies

The powder samples were pressed into self-supporting wafers of 15 mm diameter weighing approximately 15 mg by using an applied pressure of 6-8 tons per square inch for up to 60 s. The wafers were clamped into a glass tube whose one-side turbo-molecular vacuum ($10^{-7}$ Torr) connected and located in furnace. Thus the self supporting wafers were dehydrated with the following heating schedule, using an NX-(Mitsubishi) series temperature controller: 0.5 h from 25 to 100 °C, 1 h at 100 °C, 4 h from 100 to 550 °C and 4 h at 550 °C. After thermal treatment the samples inside the glass tube were cooled down to room temperature, then sealed and transferred into the drybox ($0_2 < 5$ ppm, $H_2O < 1$ ppm) in which the sample was put into a sample holder equipped with high density polyethylene window.

The level of dehydration was checked by complementary Mid- IR spectroscopy. The degree of dehydration was judged by the flatness of the baseline in the IR v(OH) stretching and (OH) deformation regions, 3400-3700 and 1600-1650 $cm^{-1}$, respectively, and was found to be complete in all cases. The far-IR spectra were recorded at Nicolet Magna-IR 750 spectrometer (using Omnic software) under $N_2$

purging by using global source and DTGS detector. The spectral resolution in all cases was 4 cm$^{-1}$ and all of the spectra have been base line corrected.

## 2.3. The Preparation and the Catalytic Reactivity of Zeolite Framework Stabilized Ruthenium(0) Nanoclusters in the Hydrolysis of Sodium Borohydride

### 2.3.1. Preparation of Ruthenium(III)-Exchanged Zeolite

In a round bottom flask (250 mL), sodium zeolite-Y was added to a solution of RuCl$_3$·3H$_2$O in 100 mL of water. The concentration of the aqueous solution was adjusted to control the degree of ion-exchange [77] and the ruthenium content in the sample. This slurry was stirred (at 700 rpm) at room temperature for 72 h. It was observed that after 72 h the opaque supernatant solution became colorless, indicating the completion of ion exchange. The sample was then filtered by suction filtration (under 0.1 Torr vacuum) using Whatman-1 filter paper, washed three times with 20 mL of deionized water and dried in oven at 100 °C for 6 h.

### 2.3.2. Testing the Catalytic Activity of the Zeolite Framework Stabilized Ruthenium(0) Nanoclusters Formed In-Situ During the Hydrolysis of Sodium Borohydride

The catalytic activity of zeolite framework stabilized ruthenium(0) nanoclusters formed in-situ during the hydrolysis of sodium borohydride was determined by measuring the rate of hydrogen generation. To determine the rate of hydrogen generation, the catalytic hydrolysis of sodium borohydride was performed using a Fischer-Porter (FP) pressure bottle. The FP bottle was connected to a line through a Swagelok TFE sealed quick connects and to an Omega PX-302 pressure transducer interfaced through an Omega D1131 digital transmitter to a computer using the RS-232 module (Figure 14). The progress of an individual hydrolysis

reaction was followed by monitoring the increase in the pressure of $H_2$ gas with the program LabVIEW 8.0.
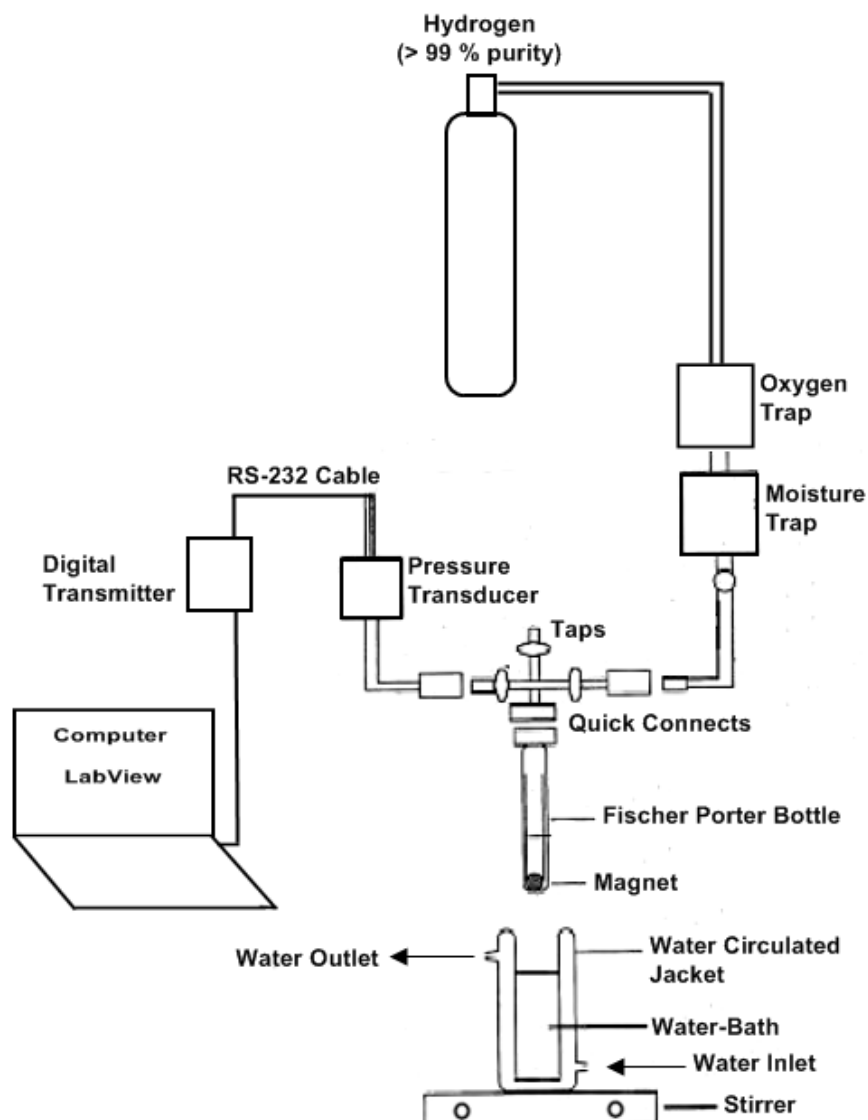


**Figure 14.** The experimental system constructed to measure the amount of hydrogen pressure evolved and consumed in the hydrolysis of sodium borohydride and the hydrogenation of aromatics, respectively.

The pressure vs time data was processed using Microsoft Office Excel 2003 and Origin 7.0 and then converted into the values in the proper unit, volume of

hydrogen (mL). In a typical experiment, 284 mg (7.47 mmol) of $NaBH_4$ was dissolved in 50 mL of water (corresponding to a maximum amount of $H_2$ gas of 30 mmol = 672 mL at $25.0 \pm 0.1$ °C and 0.91 atm pressure in the FP bottle). This solution was transferred with a 50 mL glass-pipet into the FP bottle thermostated at $25.0 \pm 0.1$ °C. Then, $Ru^{3+}$-exchanged zeolite-Y sample was added into this solution. The experiment was started by closing the FP bottle connected to the pressure transducer and turning on the stirring at 1000 rpm simultaneously. Ruthenium(III) ion was reduced and the ruthenium(0) nanoclusters were formed within the cages of zeolite- Y, catalyzing the hydrolysis of sodium borohydride. In addition to the volumetric measurement of the hydrogen evolution, the conversion of sodium borohydride to sodium metaborate was also checked by comparing the intensities of signals of sodium borohydride and metaborate anion at $\delta$= -42.1 and 9 ppm [78], respectively, in the $^{11}B$-$\{^1H\}$ NMR spectra of the solution. The same experiment was also conducted at $25 \pm 0.1$ °C using different stirring speeds: 0, 120, 240, 360, 480, 600, 720, 840, 960, 1080 and 1200 rpm. It was found that after 600 rpm, the stirring rate has no significant effect on the hydrogen generation rate. This indicates that the system is in a non-MTL (mass transfer limitation) regime at stirring rates > 600 rpm.

### 2.3.3. Control Experiment: Testing the Catalytic Activity of Ruthenium-Free Zeolite-Y in the Hydrolysis of Sodium Borohydride in the Aqueous Medium

To investigate the effect of the host material zeolite-Y on the catalytic activity of zeolite framework stabilized ruthenium(0) nanoclusters, the hydrolysis of sodium borohydride was performed in the presence of zeolite-Y. Sodium borohydride (284 mg, $[NaBH_4]$ = 150 mM) was dissolved in 50 mL of water and the solution was transferred with a 50 mL pipet into a FP bottle thermostated at $25.0 \pm 0.1$ °C, and then 474 mg of zeolite-Y (corresponds to the maxiumum amount of zeolite-Y that was used as a host material for all the tests reported for the hydrolysis of sodium borohydride in aqueous medium) was added into the FP bottle. The experiment was started by closing the reaction flask and turning on the stirring at 1000 rpm

simultaneously. The same experiment was repeated at different temperatures (20, 25, 30, 35, 40, and 45 °C).

## 2.3.4. Effect of Ruthenium Loading on the Catalytic Activity of Zeolite Framework Stabilized Ruthenium(0) Nanoclusters in the Hydrolysis of Sodium Borohydride

In a series of experiments, the catalytic activity of zeolite framework stabilized ruthenium(0) nanoclusters ([Ru] = 1mM) with a various ruthenium loading in the range of 0.10-8.4% wt Ru (0.1, 0.22, 0.4, 0.5, 0.61, 0.8, 0.95, 1.2, 1.5, 1.8, 2.3, 2.7, 3, 3.2, 3.6, 3.95, 4.3, 4.7, 5, 5.4, 6.2, 7.1, 8.4% wt Ru loadings) were tested in the hydrolysis of  sodium borohydride solution (284 mg in 50 mL, [NaBH$_4$] = 150 mM) at 25 ± 0.1 °C. The experiments were performed in the same way as described in section (**2.3.2.**). The best catalytic activity was achieved by 0.80 wt % ruthenium loaded zeolite framework stabilized ruthenium(0) nanoclusters. Therefore, in all of the tests reported hereafter, the ruthenium loading used was ≈ 0.80 wt % unless otherwise stated.

## 2.3.5.  Kinetic Studies and the Determination of Activation Parameters for the Hydrolysis of Sodium Borohydride in the Aqueous Medium Catalyzed by In-Situ Formed Zeolite Framework Stabilized Ruthenium(0) Nanoclusters

In order to establish the rate law for the catalytic hydrolysis of sodium borohydride using zeolite framework stabilized ruthenium(0) nanoclusters, two different sets of experiments were performed in the same way as described in section of (**2.3.2.**). In the first set of experiments, the concentration of sodium borohydride was kept constant at 150 mM (284 mg in 50 mL) and the ruthenium concentration was varied in the range of 0.50, 0.75, 1.00, 1.25, and 1.50 mM (316, 474, 632, 790, 948 mg of zeolite framework stabilized ruthenium(0) nanoclusters, respectively) at 25 ± 0.1 °C. In the second set of experiments, the ruthenium

concentration was held constant at 0.50 mM Ru (316 mg of zeolite framework stabilized ruthenium(0) nanoclusters in 50 mL), while sodium borohydride concentration was varied in the range of 0.075, 0.15, 0.30, 0.45, 0.60, 1.20, 2.40, 4.80 M (0.14, 0.28, 0.56, 0.84, 1.12, 2.24, 4.48, 8.96 g of NaBH$_4$, respectively) at 25 ± 0.1 °C.

Finally, we performed the catalytic hydrolysis of sodium borohydride (284 mg in 50 mL, [NaBH$_4$] = 150 mM) in the presence of 0.50 mM zeolite framework stabilized ruthenium(0) nanoclusters (351 mg zeolite framework stabilized ruthenium(0) nanoclusters with a ruthenium loading of ≈ 0.72 wt %) at various temperatures (20, 25, 30, 35, 40, and 45 °C) in order to obtain the activation energy (Ea), enthalpy ($\Delta H^{\#}$), and entropy ($\Delta S^{\#}$).

## 2.3.6. Isolability, Bottlability and Reusability of Zeolite Framework Stabilized Ruthenium(0) Nanoclusters in the Hydrolysis of Sodium Borohydride in the Aqueous Medium

After the first run of the hydrolysis of sodium borohydride (284 mg in 50 mL, [NaBH$_4$] = 150 mM), catalyzed by zeolite framework stabilized ruthenium(0) nanoclusters (316 mg, [Ru] = 0.5mM), at 25 ± 0.1 °C, the catalyst was isolated by suction filtration (under 0.1 Torr), washed three times with 20 mL of deionized water, dried under N$_2$ gas purging at room temperature, and then transferred into the glovebox.

After 1 day storage, the isolated and dried samples of zeolite framework stabilized ruthenium(0) nanoclusters were weighted and used again in the hydrolysis of sodium borohydride (284 mg in 50 mL, [NaBH$_4$] = 150 mM), and the same procedure was repeated three times after 1 week, 15 days, and 1 month. The results were expressed as the percentage of retained initial catalytic activity of zeolite framework stabilized ruthenium(0) nanoclusters and the conversion in the hydrolysis of sodium borohydride.

### 2.3.7. Determination of the Catalytic Lifetime of Zeolite Framework Stabilized Ruthenium(0) Nanoclusters in the Hydrolysis of Sodium Borohydride in the Aqueous Medium

The catalytic lifetime of zeolite framework stabilized ruthenium(0) nanoclusters in the hydrolysis of sodium borohydride was determined by measuring the total turnover number (TTO). This experiment was started with a 50 mL solution containing zeolite framework stabilized ruthenium(0) nanoclusters (316 mg, [Ru] = 0.5 mM) and sodium borohydride (0.56 g, [NaBH$_4$] = 300 mM) at 25.0 ± 0.1 °C. When the complete conversion is achieved, more sodium borohydride was added into the solution and the reaction was continued in this way until hydrogen gas evolution was slowed down to the level obtained in the ruthenium free zeolite-Y catalyzed hydrolysis of sodium borohydride (1.0 mL H$_2$/min) at 25 ± 0.1 °C.

### 2.3.8. Effect of Sodium Hydroxide on the Catalytic Activity of Zeolite Framework Stabilized Ruthenium(0) Nanoclusters in the Hydrolysis of Sodium Borohydride in the Basic Medium

The zeolite framework stabilized ruthenium(0) nanoclusters catalyzed hydrolysis of sodium borohydride was performed in solutions containing different amounts of sodium hydroxide (solutions containing 2.5, 5, 7.5, 10 wt % NaOH). Such an experiment started with the reduction of of ruthenium(III)-exchanged zeolite Y (252.5 mg with 0.80 wt % Ru loading, [Ru] = 0.67 mM) by sodium borohydride (170.4 mg, [NaBH$_4$] = 150 mM) in 30 mL of water at 25.0 ± 0.1 °C ; when no more hydrogen evolution was observed (after the complete reduction of ruthenium(III) to ruthenium(0)), then this solution was transferred into a FP bottle that contains sodium hydroxide (1.315 g for 2.5 % wt NaOH solution) and sodium borohydride (284 mg, [NaBH$_4$]= 150 mM), which had been dissolved in 20 mL of H$_2$O. Then the catalytic activity of zeolite framework stabilized ruthenium(0) nanoclusters ([Ru] =

0.4 mM) at 25.0 ± 0.1 °C in the hydrolysis of sodium borohydride in the basic medium was measured in the same way as described in the section of (**2.3.2.**).

## 2.3.9. Control Experiment: Testing the Catalytic Activity of Ruthenium-Free Zeolite-Y in the Hydrolysis of Sodium Borohydride in the Basic Medium

In a series of experiments, the catalytic activity of ruthenium free zeolite-Y was tested in the hydrolysis of sodium borohydride in the basic medium. This experiment was performed by dissolving sodium borohydride (284 mg, [NaBH$_4$]= 150 mM) and sodium hydroxide (1.32, 2.63, 3.96, and 5.26 g for 2.5, 5, 7.5, 10 wt % NaOH solutions) in 50 mL of water, transferring the solution with a 50 mL pipet into a FP bottle thermostated at 25.0 ± 0.1 °C, and adding 474 mg of zeolite-Y (corresponds to the maxiumum amount of zeolite-Y that was used as a host material for all the tests reported for the hydrolysis of sodium borohydride in the basic medium) into the FP bottle. The experiment was started by closing the reaction flask and turning on the stirring speed at 1000 rpm simultaneously. The same experiment was also repeated at different temperatures (20, 30, 35, 40, and 45 °C). In all experiments no hydrogen generation was observed, even at low sodium hydroxide concentration (2.5 wt %) and high temperature (45 °C).

## 2.3.10. Kinetic Studies and the Determination of Activation Parameters for the Hydrolysis of Sodium Borohydride in the Basic Medium Catalyzed by Preformed Zeolite Framework Stabilized Ruthenium(0) Nanoclusters

To establish the rate law for the zeolite framework stabilized ruthenium(0) nanoclusters catalyzed hydrolysis of sodium borohydride in the basic medium (in 5 wt % NaOH solution), two different sets of experiments were performed in the same way as described in the section of (**2.3.8.**). First, the concentration of sodium borohydride was kept constant at 150 mM (284 mg in 50 mL) and the ruthenium concentration was varied in the range of 0.50, 0.75, 1.00, 1.25, and 1.50 mM (316,

474, 632, 790, and 948 mg of zeolite framework stabilized ruthenium(0) nanoclusters, respectively) at 25.0 ± 0.1 °C. In the second set of experiments, ruthenium concentration was held constant at 0.50 mM (316 mg of zeolite framework stabilized ruthenium(0) nanoclusters) while sodium borohydride concentration was varied in the range of 0.15, 0.30, 0.45, 0.60, 1.20, 2.40, 4.80 M (0.28, 0.56, 0.84, 1.12, 2.24, 4.48, 8.96 g of $NaBH_4$ respectively) at 25.0 ± 0.1 °C. Then, the same experiment starting with zeolite framework stabilized ruthenium(0) nanoclusters (316 mg, [Ru] = 0.5 mM), sodium borohydride (284 mg, [$NaBH_4$]= 150 mM) in 50 mL of 5 wt % NaOH solution was performed at various temperatures (20, 25, 30, 35, 40, and 45 °C) in order to obtain the activation energy (Ea), enthalpy ($\Delta H^{\#}$), and entropy ($\Delta S^{\#}$).

.

## 2.3.11. Isolability, Bottlability and Reusability of Zeolite Framework Stabilized Ruthenium(0) Nanoclusters in the Hydrolysis of Sodium Borohydride in Basic Medium

After the first run of the hydrolysis of sodium borohydride (284 mg in 50 mL, [$NaBH_4$] = 150 mM), catalyzed by zeolite framework stabilized ruthenium(0) nanoclusters (316 mg, [Ru] = 0.5 mM) in 5 wt % NaOH solution at 25.0 ± 0.1 °C, the catalyst was isolated by suction filtration (under 0.1 Torr), washed three times with 20 mL of deionized water, dried under $N_2$ gas purging at room temperature and then transferred into the glovebox. After 1 day storage the isolated and dried samples of zeolite framework stabilized ruthenium(0) nanoclusters were weighted and used again in the hydrolysis of sodium borohydride (284 mg in 50 mL, [$NaBH_4$] = 150 mM) after 1 day, and the same procedure was repeated three times after 1 week, 15 days, and 1 month. The results were expressed as the percentage of retained initial catalytic activity of zeolite framework stabilized ruthenium(0) nanoclusters and the conversion in the hydrolysis of sodium borohydride in the basic medium.

**2.3.12. Determination of the Catalytic Lifetime of Zeolite Framework Stabilized Ruthenium(0) Nanoclusters (Ru(0)/Y) in the Hydrolysis of Sodium Borohydride in the Basic Medium**

The catalytic lifetime of zeolite framework stabilized ruthenium(0) nanoclusters in the hydrolysis of sodium borohydride in the basic medium (in 5 % wt NaOH solution) was determined by measuring the total turnover number (TTON). Such a lifetime experiment was started with a 50 mL of 5 % wt NaOH solution containing zeolite framework stabilized ruthenium(0) nanoclusters (316 mg of zeolite, [Ru] = 0.5 mM) and sodium borohydride (0.56 g, [$NaBH_4$] = 300 mM) at $25.0 \pm 0.1$ °C. When the complete conversion is achieved, more sodium borohydride was added into the solution and the reaction was continued in this way until no hydrogen gas evolution was observed.

**2.4. Zeolite Framework Stabilized Ruthenium(0) Nanoclusters Catalyzed Hydrogenation of Aromatics**

**2.4.1. The Pretreatment of Zeolite Framework Stabilized Ruthenium(0) Nanoclusters Catalyst Formed from the Borohydride Reduction of Ruthenium(III)-Exchanged Zeolite-Y**

Zeolite framework stabilized ruthenium(0) nanoclusters were prepared by following the procedure given in the section of (**2.3.2.**) by holding [$NaBH_4$] / [$Ru^{3+}$] at least 150 to achieve complete reduction of ruthenium(III) to ruthenium(0). The resultant zeolite framework stabilized ruthenium(0) nanoclusters sample was isolated from the solution by filtration using Whatman-1 filter paper under $N_2$ gas purging, washed three times with 20 mL of deionized water, and dried at room temperature under vacuum ($10^{-3}$ Torr), then transferred into the drybox ($0_2 < 5$ ppm, $H_2O < 1$ ppm).

## 2.4.2. General Procedure for the Hydrogenation of Aromatics Catalyzed by Zeolite Framework Stabilized Ruthenium(0) Nanoclusters

Hydrogenation reactions were performed using hydrogenation apparatus as previously given in Figure 14; a Fischer-Porter pressure bottle modified by Swagelock TFE-sealed quick connects and connected to a $H_2$ line and a Omega PX-302 pressure transducer interfaced through an Omega D1131 digital transmitter to a computer using the RS-232 module. The progress of individual hydrogenation reactions was followed by monitoring the loss of $H_2$ pressure on Lab View 8.0 program.

The hydrogenation experiments were performed in a similar procedure as described elsewhere [49, 50]. All reaction mixtures were prepared in a nitrogen-filled oxygen free drybox ($0_2 < 5$ ppm, $H_2O < 1$ ppm). In a drybox the catalyst was weighed into $40 \times 20$ mm borosilicate culture tube containing 5/16 in 5/8 in. Teflon coated magnetic stir bar then the substrate was transferred into this tube via gastight syringe. The culture tube was then sealed inside of the Fischer-Porter pressure bottle and Fischer-Porter bottle brought outside of the drybox and placed inside a constant temperature circulating water bath. Next the hydrogenation line was evacuated for at least 1 h, to remove any trace oxygen and water present and then the line was refilled with purified hydrogen. The Fischer-Porter bottle was then attached to the hydrogenation line via its TFE-sealed Swagelock Quick-Connects and the bottle was purged 10 times (15 s per purge, with stirring at >600 rpm). A timer was started and the pressure in the F-P bottle was then set a constant $40 \pm 1$ psig of $H_2$. The reaction was monitored on PC via RS-232 module and using Lab View 8.0 program.

The pressure vs time data was processed using Microsoft Office Excel 2003 and Origin 7.0. Reaction rates were calculated from the rate of hydrogen pressure loss as determined by the slope of the linear portion of the $H_2$ uptake curve.

### 2.4.3. Control Experiment: Detection of Mass Transfer Limitation in the Zeolite Framework Stabilized Ruthenium(0) Nanoclusters Catalyzed Hydrogenation of Cyclohexene

To obtain intrinsic kinetic data independent of external diffusion effects eleven experiments in the hydrogenation of 0.5 mL cyclohexene (in 1.5 mL cyclohexane) catalyzed by zeolite framework stabilized ruthenium(0) nanoclusters (100 mg with a ruthenium loading of 0.68 wt %, [Ru] = 3.36 mM) were conducted at $22 \pm 0.1$ °C and $40 \pm 1$ psig initial $H_2$ pressure using different stirring speeds: 0, 120, 240, 360, 480, 600, 720, 840, 960, 1080 and 1200 rpm. It was found that up to 600 rpm MTL regime is effective on the observed rate for the hydrogenation of cyclohexene (MTL regime $\leq 720$ rpm, and non-MTL regime $> 720$rpm).

### 2.4.4. Catalytic Activity of Zeolite Framework Stabilized Ruthenium(0) Nanoclusters in the Hydrogenation of Olefins and Arenes

In a series of experiments the catalytic activity of 100 mg zeolite framework stabilized ruthenium(0) nanoclusters (with a ruthenium content of 1.4 wt %) were tested in the hydrogenation of cyclohexene, toluene, benzene, *o*-xylene, and mesitylene in the cyclohexane (0.5 mL substrate + 2.5 mL of cyclohexane) at $22 \pm 0.1$ °C and $40 \pm 1$ psig initial $H_2$ pressure(at $> 720$ rpm).

### 2.4.5. Control Experiment: Testing the Catalytic Activity of Ruthenium Free Zeolite-Y in the Hydrogenation of Neat Benzene

To investigate the effect of the host material zeolite-Y on the catalytic activity of zeolite framework stabilized ruthenium(0) nanoclusters, the hydrogenation of 2.0 mL benzene (22.4 mmol) was performed in the presence of 500 mg zeolite-Y, (corresponds to maxiumum amount of zeolite-Y that used as a host material in all

the experiments reported for the hydrogenation of arenes and olefins) at $25 \pm 0.1$ °C and $40 \pm 1$ psig initial $H_2$ pressure (at > 720 rpm). The same experiment was also repeated at different temperatures (15, 20, 30, and 35 °C).

## 2.4.6. Catalytic Activity of Zeolite Framework Stabilized Ruthenium(0) Nanoclusters in the Hydrogenation of Neat Benzene Depending on Ruthenium Loading (wt %)

The catalytic activity of zeolite framework stabilized ruthenium(0) nanoclusters with a various ruthenium loading in the range of 0.4-8.4 % wt Ru (0.4, 0.5, 0.61, 0.8, 0.95, 1.4, 1.8, 2.3, 2.7, 3, 3.2, 3.6, 3.95, 4.3, 4.7, 5, 5.4, 6.2, 7.1, 8.4 % wt Ru loadings) were (in all [Ru] = 1.0 mM) tested in the hydrogenation of 1.0 mL benzene (11.2 mmol) at $22 \pm 0.1$ °C (at > 720 rpm).

## 2.4.7. The Catalytic Activity of Zeolite Framework Stabilized Ruthenium(0) Nanoclusters in the Hydrogenation of Neat Benzene Depending on Ruthenium Concentration

In a series of experiments hydrogenation of 1.0 mL benzene (11.2 mmol) was performed in the presence of 2, 4, 6, 8, 10 and 12 mM Ru (22.3, 44.6, 66.9, 89.2, 111.5 and 133.8 mg zeolite framework stabilized ruthenium(0) nanoclusters) at $22 \pm 0.1$ °C, and $40 \pm 1$ psig of initial $H_2$ pressure and > 720 rpm stirring speed.

## 2.4.8. The Catalytic Activity of Zeolite Framework Stabilized Ruthenium(0) Nanoclusters in the Hydrogenation of Neat Benzene Depending on Temperature

To obtain the activation parameters; the activation energy (Ea), enthalpy ($\Delta H^{\#}$), and entropy ($\Delta S^{\#}$), the hydrogenation of neat benzene (0.6 mL, 6.72 mmol)

was performed in the presence of zeolite framework stabilized ruthenium(0) nanoclusters ([Ru] = 11.6 mM) at 15, 20, 25, 30, 35 C, 40 ± 1 psig of initial $H_2$ pressure and > 720 rpm stirring speed.

## 2.4.9. The Catalytic Lifetime of Zeolite Framework Stabilized Ruthenium(0) Nanoclusters in the Hydrogenation of Neat Benzene

In the nitrogen filled drybox, zeolite framework stabilized ruthenium(0) nanoclusters (100 mg, 13.8 μmol Ru) was weighed into a new culture tube containing a new stirring bar then 3.0 mL benzene (33.6 mmol benzene corresponding to a maximum turnover number of 2426 mol benzene/mol Ru) was added via 5.0 mL gas-tight syringe into the culture tube. The experiment was performed in the same way as described in the section of (**2.4.2.**). The reaction was monitored as a function of time via the computer-interfaced pressure transducer of the apparatus and more $H_2$ has been added to the FP bottle (not > 40 psig for each addition) when the pressure inside lowers down to ~ 20 psig as monitored via computer interface.

## 2.4.10. Isolability, Bottlability and Reusability of Zeolite Framework Stabilized Ruthenium(0) Nanoclusters in the Hydrogenation of Neat Benzene

After the first run of the hydrogenation of 0.80 mL benzene (8.96 mmol), catalyzed by zeolite framework stabilized ruthenium(0) nanoclusters (100 mg, 12 μmol Ru) at 22.0 ± 0.1 °C, 40 ± 1 psig of initial $H_2$ pressure and > 720 rpm stirring speed. The experiments were performed in the same way as described in the section of (**2.4.2.**). At the end of the reaction the FP bottle was disconnected from the line, taken into the drybox, opened and the content of the culture tube was transferred into the Schlenk tube, resealed and connected to vacuum line ($10^{-3}$ Torr). After the evaporation of volatiles, the Schlenk tube was transferred into the glove box. After 1

day the solid residue of zeolite framework stabilized ruthenium(0) nanoclusters was weighed and used again in the hydrogenation of 0.80 mL benzene (8.96 mmol). The same procedure was repeated three times after 1 week, 15 days and 1 month. In addition to the hydrogen uptake data, the $^1$H-NMR spectrum of reaction solutions taken at the end of each run showed that the benzene is completely converted to cyclohexane (1.44 ppm).

Results of the NMR experiment clearly showed that there is no detectable unreacted benzene nor partially hydrogenated products. The results were expressed as the percentage of retained initial catalytic activity of zeolite framework stabilized ruthenium(0) nanoclusters in the hydrogenation of neat benzene.

## 2.4.11. P(C$_6$H$_{11}$)$_3$ and P(C$_6$H$_{11}$O$_3$) Poisoning of Zeolite Framework Stabilized Ruthenium(0) Nanoclusters in the Hydrogenation of Neat Benzene

In order to begin the catalyst poisoning experiments a stock solution of P(C$_6$H$_{11}$)$_3$ in benzene was prepared by dissolving 1.49 g in 9.5 mL benzene in drybox. Then, 128 mg zeolite framework stabilized ruthenium(0) nanoclusters (12 μmol Ru) was transferred into a 22 × 175 mm culture tube containing a 5/16 in 5/8 in. Teflon coated magnetic stir bar. To this was added an aliquot (24 – 720 μL) of either 26 μM or 800 μM P(C$_6$H$_{11}$)$_3$ stock solution (in benzene) using a 500 μL gastight syringe and the total volume of solution in the culture tube was adjusted to 1.5 mL by adding benzene (1.48 – 0.78 mL). The culture tube was then placed in the Fischer-Porter bottle, sealed, taken out of the drybox, placed in a constant temperature circulation water bath thermostated at 22 ± 0.1 °C and attached to the hydrogenation apparatus via the quick connects and stirred for a 10 min before the pressure was set to 40 ± 1 psig initial H$_2$ pressure. The same protocol was also followed by using 1.2 μmol – 3.0 μmol P(C$_6$H$_{11}$O$_3$).

## 2.4.12. The Leaching Test of the Zeolite Framework Stabilized Ruthenium(0) Nanoclusters

After the first run of the hydrogenation of 0.80 mL benzene (8.96 mmol), catalyzed by zeolite framework stabilized ruthenium(0) nanoclusters (100 mg, 9.4 µmol Ru) at $22.0 \pm 0.1$ °C, $40 \pm 1$ psig of initial $H_2$ pressure and > 720 rpm stirring speed, the FP bottle was detached from the line, taken into the drybox, opened and the suspension in the culture tube was filtered; the filtrate was transferred into a new culture tube and 0.5 mL benzene was added. The culture tube was placed into the FP bottle. The hydrogenation of benzene was performed in the same way as described in the section of (**2.4.2.**). No hydrogenation of benzene was observed after 8 hours. Additionally, no ruthenium metal was detected in the filtrate by ICP which had a detection limit of 24 ppb for Ru.

# CHAPTER 3

# RESULTS AND DISCUSSIONS

## 3.1. Preparation and Characterization of Zeolite Framework Stabilized Ruthenium(0) Nanoclusters

Zeolite framework stabilized ruthenium(0) nanoclusters were prepared by ion-exchange [77] of $Ru^{3+}$ ions with the extra framework $Na^+$ cations of zeolite-Y (which had previously been slurried with 0.1 M NaCl to remove sodium defect sites, washed until free of chloride and calcined in dry oxygen at 500 °C for 12 h) followed by reduction of the ruthenium(III)-exchanged zeolite-Y with sodium borohydride in the aqueous solution all at room temperature. Following this two step procedure, zeolite-Y is first added to the aqueous solution of ruthenium(III) chloride in the amount depending on the degree of ion exchange and the suspension is stirred for three days at room temperature. After filtering, copious washing with water, and drying in vacuum at room temperature, ruthenium(III)-exchanged zeolite-Y sample was obtained and characterized by XRD, ICP-OES spectroscopy.

As seen from the comparison of XRD patterns for zeolite-Y and ruthenium(III)-exchanged zeolite-Y samples (Figure 15(a), (b) and (c)), there is no noticeable change in both the intensities and positions of the Bragg peaks, indicating that neither the crystallinity nor the lattice of zeolite-Y is essentially altered by ion exchange. Next, the ruthenium(III)-exchanged zeolite-Y was reduced by sodium borohydride in aqueous solution yielding zeolite framework stabilized ruthenium(0) nanoclusters. Figure 15 (d) and (e) also depicts XRD patterns of zeolite framework

stabilized ruthenium(0) nanoclusters in addition to those of zeolite-Y and ruthenium(III)-exchanged zeolite-Y samples. A comparison of the XRD patterns clearly shows that the incorporation of ruthenium(III) ions into zeolite-Y and the reduction of ruthenium(III) ions forming the zeolite framework stabilized ruthenium(0) nanoclusters cause no observable alteration in the framework lattice and no loss in the crystallinity of zeolite-Y.
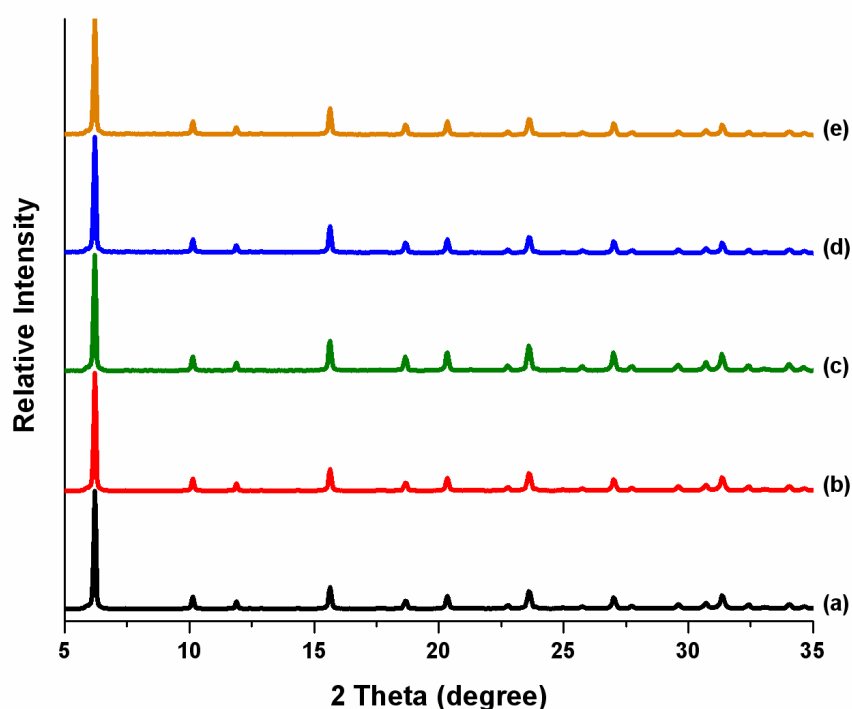


**Figure 15.** The powder XRD patterns of (a) zeolite-Y, (b) ruthenium(III)-exchanged zeolite-Y samples with a ruthenium loading of 0.1 wt % and (c) ruthenium(III)-exchanged zeolite-Y samples with a ruthenium loading of 8.4 wt %, (d) and (e) are zeolite framework stabilized ruthenium(0) nanoclusters prepared by $NaBH_4$ reduction of ruthenium(III)-exchanged zeolite-Y samples with ruthenium loadings of 0.1 and 8.4 % % wt, respectively.

The morphology and composition of zeolite framework stabilized ruthenium(0) nanoclusters were investigated by HRTEM, TEM-EDX, SEM, and ICP-OES analyses. Figure 16 shows the SEM images of zeolite framework stabilized ruthenium(0) nanoclusters with a ruthenium loading of 2.0 wt % .
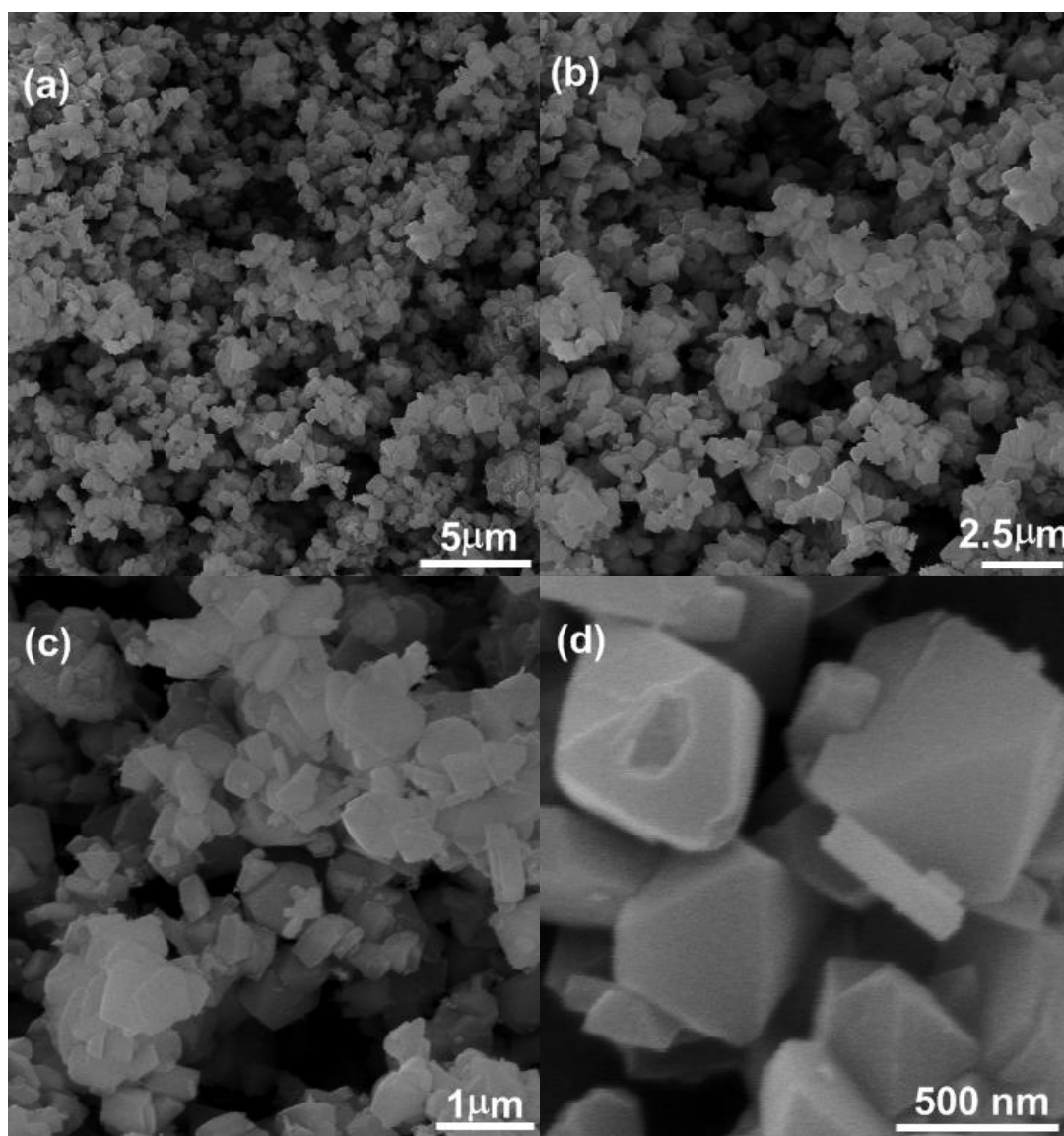


**Figure 16.** Scanning Electron Microscopy (SEM) images of zeolite framework stabilized ruthenium(0) nanoclusters without Pt-Au alloy coating taken in different magnifications.

These SEM images indicate that (*i*) there exist only crystals of zeolite-Y, (*ii*) there is no bulk ruthenium formed in observable size on the surface of the zeolite crystals, (*iii*) the method used for the preparation of zeolite framework stabilized ruthenium(0) nanoclusters doesn't cause any observable defects in the structure of zeolite-Y, a fact which is also supported by XRD results.
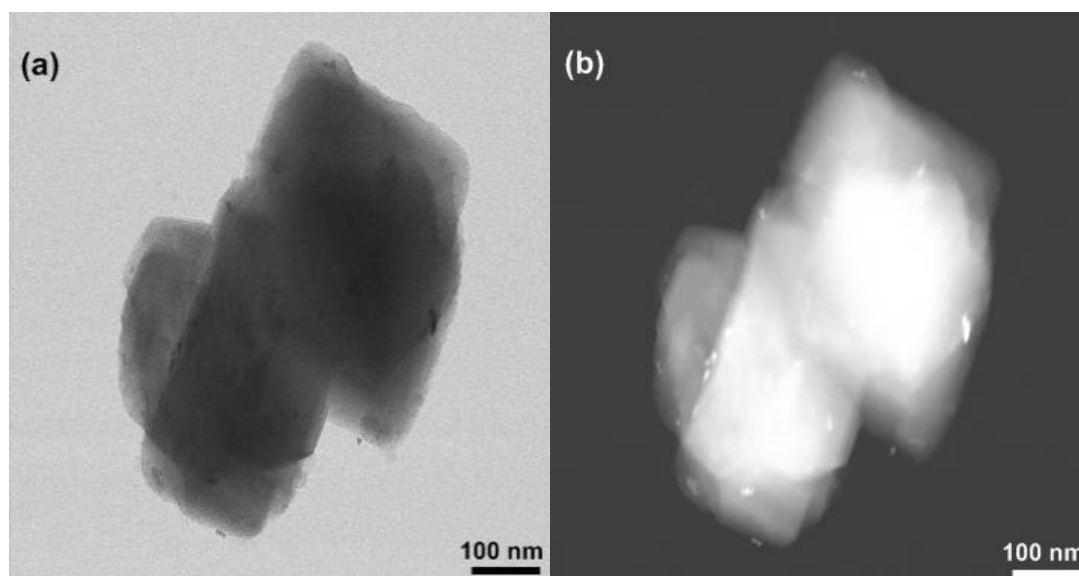


**Figure 17.** (a) TEM image, (b) zero constrast-TEM (ZC-TEM) image of zeolite framework stabilized ruthenium(0) nanoclusters with a 2.0 wt % ruthenium loading.

The TEM analyses of the zeolite framework stabilized ruthenium(0) nanoclusters with a ruthenium content of 2.0 % wt were started by taking low resolution and zero contrast TEM images as given in Figure 17. These images are indicative of the formation of some ruthenium(0) nanoclusters on the surface of zeolite, but it should be noted that these zeolite-supported ruthenium(0) nanoclusters are still stable against agglomeration as their size is less than 20 nm. The TEM image taken with higher resolution (Figure 18) shows that the distribution of ruthenium(0) nanoclusters within the framework of zeolite-Y and support that there is no bulk

ruthenium or sintered nanocluster were formed on the surface of the zeolite, which is also evidenced by SEM and low resolution TEM analyses (*vide supra*).
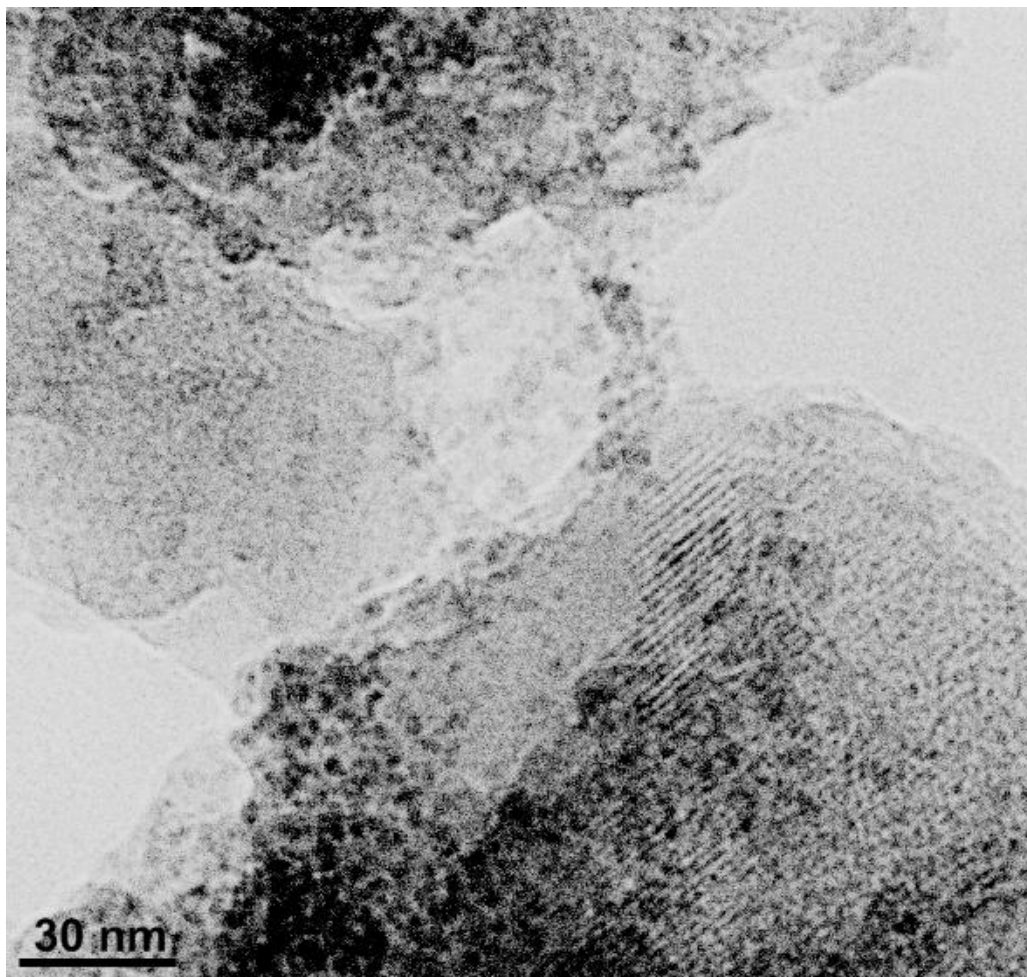


**Figure 18.** TEM image of zeolite framework stabilized ruthenium(0) nanoclusters with a 2.0 wt % ruthenium loading.

The mean particle size of ruthenium(0) nanoclusters was found to be $2.8 \pm 0.7$ nm as measured from the TEM image given in Figure 18 by using an NIH (National Institute of Health) image program [79] whereby 100 nontouching particles were counted (Figure 19).
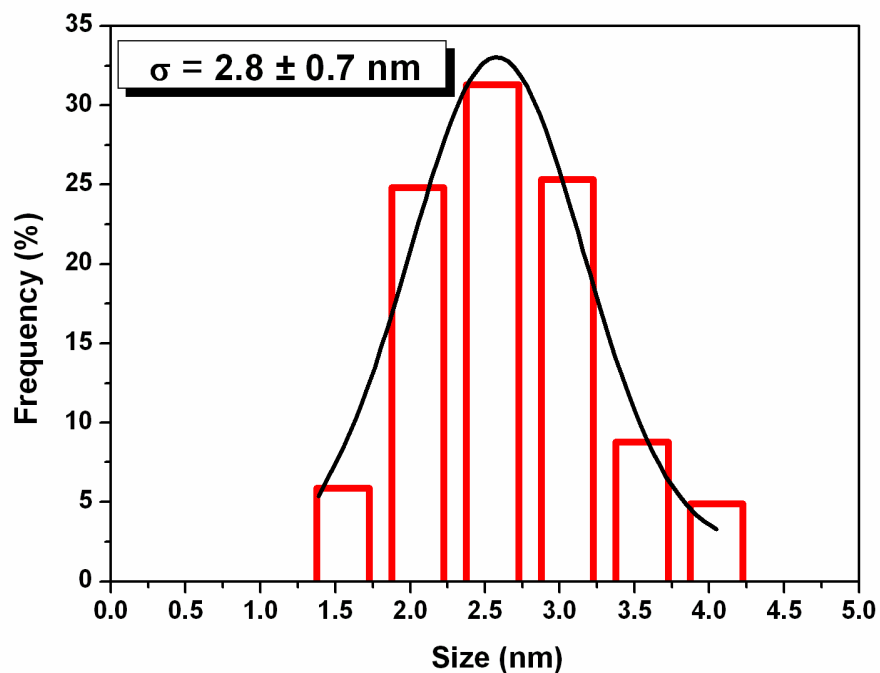
**Figure 19.** The particle size histogram of zeolite framework stabilized ruthenium(0) nanoclusters (including both zeolite surface supported and zeolite confined) constructed by counting 100 nontouching particles.

Indeed, the high resolution TEM (HRTEM) image of the same sample in Figure 20(a) shows the uniform distribution of ruthenium within the highly ordered cavities of zeolite-Y. For comparison, HR-TEM image of the plain zeolite-Y is given in Figure 20(b) ands shows that the cavities are empty.
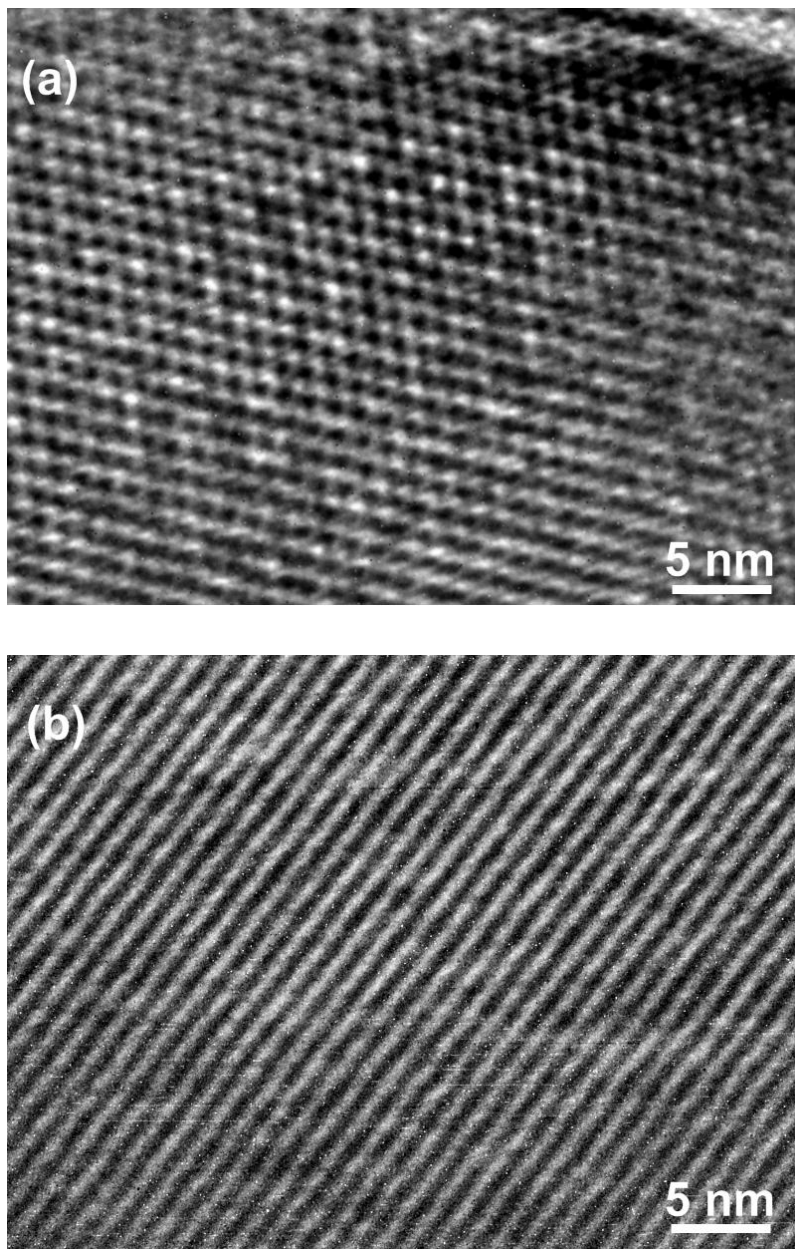
**Figure 20.** (a) High resolution TEM (HRTEM) image of the zeolite framework stabilized ruthenium(0) nanoclusters with a ruthenium contents of 2.0 wt % , (b) HRTEM image of the plain zeolite-Y.

TEM/EDX spectrum (Figure 21) taken during the TEM observation from many different areas of zeolite framework stabilized ruthenium(0) nanoclusters confirms that ruthenium is the only element detected, in addition to the zeolite framework elements (Si, Al, O, Na) and Cu from the grid.
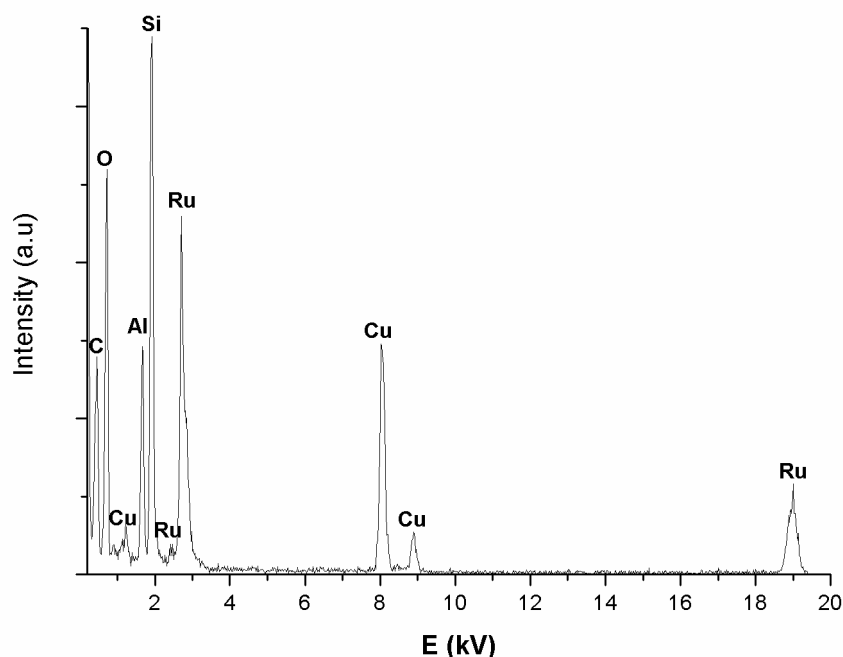


**Figure 21**. TEM/EDX spectrum of the intrazeolite ruthenium(0) nanoclusters with a ruthenium content of 2.0 wt %.

The oxidation state of ruthenium and surface composition of the zeolite framework stabilized ruthenium(0) nanoclusters were analyzed by X-ray photoelectron spectroscopy. The survey scan XPS spectrum of the sample prepared by the reduction of ruthenium(III)-exchanged zeolite-Y with a ruthenium content of 1.1 % wt, given in Figure 22 shows the presence of ruthenium in addition to the

zeolite framework elements (O, Si, Al, Na, C) as observed by TEM/EDX spectrum (*vide supra*).
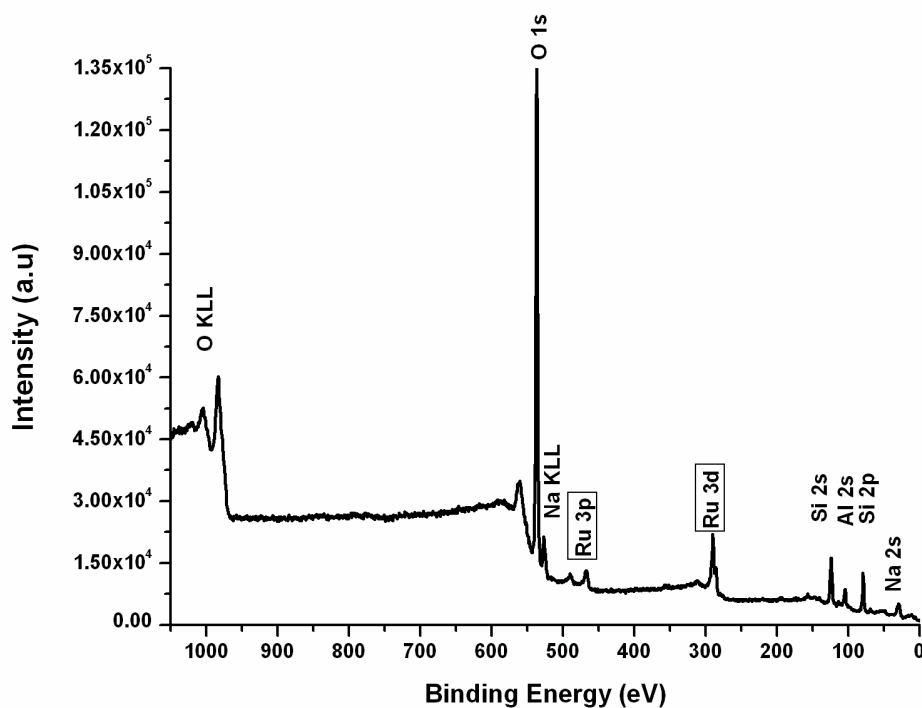


**Figure 22.** XPS survey spectrum of the zeolite framework stabilized ruthenium (0) nanoclusters with a ruthenium content of 2.0 wt %.

The high resolution Ru 3d and 3p XPS spectra of the intrazeolite ruthenium(0) nanoclusters given in Figure 23 (a) and (b), respectively gives two prominent peaks at 281.6 and 462.2 eV, readily assigned to Ru(0) $3d_{5/2}$, and Ru(0) $3p_{3/2}$, respectively [80]. The binding energies of intrazeolite ruthenium(0) nanoclusters are shifted by 2.1 and 1.2 eV, respectively, toward higher values, which might be attributed to both the quantum size effect [4] and peculiar electronic properties of the zeolite matrix [81].

49
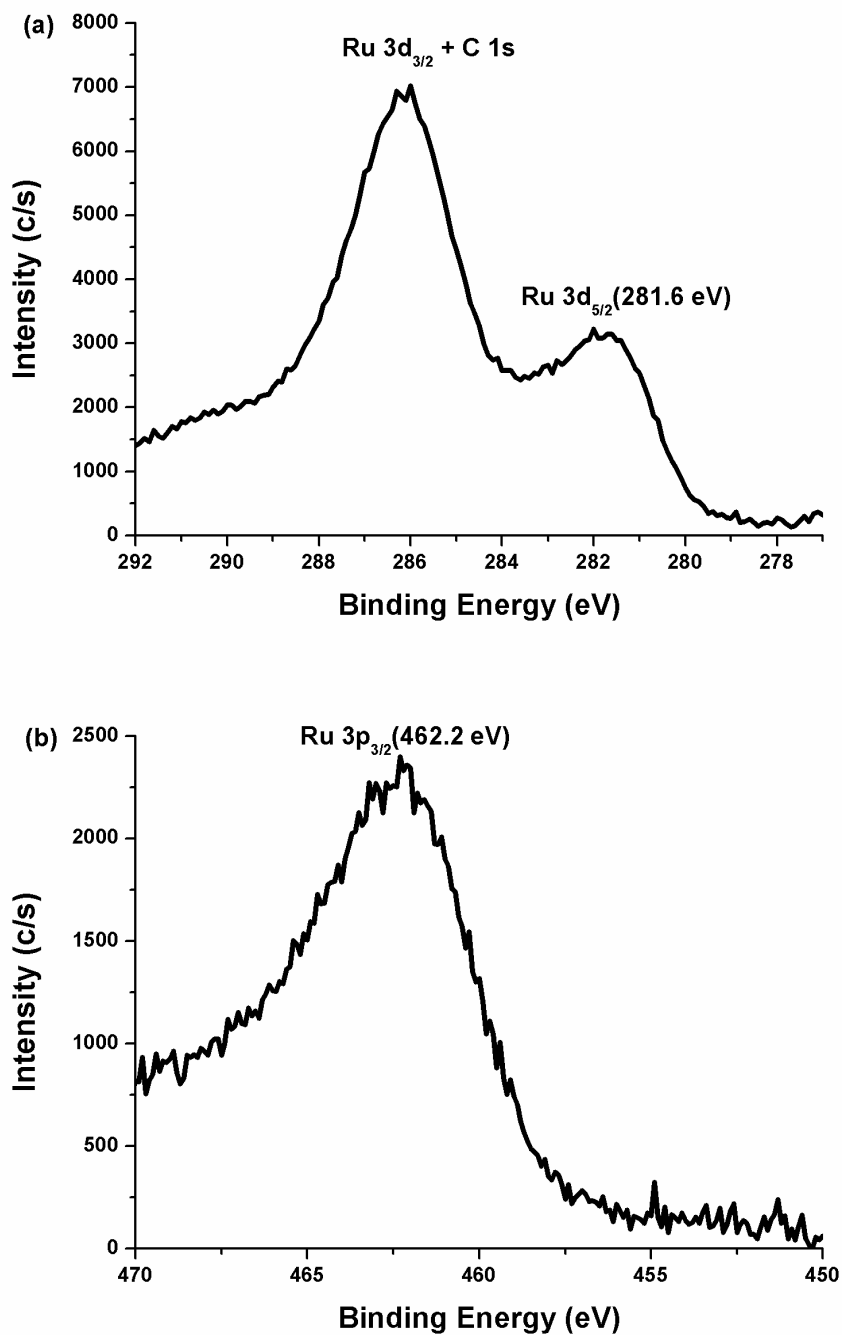
**Figure 23.** The high resolution (a) Ru 3d XPS spectrum and (b) Ru 3p XPS spectrum of the zeolite framework stabilized ruthenium(0) nanoclusters.

The interaction of ruthenium(0) nanoclusters with the framework oxygen of the zeolite cages is expected to induce a positive charge on the surface metal, which would increase the binding energies of ruthenium(0) nanoclusters. A similar effect has also been observed for the zeolite-encapsulated cobalt [82] and platinum [83] nanoparticles. In addition to the matrix effect, the high energy shift in the ruthenium binding energy might be due to the fact that electrons in the core level are strongly restricted by the atomic nucleus, as observed in the case of palladium(0) nanoclusters in zeolite-Y [84]. The interaction between the ruthenium(0) nanoclusters and the zeolite framework induces a positive charge on the surface ruthenium atoms; thus, increasing their Lewis acidity would also enhance the catalytic activity of the ruthenium(0) nanoclusters in reactions of Lewis base substrates, such as water and borohydride ion.

Although oxidation of ruthenium(0) nanoclusters during the XPS sampling procedure is a well known fact, the possibility of the existence of $RuO_2$ need to be tested by using other analytical techniques. For this purpose we analyzed zeolite framework stabilized ruthenium(0) nanoclusters by Raman spectroscopy, which is strong tool to test the existence of $RuO_2$. It was observed that the characteristics Raman peaks of $RuO_2$ [85] in the range of 400-1200 $cm^{-1}$ were missing in the Raman spectrum of zeolite framework stabilized ruthenium(0) nanoclusters (Figure 24).
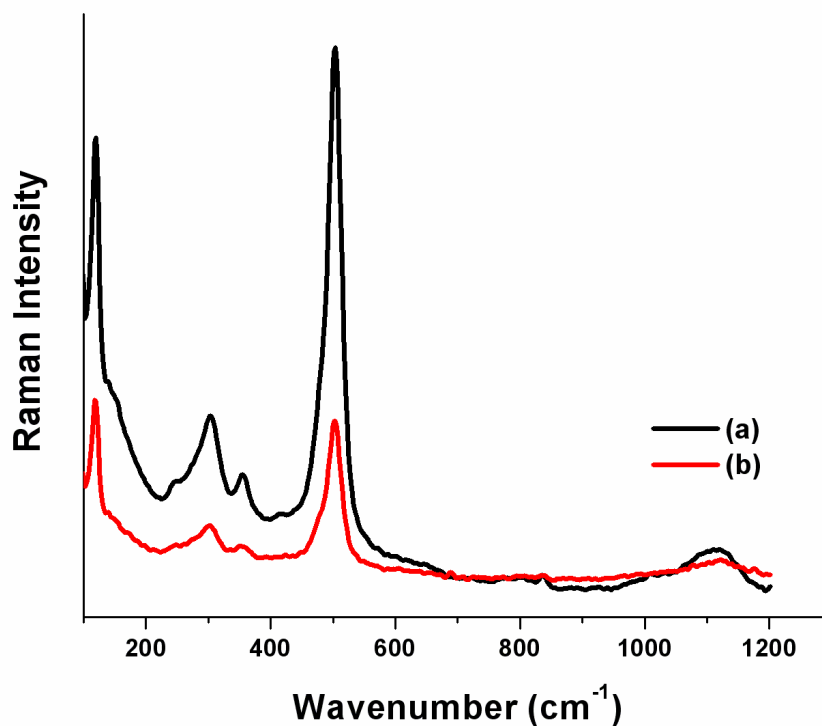
**Figure 24**. Raman spectrum of (a) zeolite-Y, (b) zeolite framework stabilized ruthenium(0) nanoclusters with a ruthenium content of 2.0 wt %.

The reduction of ruthenium(III)-exchanged zeolite-Y to zeolite framework stabilized ruthenium(0) nanoclusters was also monitored by using diffuse reflectance UV-vis spectrosocopy (Figure 25). Ruthenium(III)-exchanged zeolite-Y sample shows a band at near 320 nm attributed to d-d transition [86, 87] and it completely disappears when they are reduced with sodium borohydride. The resultant zeolite framework stabilized ruthenium(0) nanoclusters exhibits continuous absorption characteristic for ruthenium(0) nanoclusters because of the surface plasmon resonance, with a steep rise in absorbance at short wavelengths [86, 88].
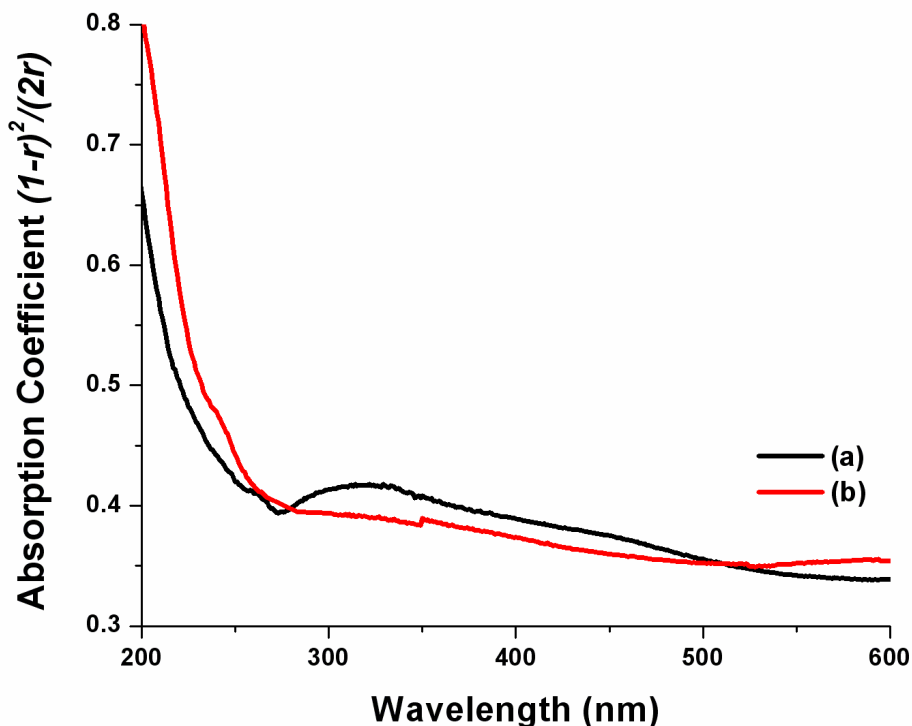
**Figure 25.** Diffuse reflectance UV-vis spectrum of (a) ruthenium(III)-exchanged zeolite-Y (b) zeolite framework stabilized ruthenium(0) nanoclusters with a ruthenium content of 2.0 wt %.

Nitrogen adsorption-desorption isotherms of zeolite-Y and zeolite framework stabilized ruthenium(0) nanoclusters are given in Figure 26 and both of them show type I shape, a characteristic of microporous materials [89]. The micropore volume and area were determined for zeolite-Y and zeolite framework stabilized ruthenium(0) nanoclusters by the *t*-plot method [90]. On passing from zeolite-Y to zeolite framework stabilized ruthenium(0) nanoclusters, both the micropore volume (from 0.333 to 0.142 cm$^3$/g) and the micropore area (from 753 to 320 m$^2$/g) are noticeably reduced. The remarkable decrease in the micropore volume and micropore area can be attributed to the encapsulation of ruthenium(0) nanoclusters in the cavities of zeolite-Y.
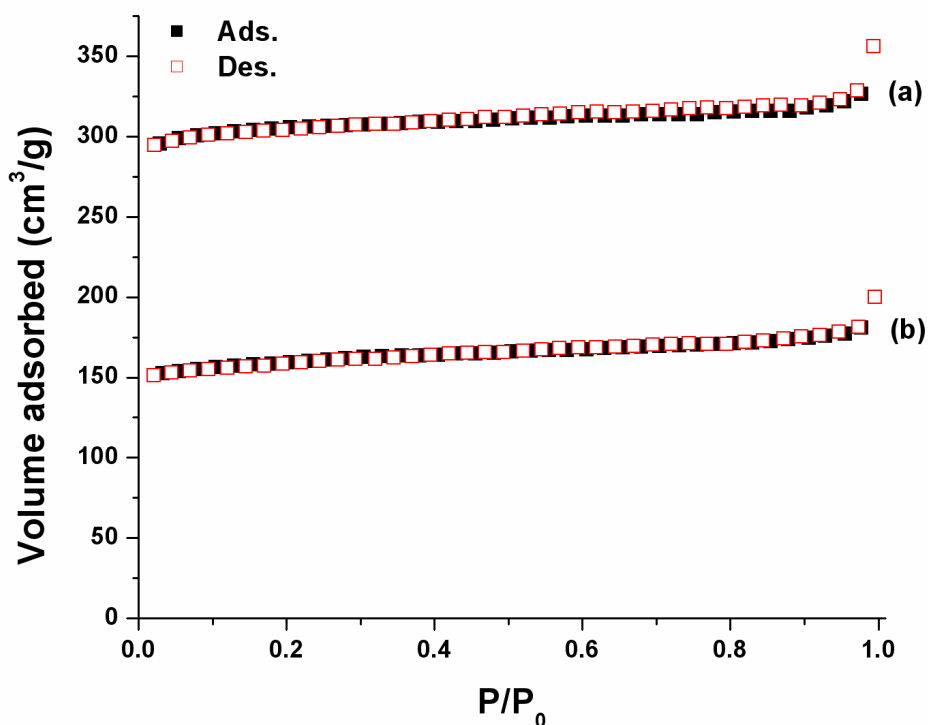
**Figure 26.** Nitrogen adsorption-desorption isotherms of (a) zeolite-Y and (b) zeolite framework stabilized ruthenium(0) nanoclusters with a ruthenium content of 2.0 wt %.

Furthermore, no hysteresis loop was observed in the $N_2$ adsorption-desorption isotherm of zeolite framework stabilized ruthenium(0) nanoclusters, indicating that the two- step procedure followed in the preparation of zeolite framework stabilized ruthenium(0) nanoclusters does not create any mesopores. However, the zeolite framework stabilized ruthenium(0) nanoclusters isolated from the hydrolysis of sodium borohydride in basic solutions show different behavior in $N_2$ adsorption-desorption. The nitrogen adsorption-desorption isotherms of zeolite framework stabilized ruthenium(0) nanoclusters samples isolated from the hydrolysis of sodium borohydride in basic solutions containing different weight percentage of NaOH (wt % NaOH = 2.5, 5.0, 7.5, 10) are given in Figures 27. The observation of hysteresis loops indicates that mesopores are generated in these samples.
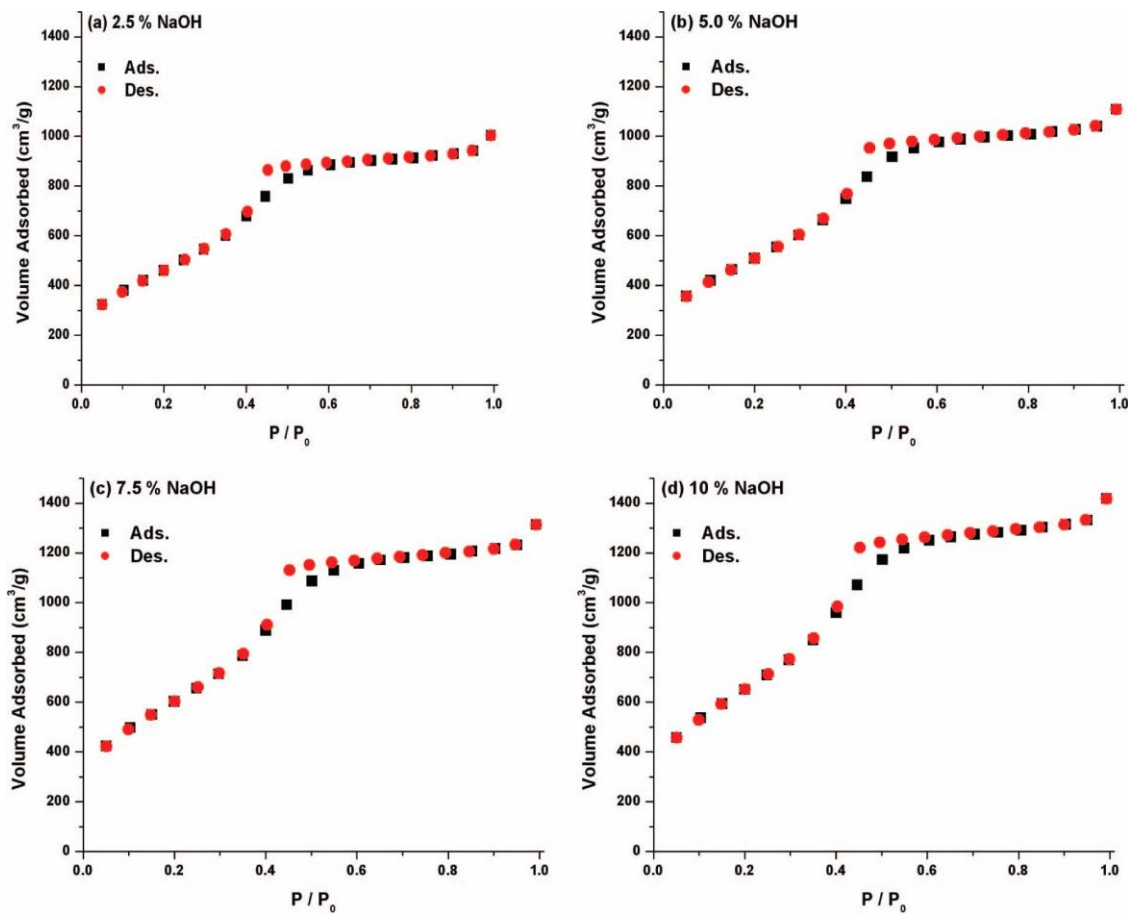
**Figure 27.** The nitrogen adsorption-desorption isotherms of zeolite framework stabilized ruthenium(0) nanoclusters with a ruthenium content of 2.0 wt %, isolated at the end of hydrolysis of sodium borohydride in (a) 2.5 wt % , (b) 5 wt % , (c) 7.5 wt %, and (d) 10 wt  % NaOH solutions.

Figure 28 shows the pore size distributions for these samples evaluated by the BJH method [91] in the mesoporous region; one observes an increase in the mean size of mesopores with the increasing concentration of sodium hydroxide initially used in the hydrolysis of sodium borohydride (*vide infra*).
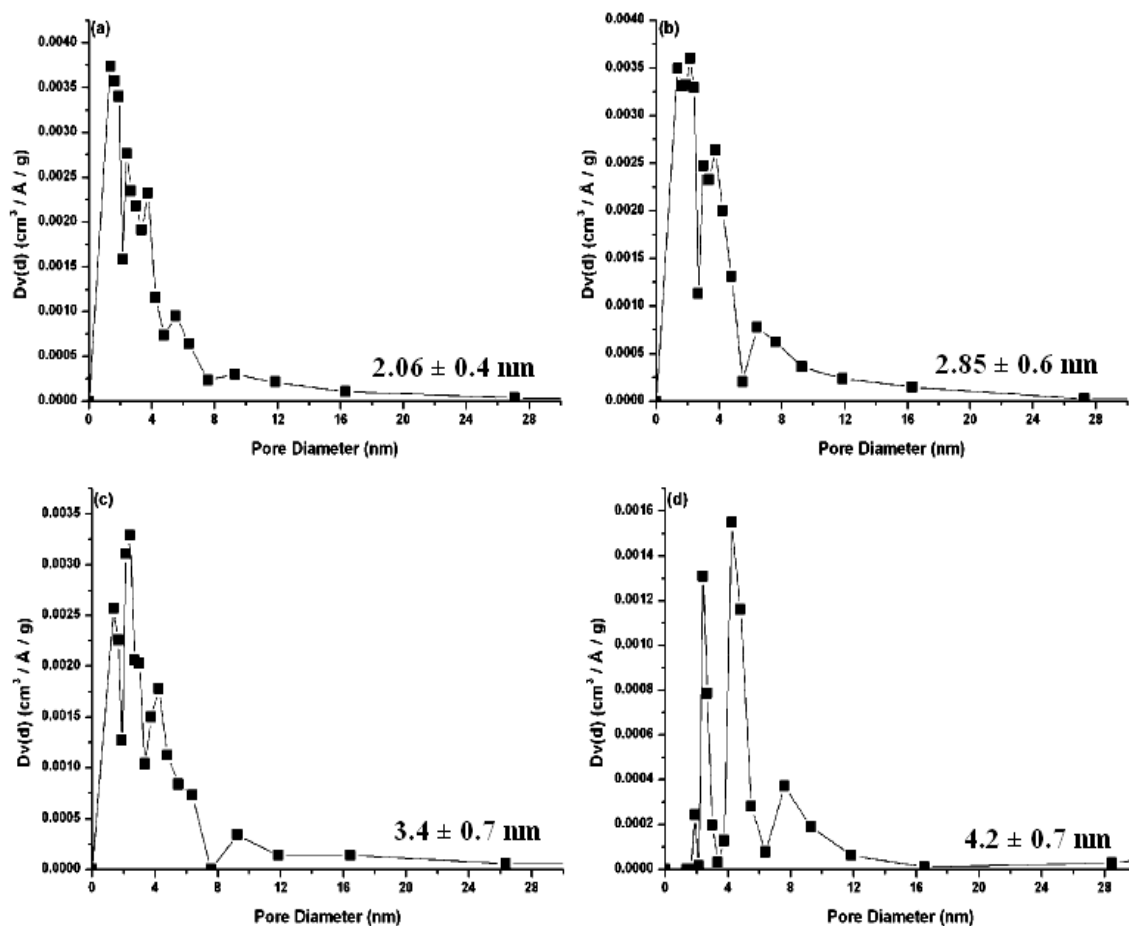
**Figure 28.** Pore size distributions and average pore diameters evaluated by the BJH method in the mesoporous region for the zeolite framework stabilized ruthenium(0) nanoclusters isolated at the end of hydrolysis of sodium borohydride in (a) 2.5 wt % , (b) 5 wt % , (c) 7.5 wt %, and (d) 10 wt % NaOH solutions.

The formation of mesopores was also observed in previous studies when NaX or NaY zeolite was treated with NaOH [92]. Although the dealuminization of the zeolite might cause mesopores, the removal of a small part of the silicon atoms in the framework by the attack of hydroxyl ions should mainly be responsible for the formation of mesopores with sizes even larger than 2 nm [92].

In the characterization of zeolite confined metal(0) nanoclusters, far-IR spectroscopy is a direct probe for location of cation sites in zeolite via their characteristic vibrational modes [93]. The combined use of the frequencies and intensities of site specific metal cation absorption bands in the far-IR spectrum allows us to secure metal cation vibrational assignments for sites I, II, III and I' in zeolite-Y as shown in Figure 29 (inset) [94]. Figure 29 shows the far-IR spectrum (300-25 cm$^{-1}$) of vacuum thermally dehydrated zeolite-Y with band assignments to cation sites [93, 94].
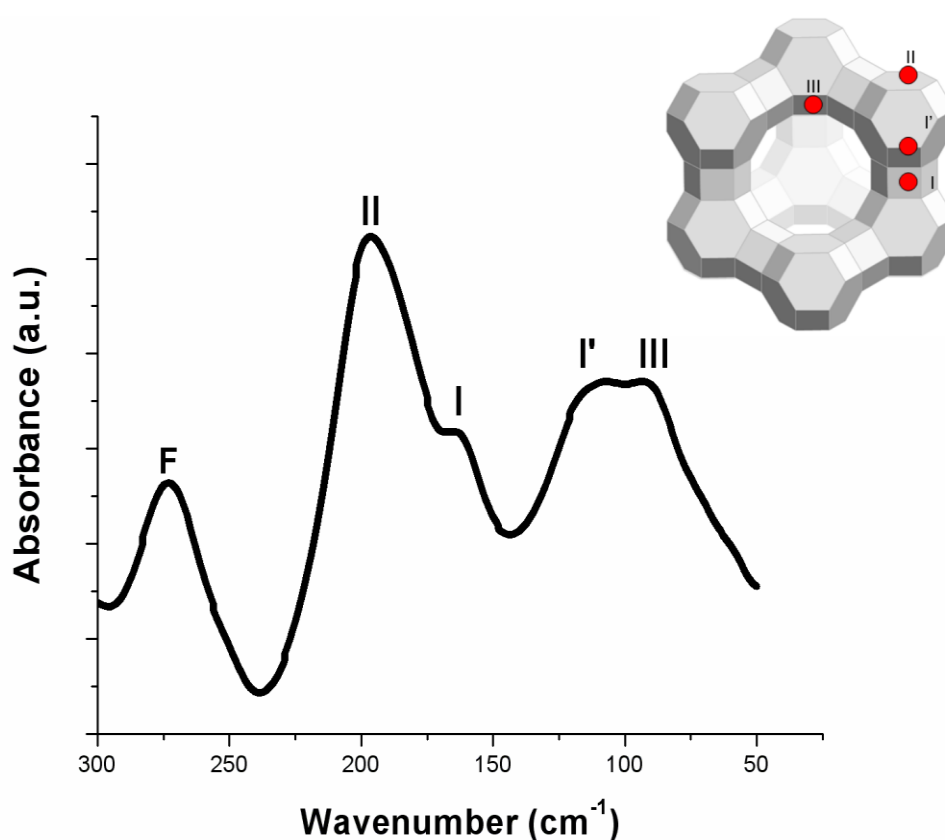


**Figure 29.** Far-IR spectrum (325- 25 cm$^{-1}$) of vacuum thermally dehydrated (10$^{-7}$ Torr, 550 °C) zeolite-Y (F denotes an oxygen framework vibration) and the framework of zeolite-Y with cation positions.

This assignment of the extra-framework cation sites in zeolite-Y has also been confirmed by $^{23}$Na-NMR spectroscopy [95]. It has been shown that there are normal modes of the charge balancing cations which can be considered to be essentially decoupled from the lattice vibrations [93]. Each cation site has a vibrational mode with characteristic frequency in the far-IR region as shown in Figure 29. The frequencies of cation translatory vibrational modes depend on the mass and charge of the cation [93]. Since $Ru^{3+}$ is trivalent and also heavier than $Na^+$ its modes are expected to be at lower frequencies than those of $Na^+$. The far-IR spectrum of ruthenium(III)-exchanged zeolite-Y with a nominal composition of $Ru_{3.2}Na_{46.4}Y$ is given in Figure 30.
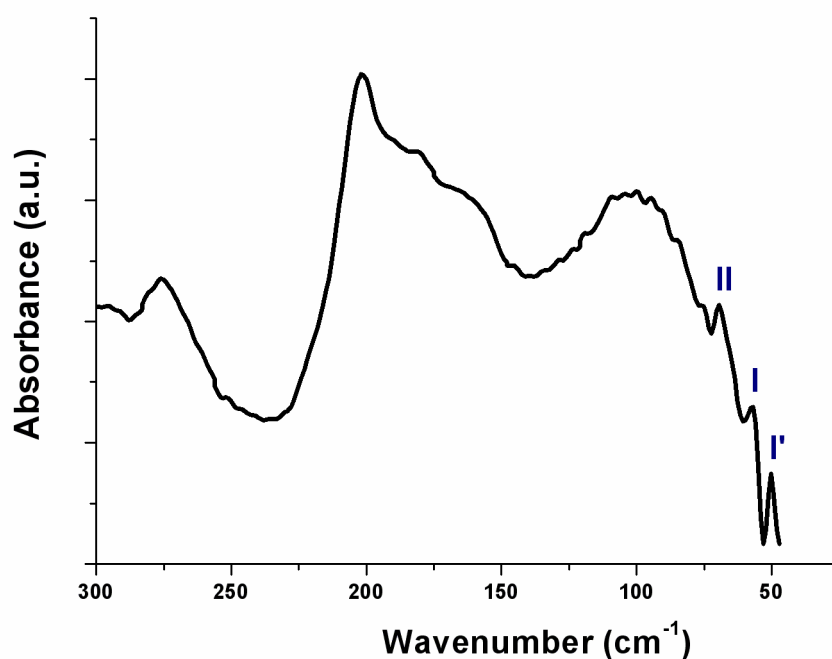


**Figure 30.** The far-IR spectrum of vacuum thermally dehydrated ($10^{-7}$ Torr, 550 °C) sample of ruthenium(III)-exchanged zeolite-Y with a nominal composition of $Ru_{3.2}Na_{46.4}Y$.

58

On passing from zeolite-Y ($Na_{56}Y$) to $Ru_{3.2}Na_{46.4}Y$ the site I, I', and II $Na^+$ cation bands in the far-IR spectra lose intensity while three lower frequency bands grow in at 79, 67 and 57 $cm^{-1}$, which are readily assigned to the $Ru^{3+}$ cation translatory modes. Comparison of the vibrational spectra of the other zeolite-Y samples with different cations [93, 94, 95] shows that the frequency order II > I > I' of cation site absorptions caused by one cation type in different sites is retained. These results reflect the occupancy of cation sites in both α and β cages by ruthenium(III) ions and the three major sites occupied are probably II, I and I'. The far-IR spectrum of zeolite framework stabilized ruthenium(0) nanoclusters prepared by the sodium borohydride reduction of ruthenium(III)-exchanged zeolite-Y sample ($Ru_{3.2}Na_{46.4}Y$) shows that the sodium cation distribution in the zeolite is essentially restored upon reduction (Figure 31).
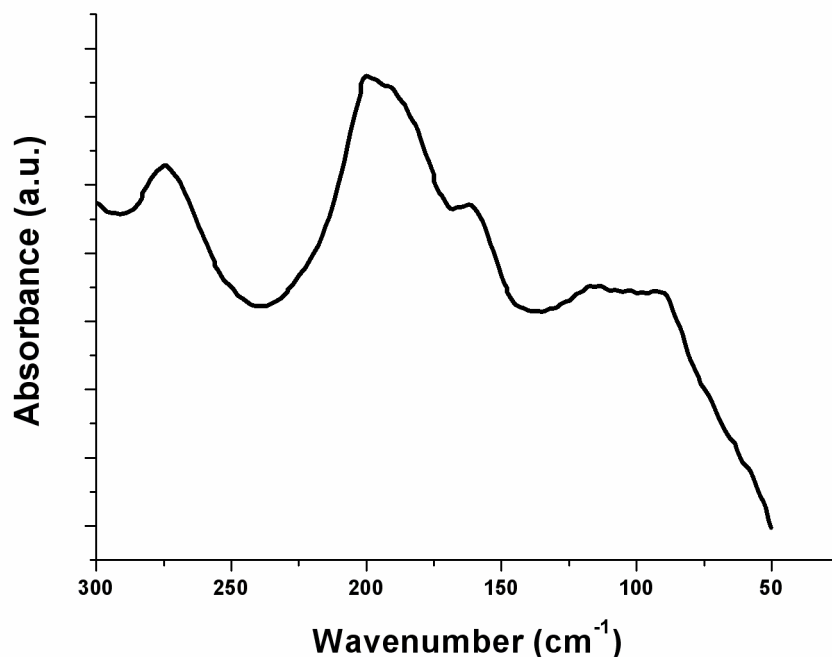


**Figure 31.** The far-IR spectrum of vacuum thermally dehydrated ($10^{-7}$ Torr, 550 °C) sample of zeolite framework stabilized ruthenium(0) nanoclusters with a nominal composition of $Ru(0)/Na_{55.4}Y$.

The cation sites left by Ru$^{3+}$ ions upon reduction are reoccupied by sodium cations coming from sodium borohydride. Hence, host framework remains intact as shown also by XRD powder pattern (*vide supra*). However, the absorption bands of sodium translatory modes experience small red shift caused by the interaction with the ruthenium(0) nanoclusters in the cages of zeolite-Y. Hence, the small red shift observed in the site specific bands of sodium cation vibrational mode can be considered as evidence for the existence of ruthenium(0) nanoclusters within the cages of sodium reloaded zeolite-Y after reduction (*see* Figues 70-74 in the Appendix for the far-IR analyses of ruthenium(III)-exchanged zeolite-Y and zeolite framework stabilized ruthenium(0) nanoclusters for the samples with higher ruthenium(0) loadings and their powder X-ray diffractions).

## 3.2. The Catalytic Activity of In-Situ Formed Zeolite Framework Stabilized Ruthenium(0) Nanoclusters in the Hydrolysis of Sodium Borohydride in the Aqueous Medium

### 3.2.1. The Catalytic Activity of Ruthenium Free Zeolite-Y in the Hydrolysis of Sodium Borohydride

In determining the catalytic activity of zeolite framework stabilized ruthenium(0) nanoclusters accurately, one has to check whether zeolite-Y catalyzes the hydrolysis of sodium borohydride. The hydrolysis of sodium borohydride in the presence of zeolite-Y was performed at various temperatures (20, 25, 30, 35, 40 and 45 °C). The results were given in Figure 32 and it was found that the hydrogen generation from the hydrolysis of sodium borohydride in the presence of zeolite-Y increases with the increasing temperature in the range of 0.6-4.2 mL of H$_2$/min for 20 and 45 °C, respectively.
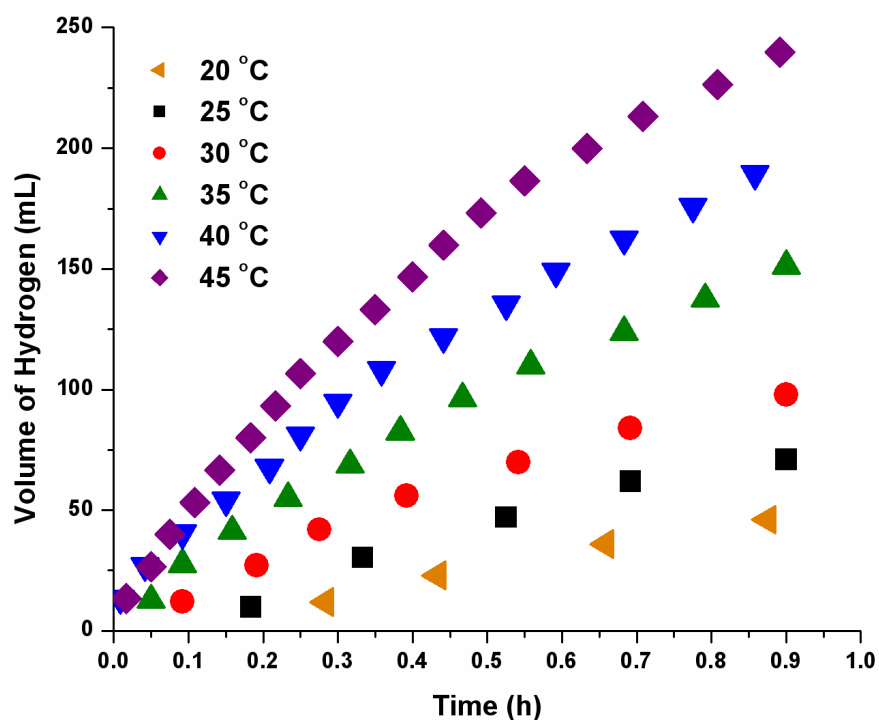
**Figure 32.** The volume of hydrogen (mL) vs time (h) graph for the ruthenium free zeolite-Y (474 mg) catalyzed hydrolysis of $NaBH_4$ (284 mg, 150 mM in 50 mL) at different temperatures.

Although the hydrolysis of sodium borohydride in the presence of zeolite-Y is slow, all of the catalytic activity results of intrazeolite ruthenium(0) nanoclusters in the hydrolysis of sodium borohydride given here were corrected by subtracting the hydrogen gas generated from the hydrolysis of sodium borohydride in the presence of zeolite-Y under otherwise identical conditions.

**3.2.2. The Effect of Ruthenium Loading on the Catalytic Activity of Zeolite Framework Stabilized Ruthenium(0) Nanoclusters in the Hydrolysis of Sodium Borohydride**

In a series of experiments, the catalytic activity of zeolite framework stabilized ruthenium(0) nanoclusters with a ruthenium loading in the range of 0.10-8.4 wt % Ru (in all [Ru] = 1.0 mM) was tested in the hydrolysis of sodium borohydride to determine the effect of ruthenium loading on the catalytic activity of zeolite framework stabilized ruthenium(0) nanoclusters. Figure 33 shows the variation in the catalytic activity of zeolite framework stabilized ruthenium(0) nanoclusters with ruthenium loading of the zeolite.
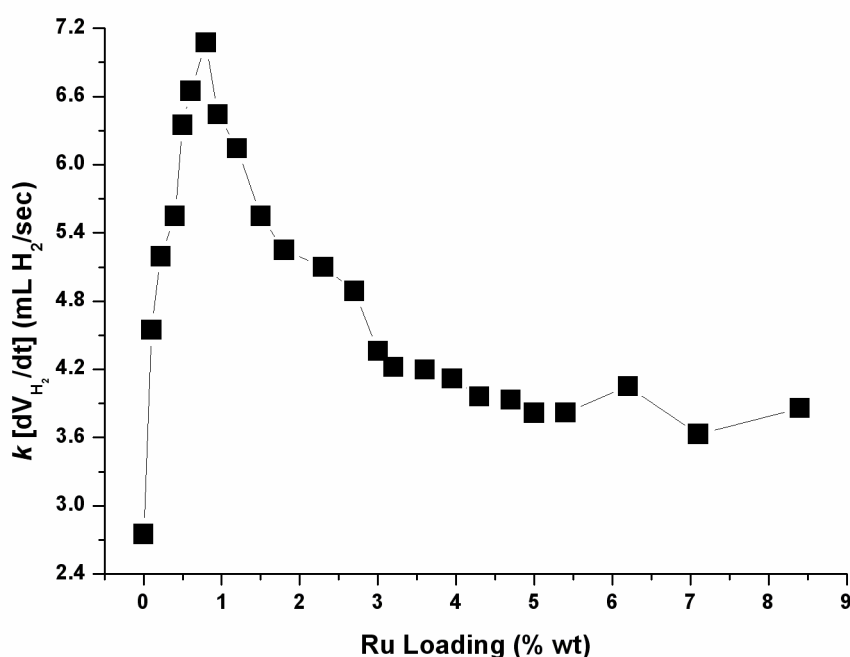


**Figure 33.** The rate of hydrogen generation (mL of $H_2$/s) versus ruthenium loadings (% wt Ru) for the zeolite framework stabilized ruthenium(0) nanoclusters (in all [Ru] =1 mM) catalyzed hydrolysis of $NaBH_4$ (284 mg, 150mM in 50 mL) at $25 \pm 0.1$ °C.

62

The variation in catalytic activity reflects the accessibility of ruthenium(0) nanoclusters in the zeolite cages by the substrate. The highest catalytic activity is obtained by using the zeolite framework stabilized ruthenium(0) nanoclusters containing 0.80 % wt Ru, most probably in this loading the majority of ruthenium(0) nanoclusters present in the supercage (α-cage), where the substrate can more readily access compared to the sodalite cage (β-cage) of zeolite-Y (Figure 34). As the ruthenium loading increases, the nanoclusters might go to the less accessible sodalite cages as well, or nanoclusters in the supercages become larger, blocking the entrance to the supercages.
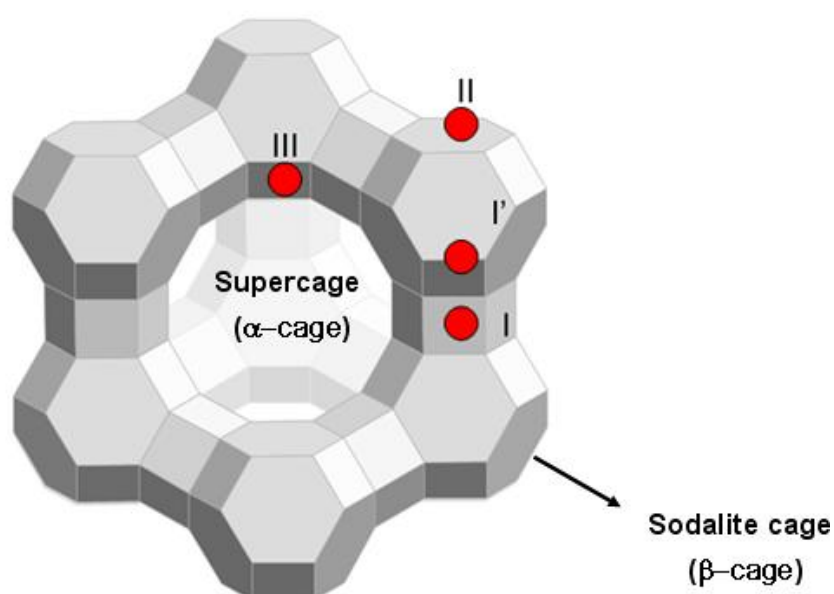


**Figure 34.** The schematic view of the zeolite-Y (FAU) framework and cation locations.

### 3.2.3. Kinetic Studies and the Determination of Activation Parameters for the Hydrolysis of Sodium Borohydride Catalyzed by Zeolite Framework Stabilized Ruthenium(0) Nanoclusters

Zeolite framework stabilized ruthenium(0) nanoclusters (with a ruthenium content of ≈ 0.8 wt %) were used as catalyst in the hydrolysis of sodium borohydride liberating hydrogen gas. Figure 35 shows the plots of hydrogen volume generated versus time during the catalytic hydrolysis of sodium borohydride solution in the presence of zeolite framework stabilized ruthenium(0) nanoclusters in different concentrations at $25 \pm 0.1$ °C. A fast hydrogen evolution starts immediately without induction period, indicating a rapid formation of the catalyst.
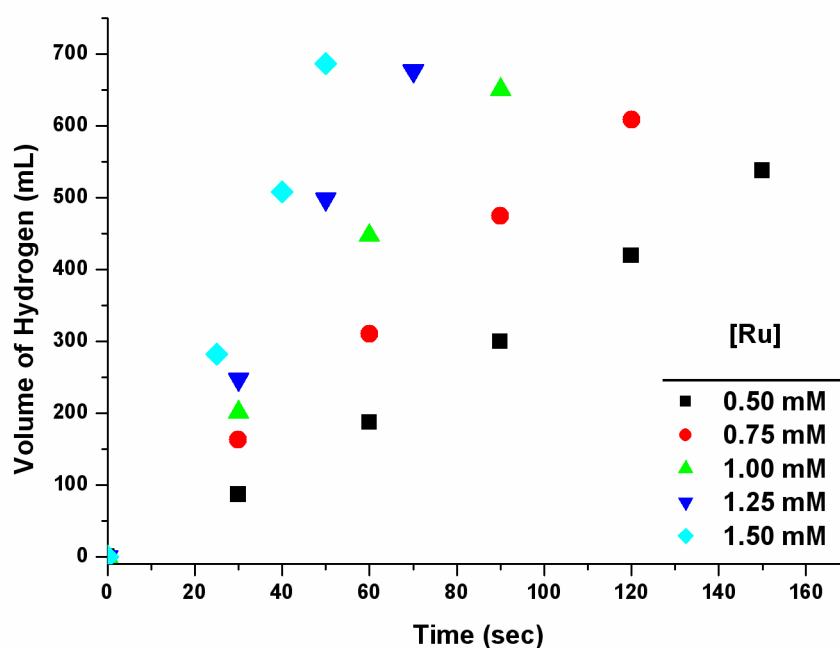


**Figure 35.** Plot of the volume of hydrogen (mL) versus time (s) for the hydrolysis of $NaBH_4$ (284 mg, 150mM in 50 mL) catalyzed by zeolite framework stabilized ruthenium(0) nanoclusters (≈ 0.8 wt % Ru loading) with different ruthenium concentrations ([Ru] = 0.50, 0.75, 1.0, 1.25, 1.50 mM) at $25.0 \pm 0.1$ °C.

The rate of hydrogen evolution is in the range of 215-823 mL of $H_2$/min, even at low catalyst concentrations (0.50-1.50 mM Ru) and room temperature. The rapid hydrolysis of sodium borohydride catalyzed by zeolite framework stabilized ruthenium(0) nanoclusters requires fast penetration of substrate into the zeolite framework as well as a potent contact of the borohydride anion and the metal atoms on the surface of ruthenium(0) nanoclusters within the cavities of zeolite. Plotting the hydrogen generation rate, determined from the linear portion of the plots in Figure 35, versus ruthenium concentration, both in logarithmic scales (Figure 36), gives a straight line with a slope of 1.04 ≈ 1.0, indicating that the hydrolysis is first-order with respect to the catalyst concentration.
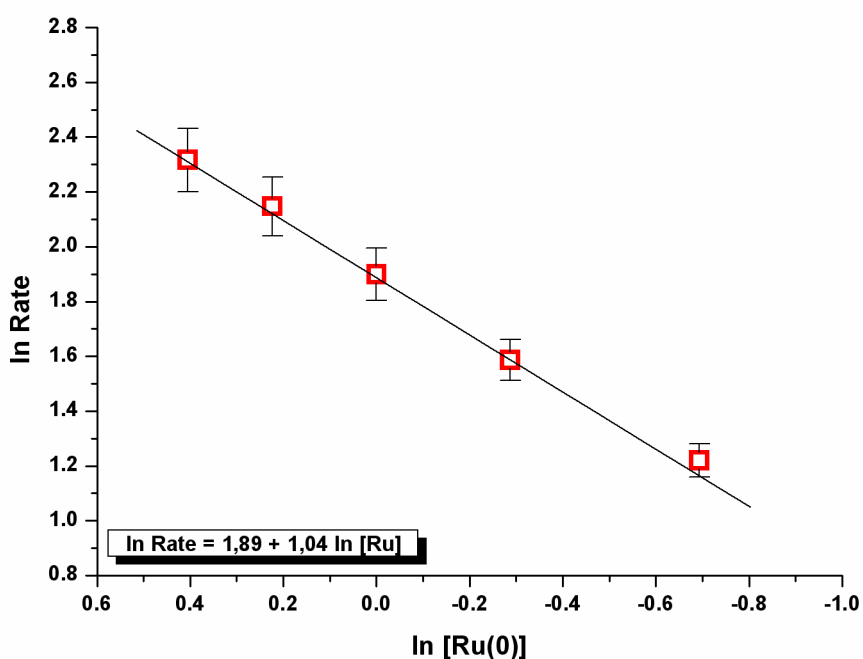


**Figure 36.** Plot of the hydrogen-generation rate versus the catalyst concentration (both in logarithmic scale) in the hydrolysis of $NaBH_4$ catalyzed by zeolite framework stabilized ruthenium (0) nanoclusters at $25.0 \pm 0.1$ °C.

The effect of substrate concentration on the hydrogen generation rate was also studied by performing a series of experiments starting with varying initial concentration of sodium borohydride while the ruthenium concentration is kept constant at 0.50 mM. Figure 37 shows the plot of hydrogen volume generated versus time for various initial concentration of sodium borohydride ([NaBH$_4$] = 0.075, 0.15, 0.30, 0.45, 0.60, 1.20, 2.40, 4.80 M).
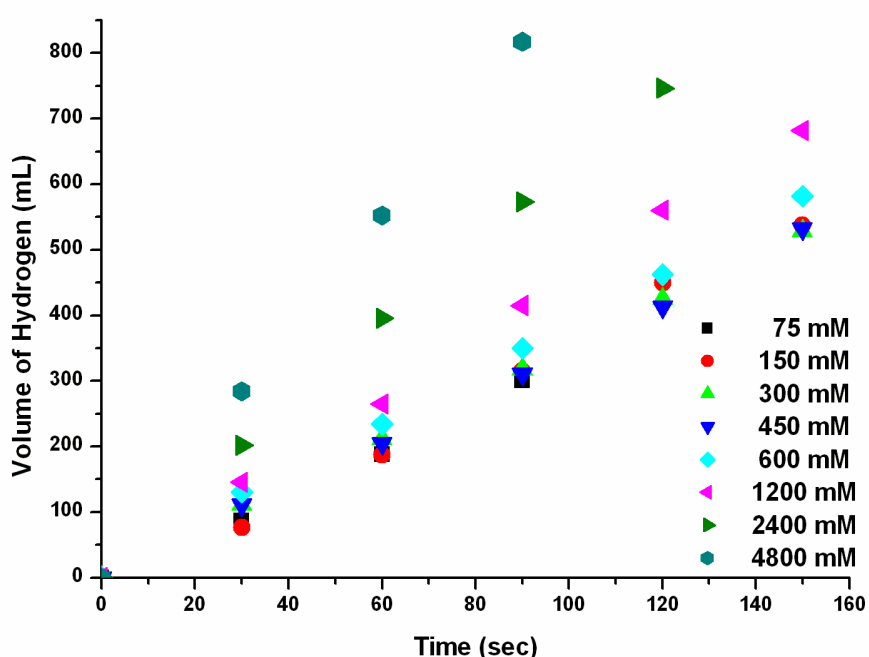


**Figure 37.** Plot of the volume of hydrogen (mL) versus time (s) for the zeolite framework stabilized ruthenium(0) nanoclusters (with a ruthenium content of ≈ 0.8% wt, [Ru] = 0.50 mM) catalyzed hydrolysis of NaBH$_4$ solution (50 mL) in different concentrations ([NaBH$_4$] = 75, 150, 300, 450, 600, 1200, 2400, 4800 mM ) at 25.0 ± 0.1 °C.

Plotting the hydrogen generation rate, determined from the linear portion of the plots in Figure 37, versus ruthenium concentration, both in logarithmic scales (Figure 38), shows that the catalytic hydrolysis of sodium borohydride proceeds

zero-order with respect to substrate concentration in dilute solutions, with an initial concentration of sodium borohydride up to 0.6 M. However, in substrate concentrations higher than 0.6 M, a positive deviation from zero order is observed.
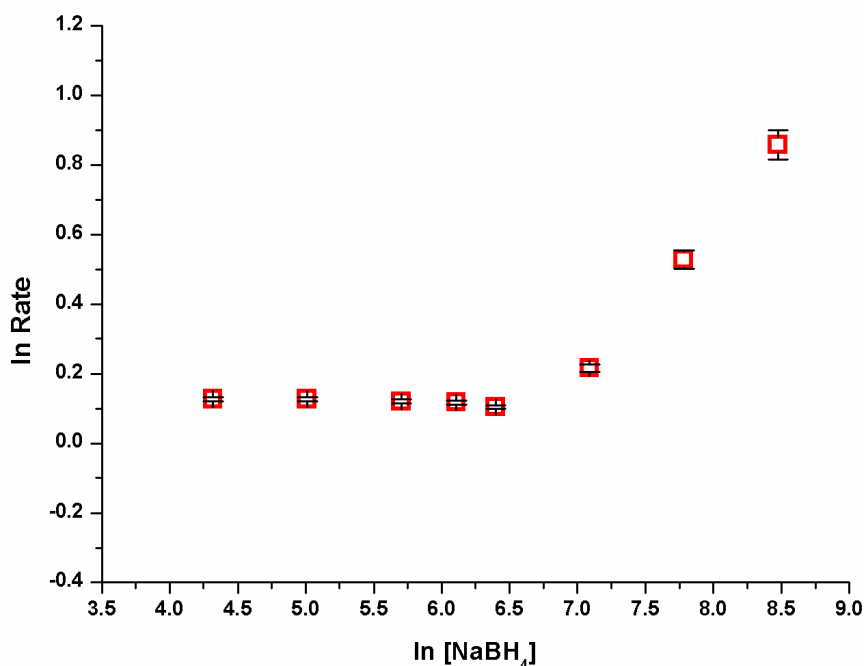


**Figure 38.** Plot of the hydrogen-generation rate versus the substrate concentration (both in logarithmic scale) in the hydrolysis of NaBH$_4$ catalyzed by zeolite framework stabilized ruthenium (0) nanoclusters at 25.0 ± 0.1 °C.

The hydrolysis of sodium borohydride was carried out at various temperatures (20, 25, 30, 35, 40 and 45 °C) starting with a 150 mM initial substrate concentration and an initial ruthenium concentration of 0.50 mM. The values of rate constant $k$ determined from the linear portions of the hydrogen volume versus time plots at six different temperatures (Figure 39) are used to create the Arrhenius, Eq. 6, [96], and Eyring-Polonyi, Eq. 7, [97] plots as shown in Figue 40 and Figure 41, respectively.

$$\ln(k) = \frac{-Ea}{RT} + \ln(A) \qquad \textbf{(6)}$$

$$\ln\frac{k}{T} = \frac{-\Delta H^{*}}{RT} + \ln\frac{k_B}{h} + \frac{\Delta S^{*}}{R} \qquad \textbf{(7)}$$

The apparent Arrhenius activation energy was found to be Ea = 49 ± 2 kJ/mol. This activation energy is slightly greater than the value found for the same hydrolysis catalyzed by acetate-stabilized ruthenium(0) nanoclusters (41 kJ/mol) [98] but it is still less than the 56 kJ/mol found for the hydrolysis of sodium borohydride catalyzed by bulk ruthenium [99] and other bulk metal catalysts: 75 kJ/mol for cobalt, 71 kJ/mol for nickel, and 63 kJ/mol for Raney nickel [100].
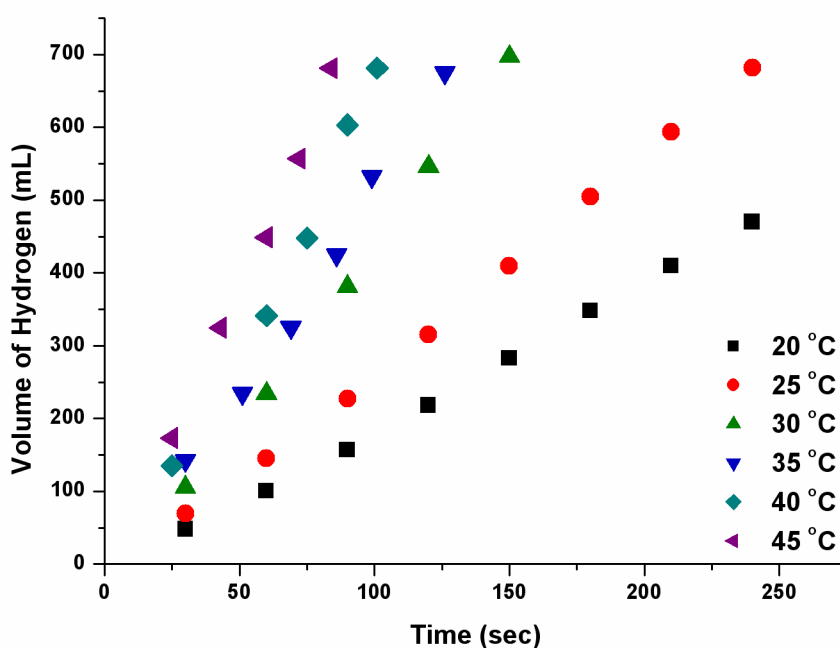


**Figure 39.** Plot of the volume of hydrogen (mL) versus time (s) for the hydrolysis of NaBH$_4$ (284 mg, 150mM in 50 mL) catalyzed by zeolite framework stabilized ruthenium(0) nanoclusters (with a ruthenium content of ≈ 0.72 wt %, [Ru] = 0.5 mM) at different temperatures (20, 25, 30, 35, 40, and 45 °C).
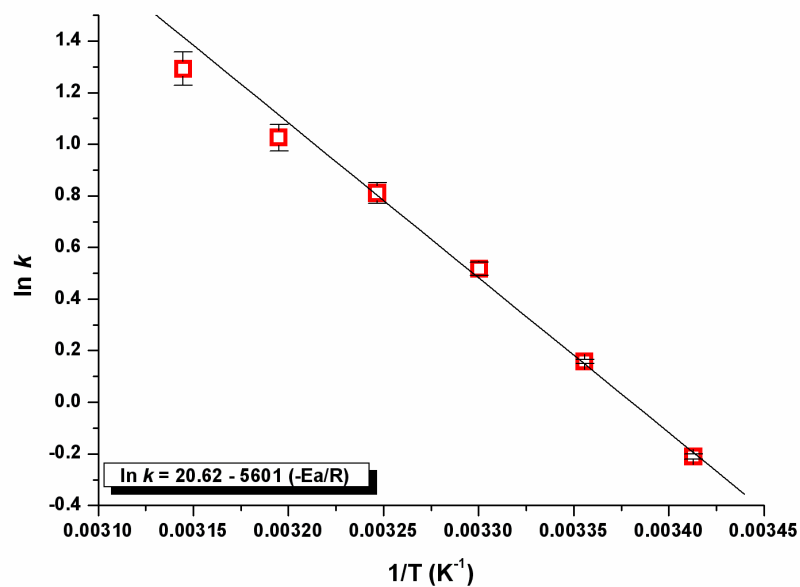
**Figure 40.** The Arrhenius plot for the zeolite framework stabilized ruthenium(0) nanoclusters catalyzed hydrolysis of sodium borohydride.
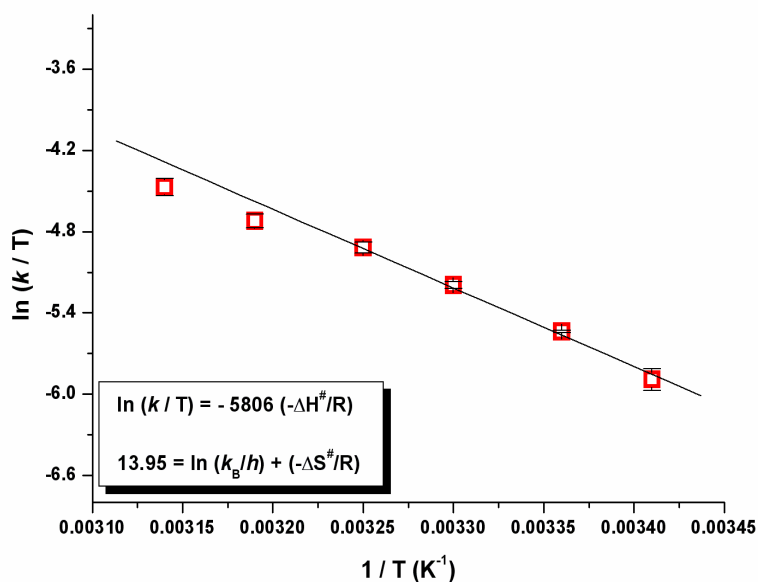


**Figure 41.** The Eyring-Polonyi plot for the zeolite framework stabilized ruthenium(0) nanoclusters catalyzed hydrolysis of sodium borohydride..

69

The Eyring-Polonyi plot given in Figure 41 gives the activation enthalpy, $\Delta H^{\#} = 48 \pm 2$ kJ/mol; and the activation entropy, $\Delta S^{\#} = -82 \pm 4$ J/K·mol, for the zeolite framework stabilized ruthenium(0) nanoclusters catalyzed hydrolysis of sodium borohydride. The small value of activation enthalpy and the large negative value of activation entropy are indicative of an associative mechanism for the ruthenium(0) nanocluster catalyzed hydrolysis of sodium borohydride, in line with the mechanism suggested for the hydrolysis of sodium borohydride given in the literature [101] consisting of $[BH_5]^*$ formed as transient.

## 3.2.4. Catalytic Lifetime of Zeolite Framework Stabilized Ruthenium(0) Nanoclusters in the Hydrolysis of Sodium Borohydride

In a catalyst lifetime experiment started with 0.50 mM Ru at $25 \pm 0.1$ °C, the zeolite framework stabilized ruthenium(0) nanoclusters were found to provide 103200 turnovers in the hydrolysis of sodium borohydride over 189 h before deactivation (Figure 42).

This is a record value of the TTO number in the catalytic hydrolysis of sodium borohydride, as the previous best value was TTO = 5170 [98] note the improvement by a factor of 20. They provide also an unprecedented value of TOF, as the initial value was 33000 mol $H_2$/mol Ru · h.
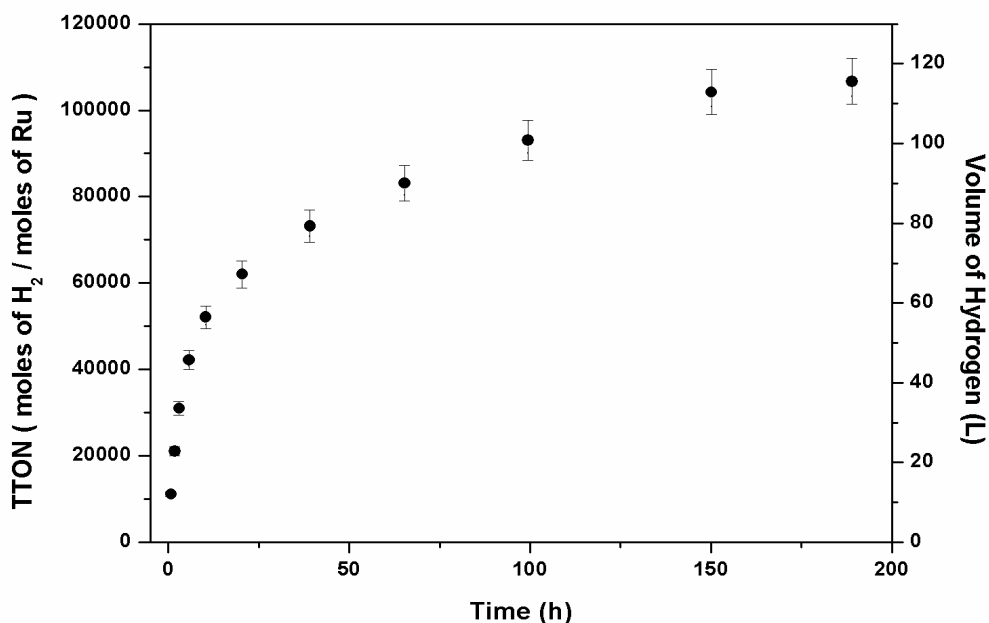
**Figure 42.** Graph of TTON (total turnover number) and volume of $H_2$ (L) versus time (h) for the zeolite framework stabilized ruthenium(0) nanoclusters catalyzed hydrolysis of sodium borohydride at $25 \pm 0.1$ °C.

## 3.2.5. Isolability, Bottlability and Reusability of Zeolite Framework Stabilized Ruthenium(0) Nanoclusters in the Hydrolysis of Sodium Borohydride

The zeolite framework stabilized ruthenium(0) nanoclusters were also tested for their isolability, bottleability, redispersibility, and reusability. After the complete hydrolysis of sodium borohydride solution (150 mM in 50 mL) catalyzed by zeolite framework stabilized ruthenium(0) nanoclusters ([Ru] = 0.5mM) at $25 \pm 0.1$ °C, the catalyst was isolated as a black powder by suction filtration, washed with water, and dried under $N_2$ purging at room temperature. Black samples of zeolite framework stabilized ruthenium(0) nanoclusters were bottled under nitrogen atmosphere and found to be stable for months.

The isolated zeolite framework stabilized ruthenium(0) nanoclusters are redispersible in aqueous solution of sodium borohydride and yet still active catalyst in the hydrolysis of sodium borohydride. Figure 43 shows the percentage of retained catalytic activity and conversion of sodium borohydride in the successive catalytic runs for the zeolite framework stabilized ruthenium(0) nanoclusters catalyzed hydrolysis of sodium borohydride at 25 ± 0.1 °C. The zeolite framework stabilized ruthenium(0) nanoclusters retain 76 % of their initial activity and provides > 99 % of conversion at the fifth run in the hydrolysis of sodium borohydride. This indicates that the zeolite framework stabilized ruthenium(0) nanoclusters are isolable, bottleable, redispersible, and yet catalytically active. In other words, they can be repeatedly used as active catalyst in the hydrolysis of sodium borohydride.
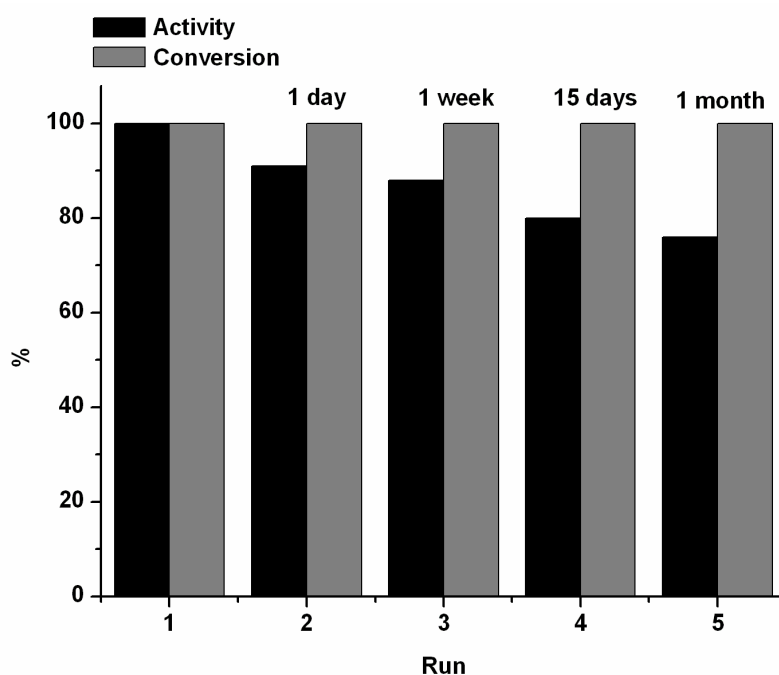


**Figure 43**. The percentage of retained catalytic activity and conversion for the zeolite framework stabilized ruthenium(0) nanoclusters catalyzed hydrolysis of sodium borohydride ([NaBH$_4$] = 150 mM) at 25.0 ± 0.1 °C.

More importantly, the complete release of hydrogen is achieved in each of the catalytic runs in the hydrolysis of sodium borohydride solution catalyzed by zeolite framework stabilized ruthenium(0) nanoclusters. The slight decrease in catalytic activity in subsequent runs may be due to the material loss during the isolation and redispersing procedure or due to passivation of nanoclusters surface by increasing the amount of boron products, e.g. metaborate, which might decrease the accessibility of active sites [102, 103].

## 3.3. The Catalytic Activity of Zeolite Framework Stabilized Ruthenium(0) Nanoclusters in the Hydrolysis of Sodium Borohydride in the Basic Medium

## 3.3.1. Kinetic Studies and the Determination of Activation Parameters for the Zeolite Framework Stabilized Ruthenium(0) Nanoclusters Catalyzed Hydrolysis of Sodium Borohydride Catalyzed in the Basic Medium

According to the established mechanism [101,104,105], in the acidic medium the hydrolysis of sodium borohydride is initiated by the attack of hydronium ion on the borohydride anion. In the basic solution, the reduction of proton concentration causes a decrease in the rate of hydrolysis. Since most of the prior studies on the catalytic hydrolysis of sodium borohydride have been carried out in alkaline medium (mostly in 5 wt % NaOH solution) [106] for comparison we also performed the hydrolysis of sodium borohydride in the basic medium by using zeolite framework stabilized ruthenium(0) nanoclusters as catalyst. In order to understand the effect of NaOH concentration on the catalytic activity of zeolite framework stabilized ruthenium(0) nanoclusters, the catalytic hydrolysis of sodium borohydride was performed in four different solutions that contain 2.5, 5, 7.5, and 10 wt % NaOH. Figure 44 shows the volume of hydrogen generated versus time during the zeolite framework stabilized ruthenium(0) nanoclusters catalyzed hydrolysis of sodium borohydride in these solutions at $25.0 \pm 0.1$ °C.
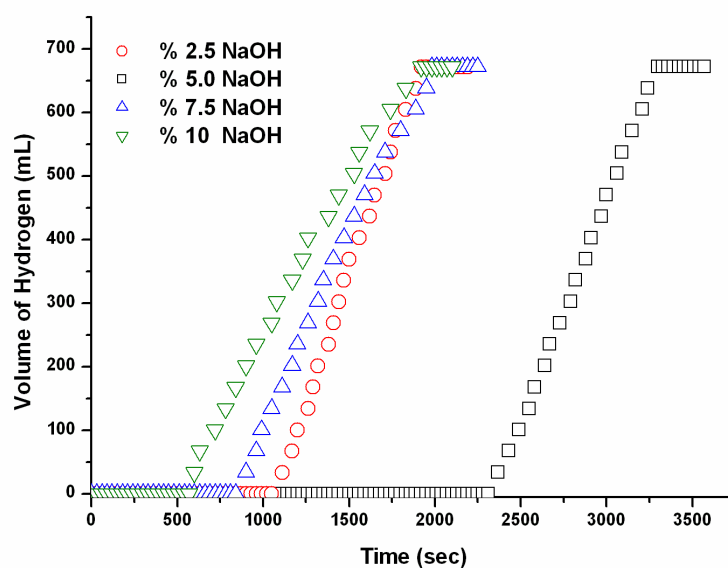
**Figure 44**. Plot of the volume of hydrogen (mL) versus time (s) for the hydrolysis of sodium borohydride ($[NaBH_4]$ = 150 mM) catalyzed by zeolite framework stabilized ruthenium(0) nanoclusters ([Ru] = 0.4 mM, with a ruthenium content of $\approx$ 0.8 % wt) in 2.5, 5, 7.5, and 10 wt % NaOH solutions at 25.0 ± 0.1 °C.

A linear hydrogen generation starts after an induction period of 10-40 min, unexpectedly, the shortest induction time was observed in the case of 10 wt % NaOH solution. This observation can be ascribed to the formation of mesopores in the framework of zeolite-Y at high NaOH concentrations as evidenced by the $N_2$ adsorption-desorption analyses of the isolated zeolite framework stabilized ruthenium(0) nanoclusters (*vide supra*). The partial removal of some framework silicon atoms by hydroxide ions may be responsible for the formation of mesopores, which leads to the easy accessibility of ruthenium(III) ion by the reducing borohydride anion. However, the rate of hydrogen generation decreases expectedly with the increasing concentration of sodium hydroxide (the observed rate constant of hydrogen generation $k_{obs}$ = 47.2, 41.2, 35.5, 29 mL of $H_2$/min in 2.5, 5, 7.5, 10 wt % NaOH solutions, respectively.

Figure 45 shows the volume of hydrogen generated versus time in the catalytic hydrolysis of sodium borohydride (150mM) in the presence of zeolite framework stabilized ruthenium(0) nanoclusters with different ruthenium concentrations (0.50-1.50 mM Ru) in 5.0% wt NaOH solution at $25.0 \pm 0.1$ °C.
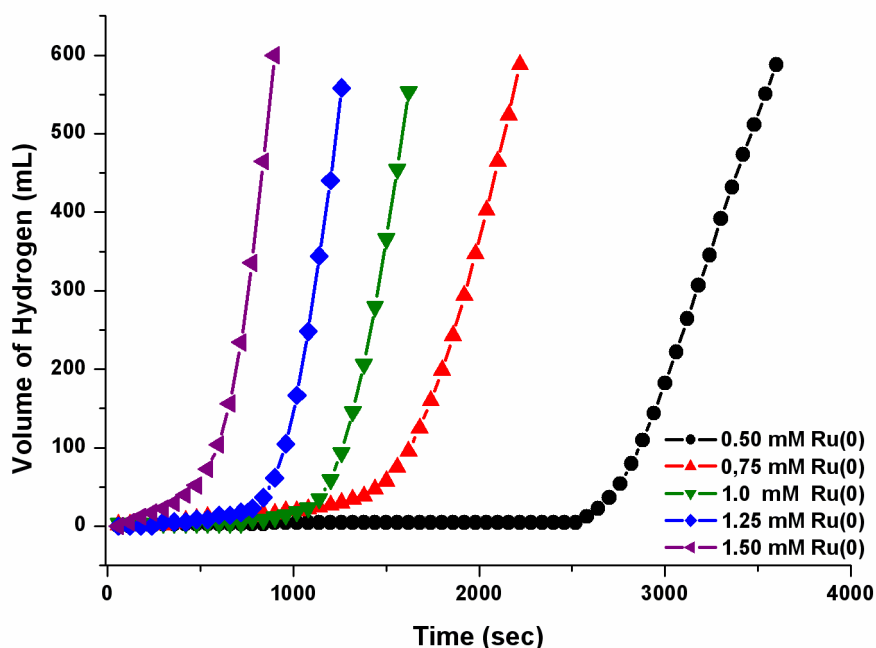


**Figure 45. .** Plot of the volume of hydrogen (mL) versus time (s) for the hydrolysis of sodium borohydride ([NaBH$_4$] = 150 mM) in 5 wt % NaOH solution catalyzed by zeolite framework stabilized ruthenium(0) nanoclusters with different ruthenium(0) concentrations (with a ruthenium content of $\approx 0\ 8$ % wt) at $25.0 \pm 0.1$ °C.

After an induction period of 6-43 minutes, a linear hydrogen generation starts with a rate of 34-71 mL H$_2$/min, depending on the ruthenium concentration at room temperature. Although the experiments in basic solution are started by using preformed catalysts, observation of induction period indicates that first the catalyst must be converted into an inactive form and, then, the active catalyst is re-formed.

Recovery of nanocluster surface, which must be oxidized by hydroxide ions, needs time, as the large borohydride ions diffuse more slowly into cages of zeolite compared to the small hydroxide ions. Additionally, the decrease in the induction period with the increasing ruthenium concentration is explained by the accessibility of more ruthenium(0) nanoclusters by borohydride ions on the way while diffusing through cavities. Plotting the hydrogen generation rate versus ruthenium concentration, both on logarithmic scales, gives a straight line (Figure 46), the slope of which is found to be 0.73.
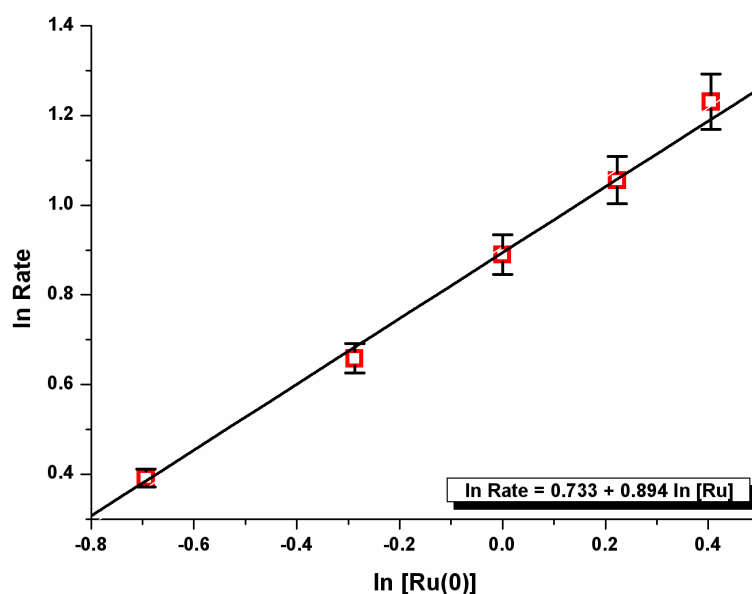


**Figure 46**. Plot of the hydrogen eneration rate versus the catalyst concentration (both in logarithmic cale) for the zeolite framework stabilized ruthenium(0) nanoclusters catalyzed hydrolysis of $NaBH_4$ ($[NaBH_4]$ = 150 mM) in 5 wt % NaOH solution at $25.0 \pm 0.1$ °C.

This result indicates that the hydrolysis is close to first-order with respect to the catalyst concentration. The slight deviation from the first-order may be attributed to the formation of mesopores in the presence of sodium hydroxide. The effect of

substrate concentration on the hydrogen generation rate was also studied by performing a series of experiments starting with various initial concentration of sodium borohydride while the catalyst concentration is kept constant at 0.50 mM Ru in 5% wt NaOH solution at $25.0 \pm 0.1$ °C. Figure 47 shows the plot of hydrogen volume generated versus time for various sodium borohydride concentrations. It is obvious that the catalytic hydrolysis is zero-order with respect to substrate concentration in dilute solutions with initial sodium borohydride concentration up to 0.6 M also in the presence of 5 wt % NaOH, but it deviates from the zero-order in substrate concentrations higher than 0.6 M (Figure 48).
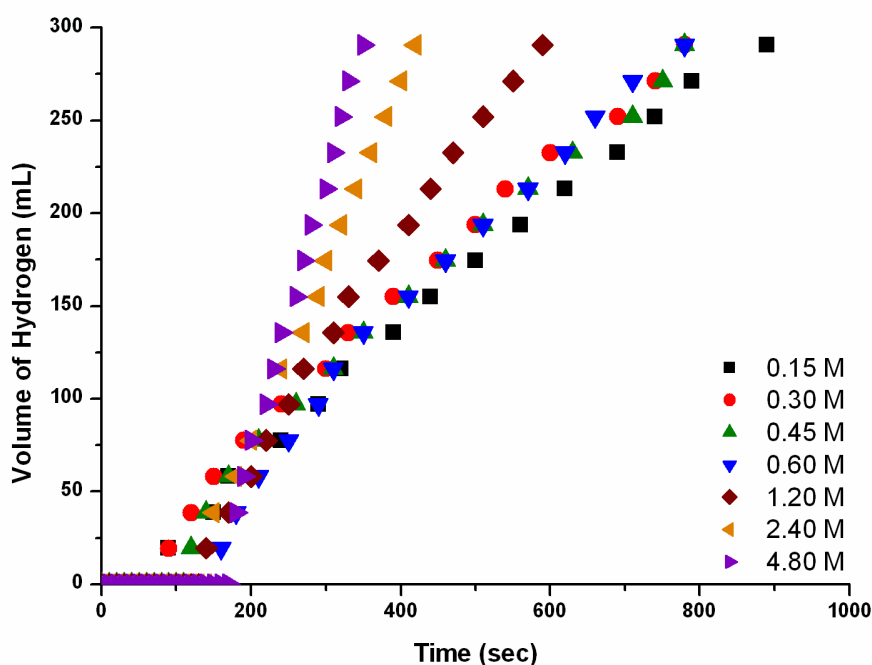


**Figure 47.** Plot of the volume of hydrogen (mL) versus time (s) for the zeolite framework stabilized ruthenium(0) nanoclusters ([Ru] = 0.50 mM, with a ruthenium content of $\approx 0.8$ wt %) catalyzed hydrolysis of $NaBH_4$ in 5 wt % NaOH solution with different $NaBH_4$ concentrations at $25.0 \pm 0.1$ °C.
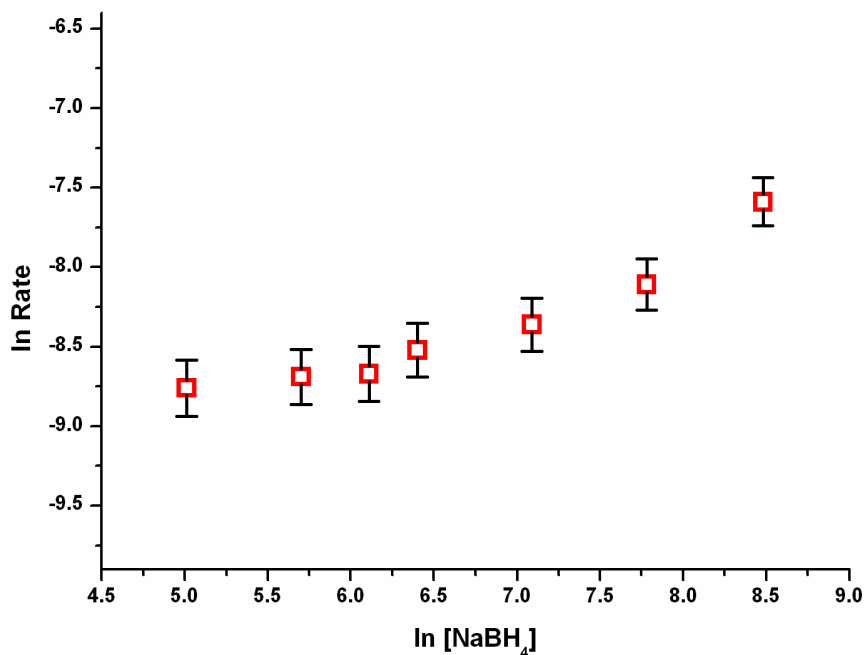
**Figure 48**. Plot of the hydrogen generation rate versus substrate concentration (both in logarithmic scale) for the zeolite framework stabilized ruthenium(0) nanoclusters catalyzed hydrolysis of sodium borohydride in 5 wt % NaOH solution at $25.0 \pm 0.1$ °C.

The hydrolysis of sodium borohydride was carried out at various temperatures in the range of 20-45 °C starting with the initial substrate concentration of 150 mM $NaBH_4$ and an initial catalyst concentration of 0.50 mM Ru in 5 wt % NaOH solution (Figure 49). The values of rate constant k determined from the linear portions of the $H_2$ volume versus time plots at six different temperatures are used to calculate the activation parameters Arrhenius activation energy, Ea = $34.9 \pm 2$ kJ/mol (Figure 50); activation enthalpy, $\Delta H^{\#} = 32 \pm 2$ kJ/mol; and activation entropy, $\Delta S^{\#} = -139 \pm 4$ J/K· mol (Figure 51) that were found for the zeolite framework stabilized ruthenium(0) nanoclusters catalyzed hydrolysis of 150 mM sodium borohydride in 5 wt % NaOH solution.
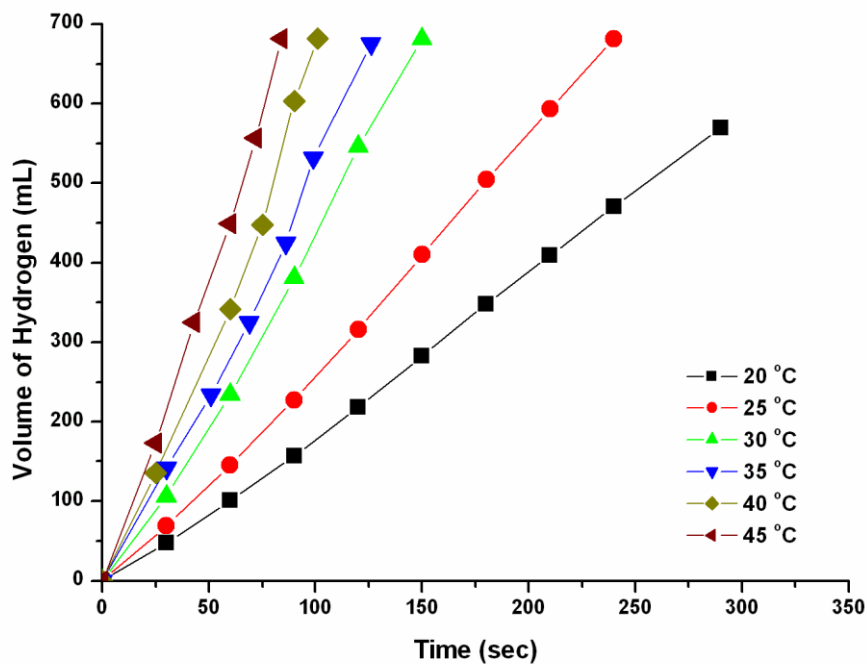
**Figure 49**. Plot of the volume of hydrogen (mL) generated versus time (s) (induction time periods were not shown for clarity) for the hydrolysis of 50 mL of 150 mM sodium borohydride in 5 wt % NaOH solution at different temperatures catalyzed by zeolite framework stabilized ruthenium(0) nanoclusters ([Ru] = 0.5 mM, with a ruthenium content of ≈ 0.8 % wt).

The value of activation energy is lower than the value of 47 kJ/mol found for bulk ruthenium at 5.6 M $NaBH_4$ concentration [107]. Table 1 shows the activation energies determined for the hydrolysis of sodium borohydride in basic medium catalyzed by other catalysts for comparison. The observed small value of activation enthalpy and the large negative value of activation entropy reveal that the zeolite framework stabilized ruthenium(0) nanoclusters catalyzed hydrolysis of sodium borohydride followed associcative mechanism in basic medium.
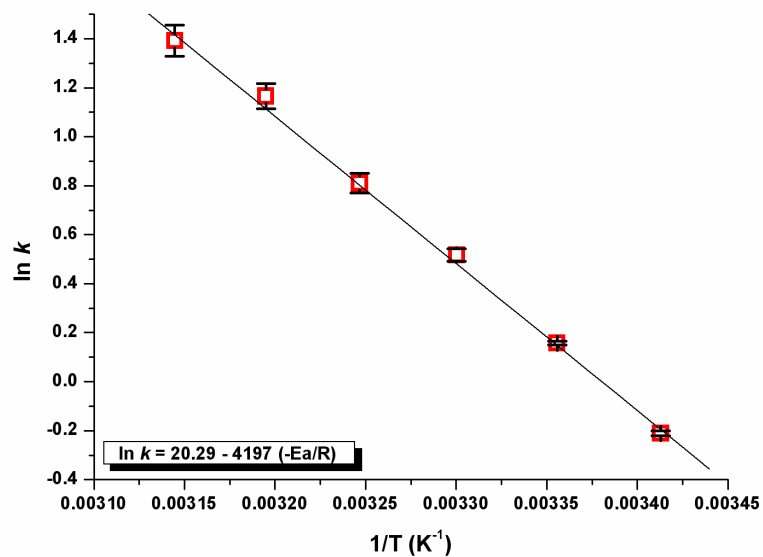
**Figure 50.** The Arrhenius plot for the zeolite framework stabilized ruthenium(0) nanoclusters catalyzed hydrolysis of sodium borohydride in 5 wt %  NaOH solution.
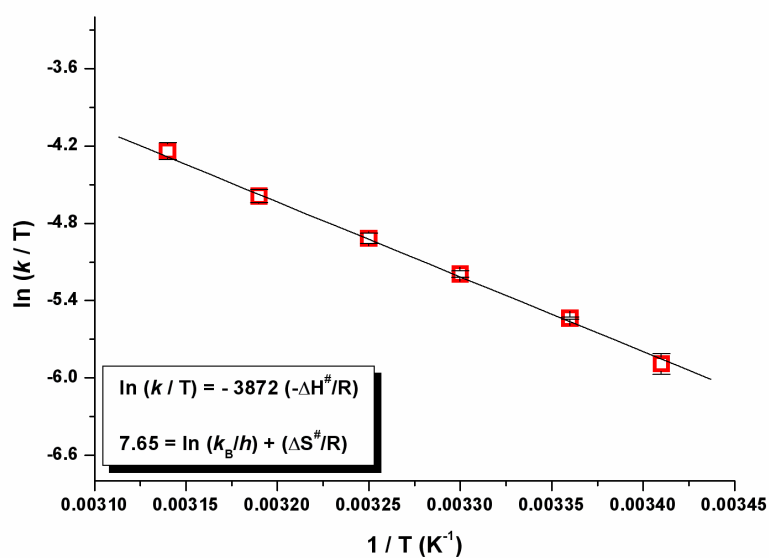


**Figure 51**. The Eyring-Polonyi plot for the zeolite framework stabilized ruthenium(0) nanoclusters catalyzed hydrolysis of sodium borohydride in 5 wt % NaOH solution.

80

**Table 1.** The catalyst systems employed in the hydrolysis of sodium borohydride in the basic medium and obtained activation energies in different reaction conditions.

| Entry | Catalyst | Ea (kJ/mol) | NaBH$_4$ | NaOH | Reference |
|-------|----------|-------------|----------|------|-----------|
| 1 | Ru(0) NC's | 43 | 0.15 M | 10 % | [98] |
| 2 | Ru-IRA 400 | 47 | 20 % | 10 % | [107] |
| 3 | Ni-Co-B | 62 | 0.16 g | 15 % | [108] |
| 4 | Co-B / Ni foam | 33 | 20 % | 10 % | [109] |
| 5 | Ni$_x$B | 38 | 1.5% | 10 % | [110] |
| 6 | Co-B | 45 | 2 % | 5 % | [111] |
| 7 | Co/γ-Al$_2$O$_3$ | 33 | 5 % | 5 % | [112] |
| 8 | Co-B/ C | 58 | 0.2 M | 20 mmol | [113] |
| 9 | Ru promoted sulphated Zr | 76 | 0.6 M | 1.3 M | [114] |
| 10 | Pt/LiCoO$_2$ | 70 | 10 % | 5 % | [115] |
| 11 | Ru/LiCoO$_2$ | 68 | 10 % | 5 % | [115] |
| 12 | Co-Mn-B nanocomposites | 55 | 5 % | 5 % | [116] |
| 13 | Ru/C | 67 | 1 M | 4 % | [117] |
| 14 | PtPd@CNT | 19 | 15 mM | 1 % | [118] |
| 15 | Co-W-B/Ni | 29 | 20 % | 5 % | [119] |
| 16 | Ru/IR-120 | 50 | 5 % | 1 % | [120] |
| 17 | **Ru(0)/Zeolite-Y** | **35** | **0.15 M** | **5 %** | [121] |

### 3.3.2. Catalytic Lifetime of Zeolite Framework Stabilized Ruthenium(0) Nanoclusters in the Hydrolysis of Sodium Borohydride in the Basic Medium

In a catalyst lifetime experiment started with 0.5 mM Ru in 5 wt % NaOH solution, the zeolite framework stabilized ruthenium(0) nanoclusters were found to provide a record TTON of 27200 and an exceptional TOF up to 4000 mol $H_2$/mol Ru ·h in the hydrolysis of sodium borohydride over 28 h before deactivation (Figure 52).
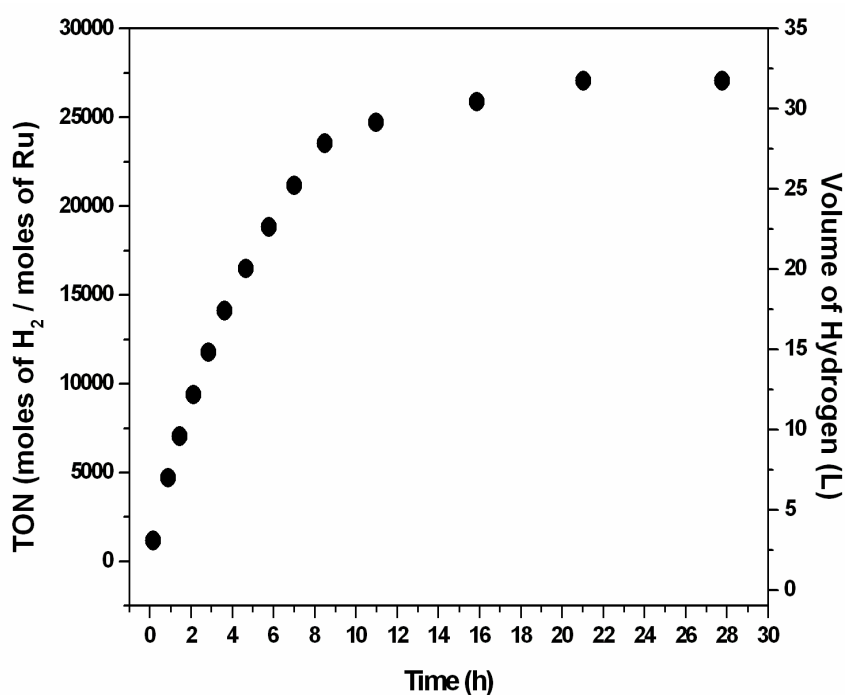


**Figure 52**. Graph of TTON (total turnover number) and volume of $H_2$ (L) versus time for the zeolite framework stabilized ruthenium(0) nanoclusters catalyzed hydrolysis of sodium borohydride in 5 wt % NaOH solution at $25 \pm 0.1$ °C.

### 3.3.3. Isolability, Bottlability and Reusability of Zeolite Framework Stabilized Ruthenium(0) Nanoclusters in the Hydrolysis of Sodium Borohydride in the Basic Medium

The zeolite framework stabilized ruthenium(0) nanoclusters at the end of the hydrolysis of sodium borohydride in 5 wt % NaOH solution could also be isolated as a black powder, which is stable under inert nitrogen atmosphere. The isolated ruthenium(0) nanoclusters are redispersible in basic solution (5 wt % NaOH) of sodium borohydride and yet still active catalyst. Figure 53 shows the percentage of catalytic activity that retained and the conversion of sodium borohydride in the successive catalytic runs for the zeolite framework stabilized ruthenium(0) nanoclusters catalyzed hydrolysis of sodium borohydride in 5 wt % NaOH solution at $25.0 \pm 0.1$ °C.
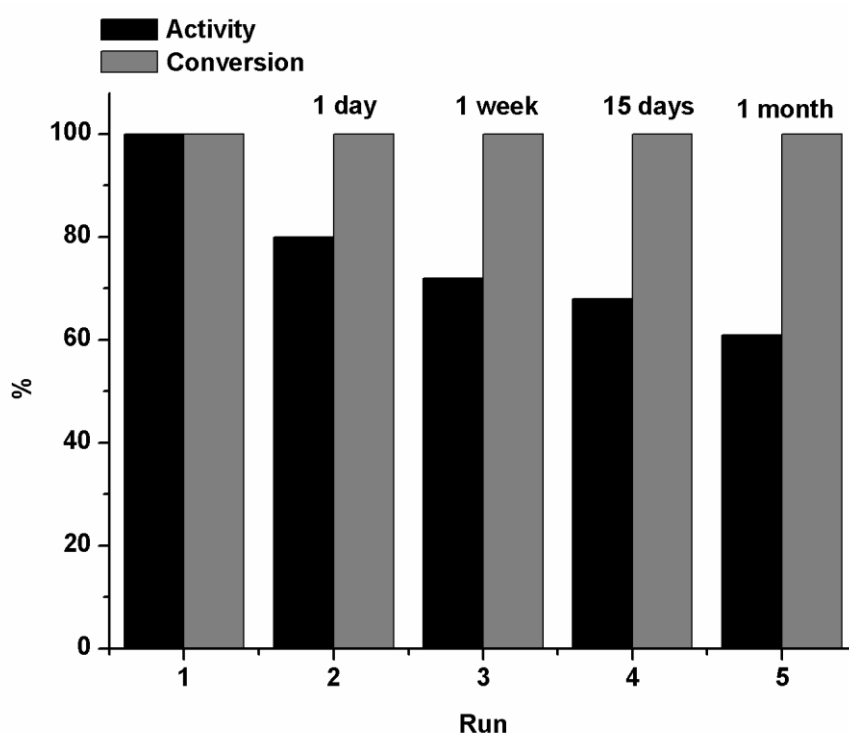


**Figure 53**. The percentage of the retained catalytic activity and conversion in the successive catalytic runs for the zeolite framework stabilized ruthenium(0) nanoclusters catalyzed sodium borohydride in 5 wt % NaOH solution at $25.0 \pm 0.1$ °C.

It is remarkable to note that the zeolite framework stabilized ruthenium(0) nanoclusters redispersed after 1 month bottling under nitrogen atmosphere retain 61 % of their initial activity and provide > 99% conversion at the fifth run in the hydrolysis of sodium borohydride. This indicates that the zeolite framework stabilized ruthenium(0) nanoclusters are isolable, bottleable, and redispersible and yet catalytically active in the hydrolysis of sodium borohydride even in basic medium. Additionally it should be noted that the resultant ruthenium(0) nanoclusters and host material exhibit high durability against agglomeration and amorph formation as evidenced by TEM and XRD analyses of the sample harvested at the end of the fifth reuse from the hydrolysis of sodium borohydride in the basic medium (see Figures 75- 76 in the Appendix).

## 3.4. The Catalytic Activity of Zeolite Framework Stabilized Ruthenium(0) Nanoclusters in the Hydrogenation of Aromatics

The zeolite framework stabilized ruthenium(0) nanoclusters were also tested for their catalytic activity in the hydrogenation of aromatics. After the complete hydrolysis of sodium borohydride solution catalyzed by zeolite framework stabilized ruthenium(0) nanoclusters at $25 \pm 0.1$ °C, the catalyst was isolated from the solution as a black powder by filtration under $N_2$ gas purging, washed with deionized water, and dried at room temperature under vacuum ($10^{-3}$ Torr). Black samples of zeolite framework stabilized ruthenium(0) nanoclusters were bottled under nitrogen atmosphere and used as catalyst in the catalytic hydrogenation reactions.

**3.4.1. Control Experiment: Detection of Mass-Transfer Limitation in the Zeolite Framework Stabilized Ruthenium(0) Nanoclusters Catalyzed Hydrogenation of Cyclohexene**

The catalytic hydrogenation of cyclohexene in the cyclohexane started by agitating the zeolite framework stabilized ruthenium(0) nanoclusters in the reaction solution at $25 \pm 0.1$ °C and $40 \pm 1$ psig initial $H_2$ pressure and the progress of the reaction was followed by monitoring the hydrogen uptake which can be converted to the concentration loss of substrate by using the stoichiometry. The complete hydrogenation of cyclohexene was also confirmed by checking the ^{1}H NMR spectra of the reaction solution at the end of the reaction.

The hydrogenation of cyclohexene performed in this way showed that zeolite framework stabilized ruthenium(0) nanoclusters are very active catalyst in this reaction (Figure 54), a linear hydrogenation starts immediately without induction period as the catalyst is preformed . They provide a TOF value of 6120 mol cyclohexene/mol Ru·h in the hydrogenation of cyclohexene at $22 \pm 0.1$ °C and $40 \pm 1$ psi $H_2$.

First of all, in order to address the most important issue; whether the zeolite framework stabilized ruthenium(0) nanoclusters catalyzed hydrogenation reaction at the interface of gas and condensed phases is under mass transfer limitation (MTL) regime [122] the dependence of reaction rate on the stirring speed was investigated.
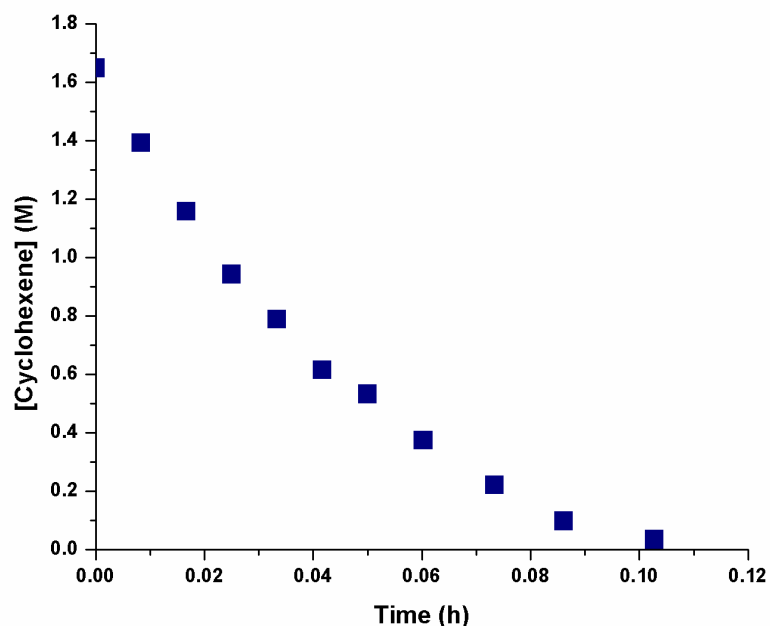
**Figure 54**. Plot of concentration of cyclohexene (M) vs time (h) for the zeolite framework stabilized ruthenium(0) nanoclusters catalyzed hydrogenation of cyclohexene (0.5 mL cyclohxene in 2.5 mL cyclohexane, 4.6 mM Ru).

In order to demonstrate the effect of stirring speed eleven independent experiments were performed for the zeolite framework stabilized ruthenium(0) nanoclusters catalyzed hydrogenation of cyclohexene under the under the same conditions (0.5 mL cyclohexene in 1.5 mL cyclohexane, [Ru] = 3.4 mM, $22 \pm 0.1$ °C and $40 \pm 1$ psi $H_2$), but using different stirring speed: 0, 120, 240, 360, 480, 600, 720, 840, 960, 1080 and 1200 rpm.The rate of cyclohexene hydrogenation was plotted against the stirring speed in Figure 55.

The inspection of the plot shows that the hydrogenation proceeds under non-MTL regime when the stirring speed is greater than 600 rpm. Additionally, in control experiments performed at a constant stirring speed of 720 rpm, doubling the catalyst concentration resulted in an increase in the hydrogenation rate by a factor of 2. This linear rate dependence on the catalyst concentration requires that the observed initial rate of hydrogenation is not influenced by mass-transfer limitation when the stirring speed is 720 rpm.
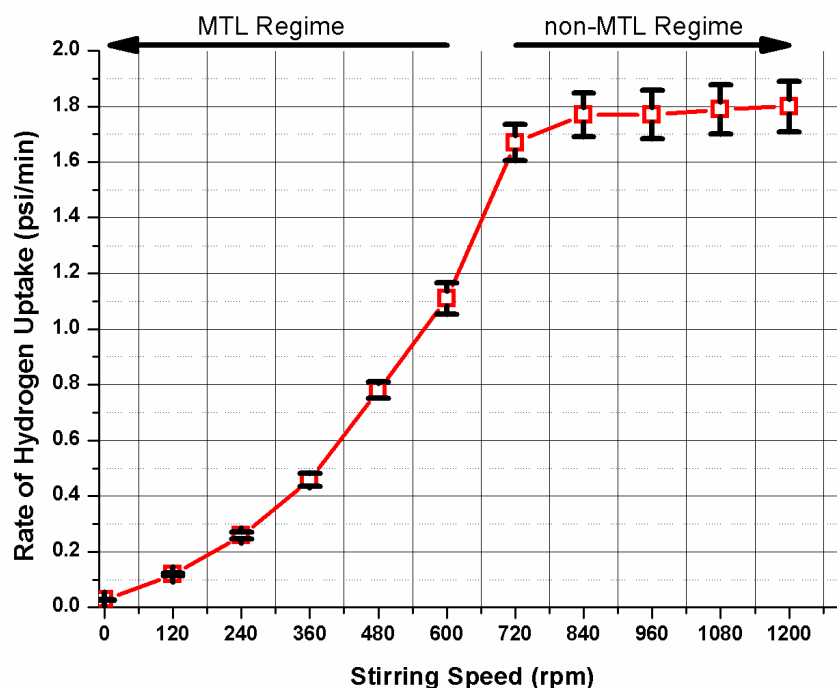
**Figure 55**. Plot of rate of hydrogen uptake (psi/min) versus stirring speed (rpm) for the zeolite framework stabilized ruthenium(0) nanoclusters catalyzed hydrogenation of cyclohexene (0.5 mL cyclohxene in 1.5 mL cyclohexane, 3.4 mM Ru), all at $22 \pm 0.1$ °C and $40 \pm 1$ psi initial $H_2$ pressure.

## 3.4.2. The Catalytic Activity of the Zeolite framework stabilized Ruthenium(0) Nanoclusters in the Catalytic Hydrogenation of Aromatics

Zeolite framework stabilized ruthenium(0) nanoclusters are also found to be highly active catalyst in the hydrogenation of aromatics. Figures 56-59 show the plots of concentration loss of aromatics vs. time for the hydrogenation of aromatics (benzene, toluene, *o*-xylene and mesitylene) catalyzed by zeolite framework stabilized ruthenium(0) nanoclusters at $22 \pm 0.1$ C and with a $40 \pm 1$ psig initial $H_2$ pressure. For all of the substrates the hydrogenation starts immediately without induction period as a preformed catalyst is used and.continues until the consumption of benzene, toluene, *o*-xylene and mesitylene with initial TOF values of 1980, 900, 550 and 45 h$^{-1}$, respectively.

In the series of benzene, toluene, *o*-xylene, and mesitylene, the hydrogenation rate decreases with the increasing number of methyl substituent, because of the electronic effect on the aromatic ring due to the addition of methyl groups [123]. Additionally, the observation of the slowest hydrogenation rate for mesitylene can also be explained by Lennard-Jones kinetic diameter of mesitylene (7.6 Å), which is larger than the supercage aperture of zeolite-Y (7.4 Å) [77].
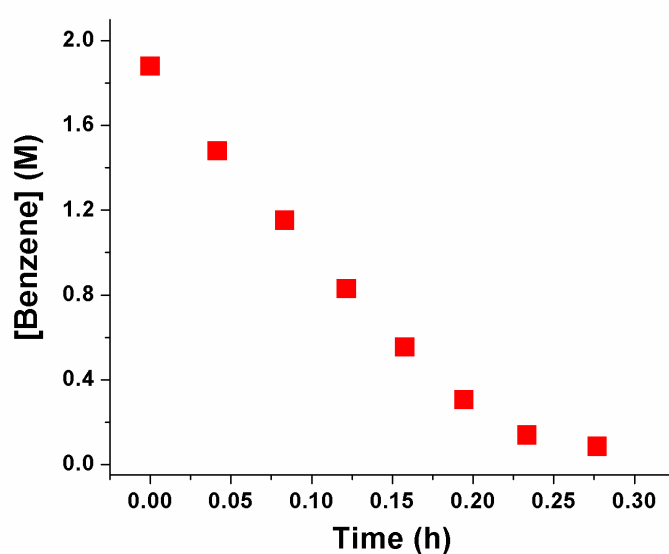


**Figure 56**. Plot of concentration (M) versus time (h) for the hydrogenation of benzene (0.5 mL benzene in 2.5 mL cyclohexane) catalyzed by zeolite framework stabilized ruthenium(0) nanoclusters ([Ru] = 4.6 mM) at 22 ± 0.1 C with 40 ± 1 psig inital $H_2$ pressure and > 720 rpm stirring speed.
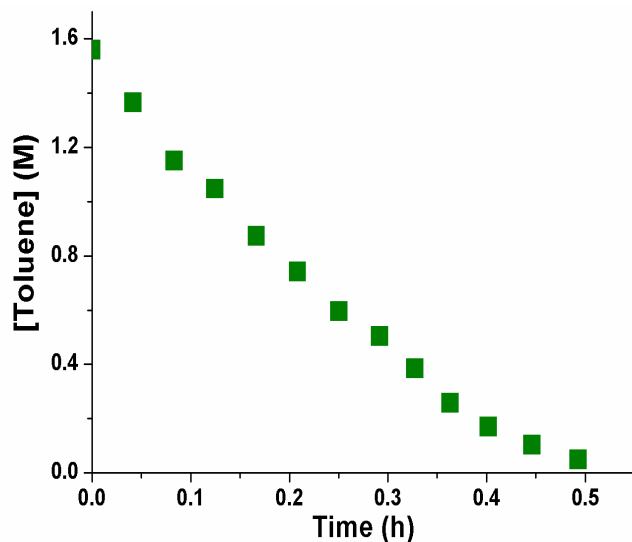
**Figure 57**. Plot of concentration (M) versus time (h) for the hydrogenation of toluene (0.5 mL toluene in 2.5 mL cyclohexane) catalyzed by zeolite framework stabilized ruthenium(0) nanoclusters ([Ru] = 4.6 mM) at $22 \pm 0.1$ C with $40 \pm 1$ psig inital $H_2$ pressure and > 720 rpm stirring speed.
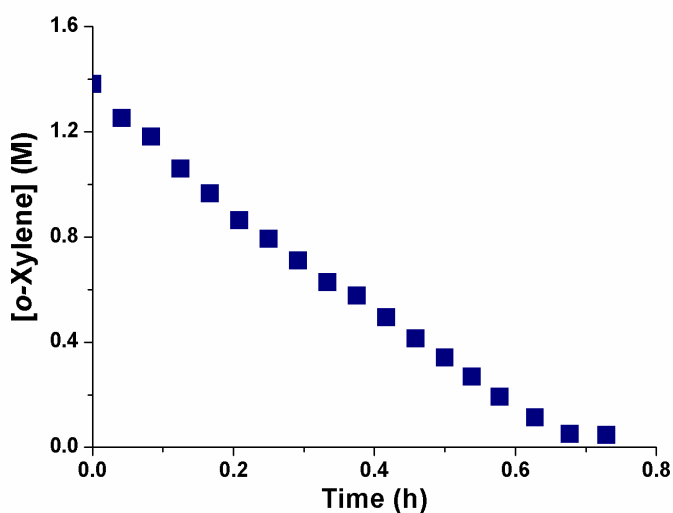


**Figure 58.** Plot of concentration (M) versus time (h) for the hydrogenation of *o*-xylene (0.5 mL *o*-xylene in 2.5 mL cyclohexane) catalyzed by zeolite framework stabilized ruthenium(0) nanoclusters ([Ru] = 4.6 mM) at $22 \pm 0.1$ C with $40 \pm 1$ psig inital $H_2$ pressure and > 720 rpm stirring speed.
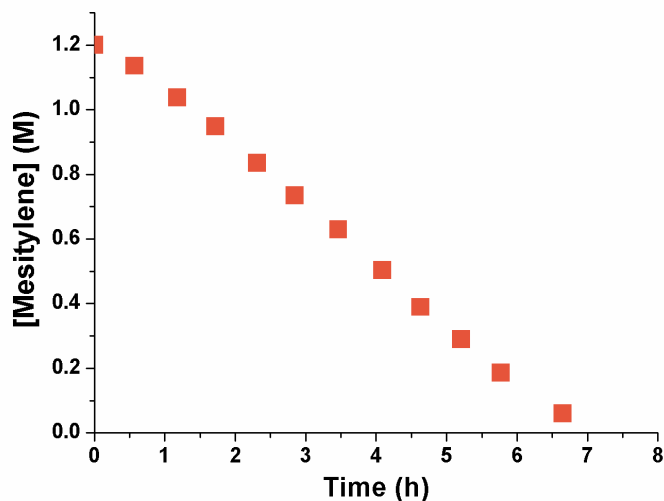
**Figure 59**. Plot of concentration (M) versus time (h) for the hydrogenation of mesitylene (0.5 mL mesitylene in 2.5 mL cyclohexane) catalyzed by zeolite framework stabilized ruthenium(0) nanoclusters ([Ru] = 4.6 mM) at 22 ± 0.1 C with 40 ± 1 psig inital $H_2$ pressure and > 720 rpm stirring speed.

## 3.4.3. The Catalytic Activity of the Zeolite Framework Stabilized Ruthenium(0) Nanoclusters in the Catalytic Hydrogenation of Benzene in the Solvent Free System Depending on Ruthenium Loading, Ruthenium Concentration and Temperature

The catalytic activity of zeolite framework stabilized ruthenium(0) nanoclusters was also tested in the hydrogenation of benzene, which is a well-known test reaction for the hydrogenation of aromatics, in the solvent free system and found to be highly active active catalyst under mild conditions at 22 ± 0.1 C and with a 40 ± 1 psig initial $H_2$ pressure (*vide infra*). However, before performing further experiments for the zeolite framework stabilized ruthenium(0) nanoclusters catalyzed hydrogenation of neat benzene an important control reaction need to be performed: determination of the most active ruthenium loading because the catalytic activity is expected to depend on the ruthenium loading of zeolite framework stabilized ruthenium(0) nanoclusters as previously demonstrated in the hydrolysis of sodium borohydride. For this purpose a series of experiments were performed starting with

zeolite framework stabilized ruthenium(0) nanoclusters ([Ru] = 10 mM) with different ruthenium loadings in the range of 0.4-8.4% wt were tested in the hydrogenation of neat benzene to determine the effect of ruthenium loading on the catalytic activity. The variation in the catalytic activity of zeolite framework stabilized ruthenium(0) nanoclusters depending on the ruthenium loading given in Figure 60 reflects the accessibility of ruthenium(0) nanoclusters in the zeolite cages by the substrate.
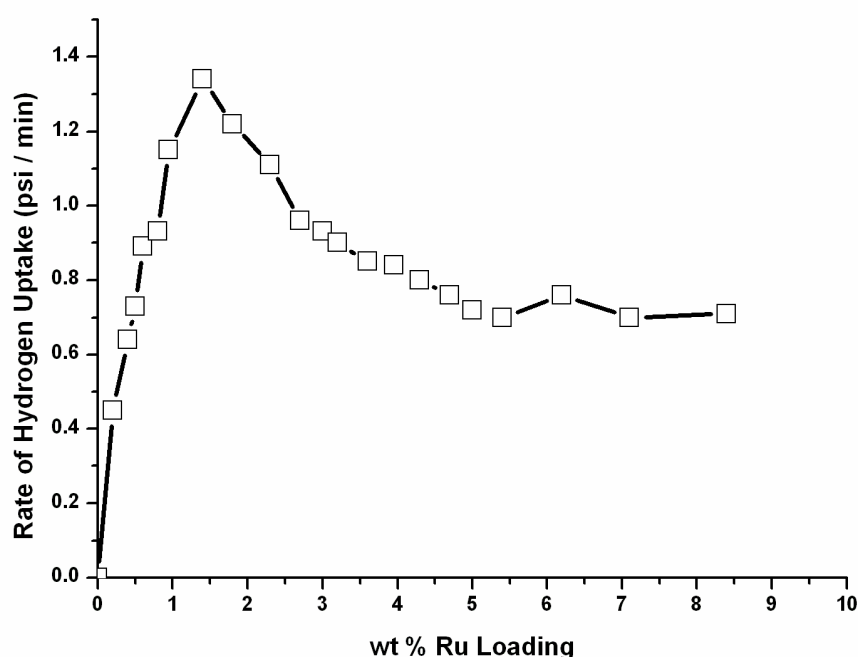


**Figure 60.** The rate of hydrogen uptake (psi $H_2$/min) versus ruthenium loading in the range of 0.4 - 8.4 % wt Ru (0.4, 0.5, 0.61, 0.8, 0.95, 1.4, 1.8, 2.3, 2.7, 3, 3.2, 3.6, 3.95, 4.3, 4.7, 5, 5.4, 6.2, 7.1, 8.4) determined from the hydrogenation of 1.0 mL benzene (11.2 mmol) catalyzed by zeolite framework stabilized ruthenium(0) nanoclusters (in all [Ru] = 10 mM) at 22 ± 0.1 °C with a 40 ± 1 psig initial $H_2$ pressure and > 720 rpm stirring speed.

The highest catalytic activity was obtained by using zeolite framework stabilized ruthenium(0) nanoclusters with a metal loading of 1.40 % wt Ru, in which

ruthenium(0) nanoclusters are most probably present in the supercages ($\alpha$-cages), where the substrate can more readily access to ruthenium(0) nanoclusters compared to sodalite cages ($\beta$-cages) of zeolite-Y (Figure 34, *vide supra*). During the drying performed under vacuum ($10^{-3}$ Torr), the possible migration of ruthenium(0) nanoclusters from sodalite cages to supercages may lead to observation of different value for the most active ruthenium loading of zeolite framework stabilized ruthenium(0) nanoclusters in the hydrogenation of neat benzene (1.4 % wt Ru) from the same of that obtained in the hydrolysis sodium borohydride (0.8 wt % Ru), in which the active catalyst formed in-situ during the hydrolysis of sodium borohydride.
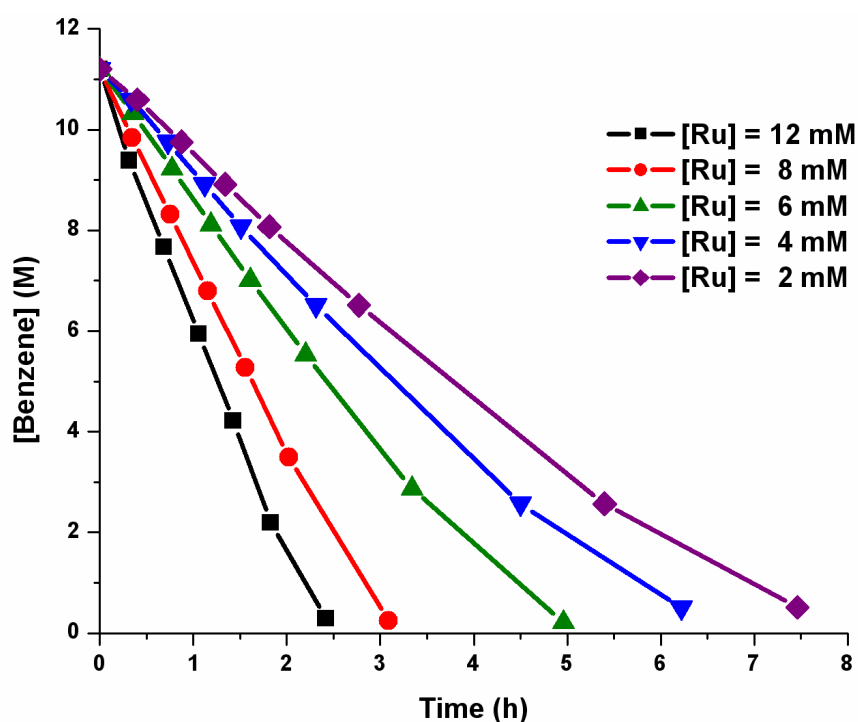


**Figure 61**. Plot of the concentration of benzene (M) versus time (h) for the hydrogenation of neat benzene (1.0 mL, 11.2 mmol) catalyzed by zeolite framework stabilized ruthenium(0) nanclusters with different ruthenium concentrations (2, 4, 6, 8, 10 and 12 mM Ru) at $22 \pm 0.1$ °C with $40 \pm 1$ psig inital $H_2$ pressure and $> 720$ rpm stirring speed.

Then the effect of ruthenium concentration on the catalytic activity of zeolite framework stabilized ruthenium(0) nanoclusters was investigated by performing a series of experiments. Figure 61 shows the plots of benzene concentration versus time during the hydrogenation of neat benzene (1.0 mL, 11.2 mmol) in the presence of zeolite framework stabilized ruthenium(0) nanoclusters with different ruthenium concentrations (2-12 μmol Ru) at $22 \pm 0.1$ °C. It was found that zeolite framework stabilized ruthenium(0) nanoclusters are highly activie catalyst in the hydrogenation of neat benzene even at low ruthenium concentrations such as the hydrogenation rate of 0.98 mmol benzene/h can be achieve by using zeolite framework stabilized ruthenium(0) nanoclusters that contain only 2 mM ruthenium. The rate of hydrogenation determined from the linear portion of the plots in Figure 61. Plotting the hydrogenation rate versus ruthenium concentration, both in logarithmic scales (Figure 62), gives a straight line with a slope of 0.93 1.0 indicating that the hydrogenation of neat benzene is first order with respect to the ruthenium concentration.



In Rate = 0.9258 In [Ru] - 0.6727
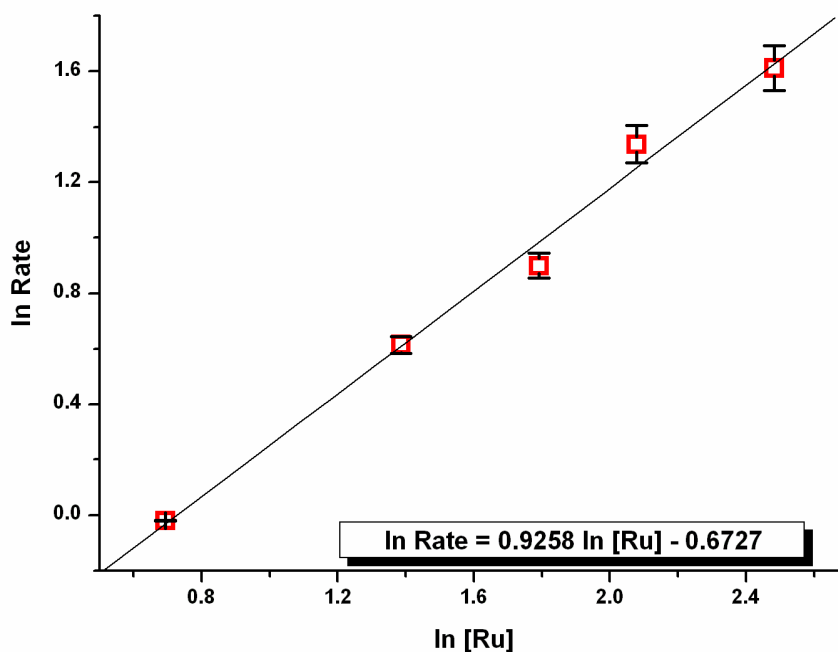
**Figure 62**. Plot of the hydrogenation rate versus ruthenium concentration (both in logarithmic scale) for zeolite framework stabilized ruthenium(0) nanoclusters catalyzed hydrogenation of neat benzene at $22 \pm 0.1$ °C with $40 \pm 1$ psig inital $H_2$ pressure and > 720 rpm stirring speed.

The hydrogenation of neat benzene (1.0 mL, 11.2 mmol) in the presence of zeolite framework stabilized ruthenium(0) nanoclusters (64 mg with a ruthenium loading of 1.4 % wt corresponds to 0.0069 mmol Ru) was also carried out at various temperatures in the range of 15-35 °C at 40 ± 1 psi $H_2$ and the results are illustrated in Figure 63 indicates the exceptional catalytic activity of zeolite framework stabilized ruthenium(0) nanoclusters even at low temperatures (15 °C).
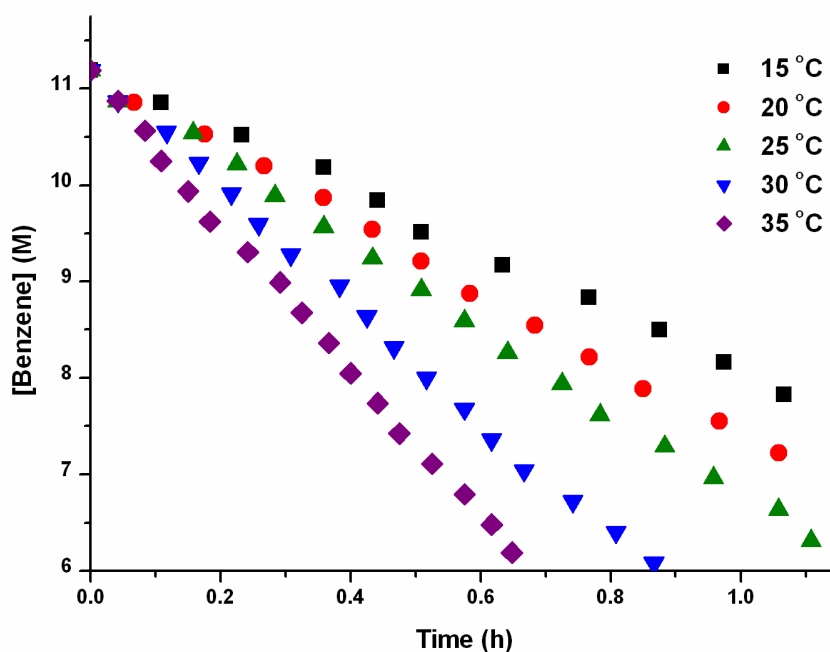


**Figure 63**. Plot of the concentration of benzene (mol/L) versus time (h) for the hydrogenation of benzene (1.0 mL, 11.2 mmol) catalyzed by zeolite framework stabilized ruthenium(0) nanoclusters ([Ru] = 12 mM) at different temperatures and 40 ± 1 psig of $H_2$ and > 720 rpm stirring speed.

The values of rate constant k, determined from the linear portion of the plot for each temperature (Figure 63), are used to calculate the activation energy: Arrhenius activation energy was found to be Ea = 32 ± 1 kJ/mol for the zeolite framework stabilized ruthenium(0) nanoclusters catalyzed hydrogenation of neat benzene as shown in the Figure 64. The value of activation energy is lower than the

value of 35 kJ/mol found for the hydrogenation of benzene catalyzed by platinum(0) nanoparticles [124], 36.5 kJ/mol for Ni-MCM-41 [125] and comparable with 30 kJ/mol for Pd/C catalyst [126].
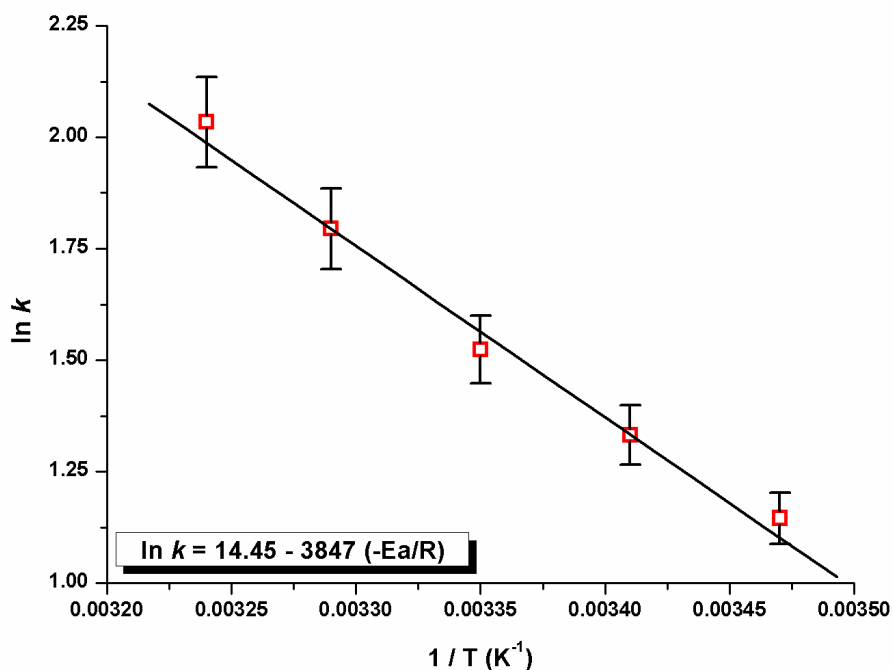


**Figure 64**. The Arrhenius plot for the zeolite framework stabilized ruthenium(0) nanoclusters catalyzed hydrogenation of neat benzene.

The Eyring-Polonyi plot of zeolite framework stabilized ruthenium(0) nanoclusters catalyzed neat benzene hydrogenation (Figure 65) gives the activation enthalpy activation enthalpy, $\Delta H^{\#} = 32 \pm 2$ kJ/mol; and activation entropy, $\Delta S^{\#} = -139 \pm 4$ J/K· mol and these values are indicative of associative mechanism as observed other heterogeneous catalysts mediated benzene hydrogenation [127].

**Figure 65**. The Eyring-Polonyi plot for the zeolite framework stabilized
ruthenium(0) nanoclusters catalyzed hydrogenation of neat benzene.

## 3.4.4. The Catalytic Lifetime of Zeolite Framework Stabilized Ruthenium(0) Nanoclusters in the Hydrogenation of Neat Benzene

The catalytic lifetime of zeolite framework stabilized ruthenium(0)
nanoclusters in the hydrogenation of neat benzene was determined by measuring the
total turnover number (TTO). Figure 66 shows the loss of benzene amount (in mmol)
versus time (h) in the catalytic lifetime experiments of zeolite framework stabilized
ruthenium(0) nanoclusters in the hydrogenation of neat benzene starting with 3 mL
(33.6 mmol benzene) and 4.6 mM zeolite framework stabilized ruthenium(0)
nanoclusters at $22 \pm 0.1$ °C and $40 \pm 1$ psig initial $H_2$ pressure.

96
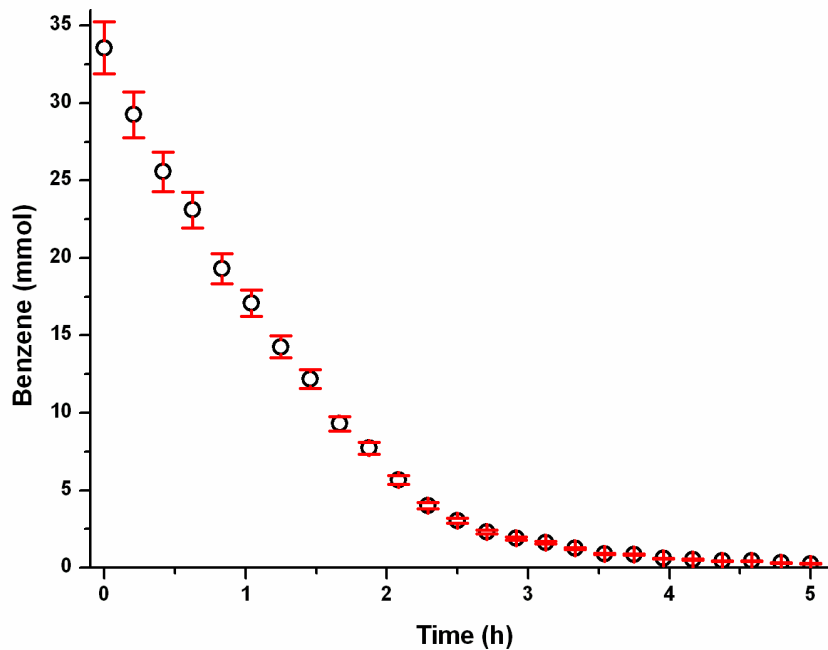
**Figure 66**. Graph of benzene consumption versus time for the zeolite framework stabilized ruthenium(0) nanoclusters catalyzed hydrogenation of neat benzene (3 mL benzene and [Ru] = 4.6 mM) at $22 \pm 0.1$ °C and $40 \pm 1$ psig initial $H_2$ pressure and >720 rpm stirring speed.

They provide a TTON of 2420 mol benzene / mol Ru and and a TOF value of 1040 mol benzene / mol Ru· h which remains almost constant during the reaction up to 90 % benzene conversion (Figure 66).The catalytic activity and the lifetime of zeolite framework stabilized ruthenium(0) nanoclusters are indisputably superior to those obtained for the hydrogenation of benzene under mild conditions (*see* Table 2).

**Table 2.** The top seventeen, best catalyst systems in terms of the activity measurable shown in the table tabulated from a SciFinder literature search of "benzene hydrogenation" (>1900 citations) refined by "benzene hydrogenation at room temperature" (~95 hits), with those seventeen studies arranged chronologically.

| entry | precatalyst | conditions [t (°C) / $P_{H2}$ / solvent] | TTON | TOF | Reference |
|---|---|---|---|---|---|
| 1 | [RhCl(1,5-hexadiene)]$_2$ | 20 °C / 1 atm / water | - | - | [128] |
| 2 | [Rh(COD)Cl]$_2$ | 25 °C / 1 atm / neat | - | 16 | [129] |
| 3 | [Rh(COD)H]$_4$ | 25 °C / bubbling / neat | - | - | [130] |
| 4 | Rh(0) NP's | 20 °C / 1 atm / water | - | 57 | [131] |
| 5 | Rh(0) NP's | 20 °C / 1 atm / water | - | 90 | [132] |
| 6 | Rh(0) NP's | 20 °C / 1 atm / water | 300 | 84 | [133] |
| 7 | [(Cp*)Zr(CH$_3$)$_3$]@Al$_2$O$_3$ | 25 °C / 1 atm / neat | - | 960 | [134] |
| 8 | Ir(0) NP's | 25 °C / 2.7 atm / neat | - | 375 | [135] |
| 9 | Rh(0) NP's | 22 °C / 1 atm / hexane | - | 600 | [136] |
| 10 | Ru(0) NP's | 20 °C / 30 atm / neat | - | 268 | [137] |
| 11 | Rh(0) NP's | 20 °C / 1 atm / water | - | 114 | [138] |
| 12 | Ru(0) NP's | 20 °C / 1 atm / water | - | 24 | [139] |
| 13 | Ru(0) NP's | 20 °C / 2.1 atm / water | - | 600 | [140] |
| 14 | Rh/AlO(OH) | 25 °C / 1 atm / hexane | - | 690 | [141] |
| 15 | Intrazeolite Ru(0) NC's | 22 °C / 2.7 atm / neat | **2420** | **1040** | [142] |
| 16 | Rh(0) NP's | 25 °C / 1 atm / water | - | 300 | [143] |
| 17 | Rh(0) NC's@CNT | 25 °C / 10 atm / neat | - | 1038 | [144] |

**3.4.5. The Isolability and Reusability of Zeolite Framework Stabilized Ruthenium(0) Nanoclusters in the Hydrogenation of Neat Benzene**

The zeolite framework stabilized ruthenium(0) nanoclusters were also tested for their isolability, bottleability and reusability. After the complete hydrogenation of benzene catalyzed by zeolite framework stabilized ruthenium(0) nanoclusters, the catalyst was isolated as black powder by evaporating the volatiles in vacuum and further dried under $N_2$ purging at room temperature. Black samples of zeolite framework stabilized ruthenium(0) nanoclusters were bottled under nitrogen atmosphere and found to be stable for months of storage.
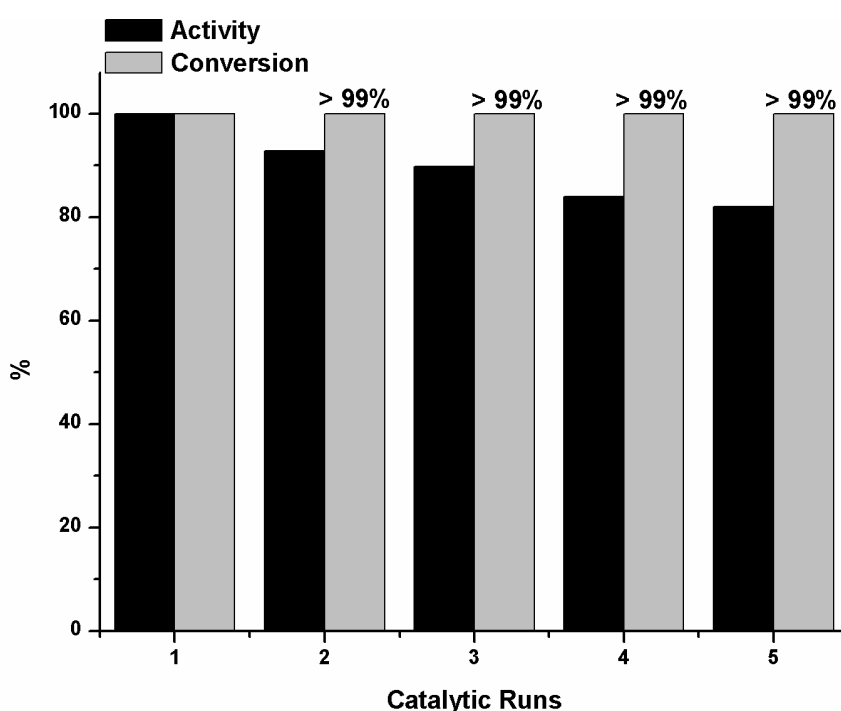


**Figure 67**. The percentage of catalytic activity retained and conversion of benzene (0.80 mL benzene corresponding to 8.96 mmol) to cyclohexane in the successive catalytic runs for zeolite framework stabilized ruthenium(0) nanoclusters catalyzed hydrogenation of neat benzene ([Ru] = 11.8 mM) at $22.0 \pm 0.1$ °C with $40 \pm 1$ psig of initial $H_2$ pressure and > 720 rpm stirring speed.

The isolated zeolite framework stabilized ruthenium(0) nanoclusters are redispersible in benzene, and yet still active catalyst in the hydrogenation of neat benzene. Figure 67 shows the percentage of catalytic activity retained in the successive catalytic runs (after 1 day, 1 week, 15 days and 1 month) for zeolite framework stabilized ruthenium(0) nanoclusters catalyzed hydrogenation of neat benzene at $22.0 \pm 0.1$ °C. Zeolite framework stabilized ruthenium(0) nanoclusters retain 81 % of their initial activity and provides complete hydrogenation of neat benzene to cyclohexane even at the fifth run (after 1 month). The slight decrease in catalytic activity in subsequent runs may be due to passivation of nanoclusters and slight agglomeration of surface supported ruthenium(0) nanoclusters as evidenced by their TEM analysis (*see* Figure 77 in Appendix). Additionally, it should be noted that the crystallinity of the host material retains its stability as proved by XRD analysis (*see* Figure 78 in Appendix).

### 3.4.6. Leaching Test of Zeolite framework stabilized Ruthenium(0) Nanoclusters in the Hydrogenation of Neat Benzene

In a control experiment, no ruthenium was detected (by ICP, detection limit 24 ppb for Ru) in the filtrate obtained by filtration of the reaction mixture after the first run of hydrogenation. The hydrogenation experiment of fresh benzene performed by using the filtrate as catalyst, no hydrogen uptake was observed over 12 hours. These experiments confirm the stability of ruthenium(0) nanoclusters, which retains within the zeolite matrix (no ruthenium passes into the solution during the suction filtration). Another control experiment was also performed to show that the hydrogenation of benzene is completely stopped by the removal of zeolite framework stabilized ruthenium(0) nanoclusters.

### 3.4.7. $P(C_6H_{11})_3$ and $PC_6H_{11}O_3$ Poisoning of Intrazeolite Ruthenium(0) Nanoclusters in the Hydrogenation of Neat Benzene

It is crucial in zeolite confined metal particle catalysis to know the percentage of catalytically active sites present on the external surface and/or inside the host material. In our case, the slow hydrogenation of mesitylene as discussed in the section of (**3.4.2.**) indicates that some ruthenium(0) nanoclusters locate on the surface of zeolite-Y as the kinetic diameter of mesitylene is larger than the supercage aperture of zeolite-Y and its hydrogenation can not be catalyzed by ruthenium(0) nanoclusters present in the cages of zeolite-Y.

To investigate the distribution of ruthenium(0) nanoclusters on the external surface or within the cages of zeolite-Y, a series of poisoning experiments for the Ru(0)/NaY catalyzed hydrogenation of neat benzene were performed by using two different phosphine ligands as poison; tricyclohexylphosphine ($P(C_6H_{11})_3$), and 4-ethyl-2,6,7-trioxa-1-phosphabicyclo[2.2.2]octane ($P(OCH_2)_3CCH_2CH_3$ or shortly $PC_6H_{11}O_3$), having kinetic diameters of 10.9 Å and 4.6 Å, respectively (Figure 68) [145].



(a)          (b)
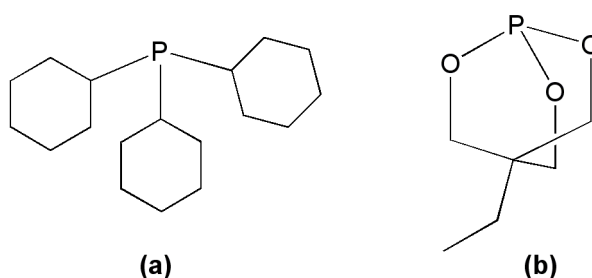
**Figure 68.** The structures of tricyclohexylphosphine ($P(C_6H_{11})_3$), and 4-ethyl-2,6,7-trioxa-1-phosphabicyclo[2.2.2]octane ($P(OCH_2)_3CCH_2CH_3$).

The hydrogenation of neat benzene catalyzed by zeolite framework stabilized ruthenium(0) nanoclusters was conducted in the presence of phosphine ligand in

various phosphine/ruthenium molar ratio at $22.0 \pm 0.1$ °C. The initial rate of benzene hydrogenation was determined in each of independent experiments at various phosphine/ruthenium ratios and divided by the hydrogenation rate of neat benzene in the absence of phosphine at $22.0 \pm 0.1$ °C to obtain the relative activity (initial rate of benzene hydrogenation in the presence of poison over the one in the absence of poison). Figure 69 shows the plots of relative hydrogenation rate of neat benzene versus the phosphine/ruthenium molar ratio for both of the phosphine poisons.



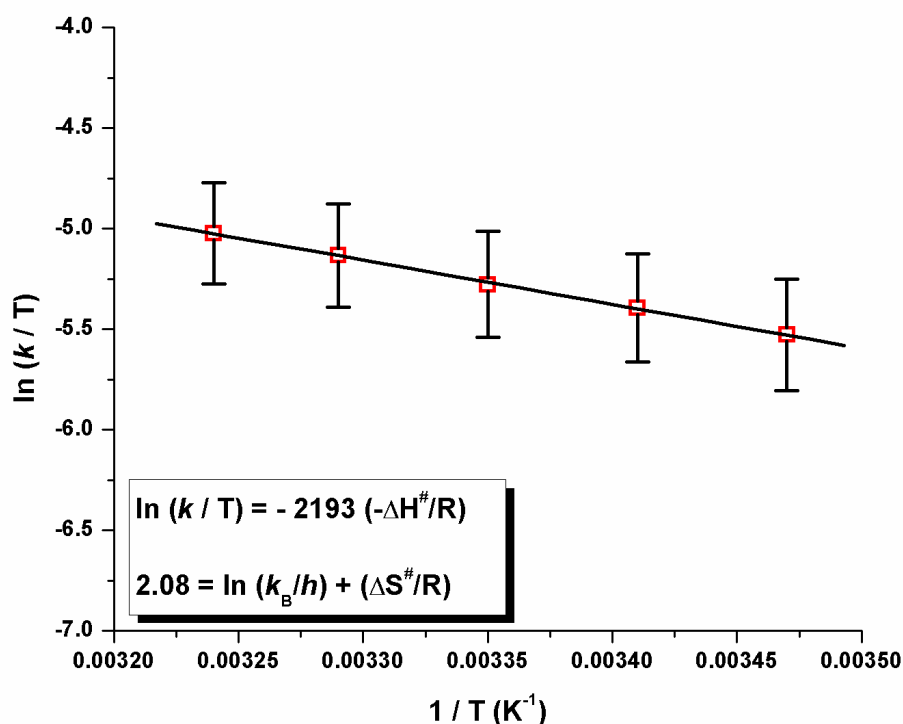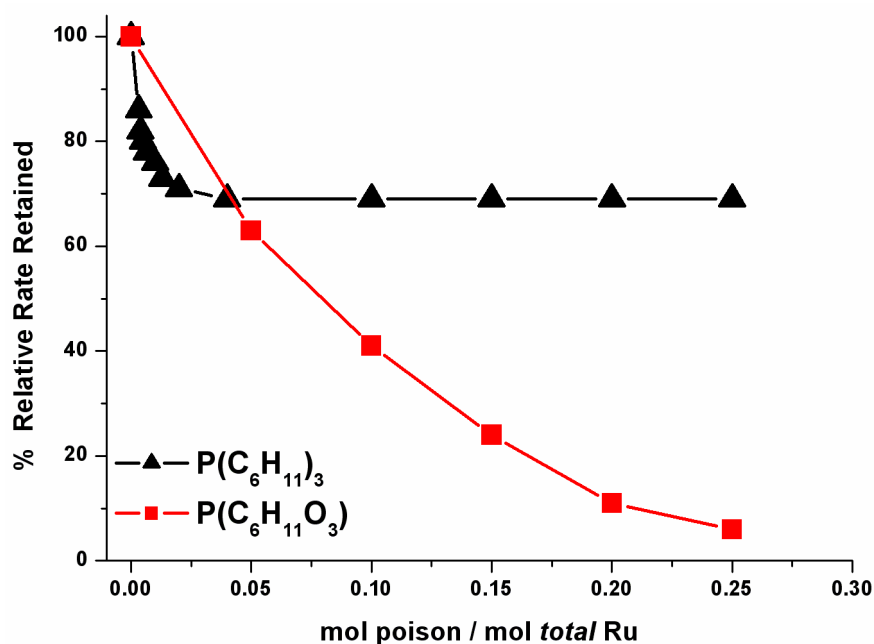**Figure 69**. Plot of percent relative rate retained versus the poison/Ru molar ratio for the zeolite framework stabilized ruthenium(0) nanoclusters catalyzed hydrogenation of neat benzene in the presence of $P(C_6H_{11})_3$ or $PC_6H_{11}O_3$ at $22.0 \pm 0.1$ °C with $40 \pm 1$ psig of initial $H_2$ pressure and $> 720$ rpm stirring speed.

In the hydrogenation experiments performed in the presence of $PC_6H_{11}O_3$ the catalytic activity of zeolite framework stabilized ruthenium(0) nanoclusters decreases almost linearly with the increasing concentration of phosphine and the hydrogenation of neat benzene stops when 0.25 equivalents of $PC_6H_{11}O_3$ per ruthenium is added to benzene (Figure 69). The observation that the benzene hydrogenation is completely

poisoned by less than 1 equivalent of phosphine is a compelling evidence for that it is a heterogeneous catalysis [146,147].

In poisoning experiments with $P(C_6H_{11})_3$ the activity of the catalyst in the hydrogenation of neat benzene also decreases initially with the increasing phosphine/ruthenium molar ratio up to 0.04, then remains unchanged beyond this ratio. The dissimilarity of two phosphine ligands in poisoning the zeolite framework stabilized ruthenium(0) nanocluster catalyst in the hydrogenation of neat benzene arises from the size difference. While the small phosphine $PC_6H_{11}O_3$ (kinetic diameter is 4.6 Å) can readily enter the supercages through the 7.4 Å aperture of zeolite-Y [77], the large phoshine $P(C_6H_{11})_3$ (kinetic diameter is 10.9 Å) cannot enter the zeolite cages, thus, remain outside. Therefore, the large $P(C_6H_{11})_3$ can poison only the ruthenium(0) nanoclusters on the external surface of zeolite, while the small $PC_6H_{11}O_3$ deactivates all the ruthenium(0) nanoclusters in the cavities and on the external surface of zeolite. The results of the poisoning experiments given in Figure 61 indicate that the zeolite framework stabilized ruthenium(0) nanoclusters sample has 31 % of catalytically active ruthenium(0) nanoclusters on the external surface of zeolite-Y and 69 % in the cavities of zeolite-Y.

# CHAPTER 4

## CONCLUSIONS

In summary, our study of the preparation and characterization of zeolite framework stabilized ruthenium(0) nanoclusters catalyst for the hydrolysis of sodium borohydride and the hydrogenation of arenes has led to the following conclusions and insights;

- Zeolite framework stabilized ruthenium(0) nanoclusters were prepared by a novel and simple method comprising the ion-exchange of $Ru^{3+}$ ions with the extra framework $Na^+$ ions in zeolite-Y, followed by reduction of the $Ru^{3+}$ ions in the cavities of zeolite-Y with sodium borohydride in aqueous solution at room temperature.

- The characterization of zeolite framework stabilized ruthenium(0) nanoclusters by using using ICP-OES, XRD, TEM, HR-TEM, TEM-EDX, SEM, XPS, DR-UV-vis, far-IR, mid-IR, Raman spectroscopy and $N_2$ adsorption-desorption technique reveals the formation of ruthenium(0) nanoclusters mostly within the cavities of zeolite-Y whereby the host material retains its crystallinity and microporous stability.

- The far-IR analyses of zeolite-Y, ruthenium(III)-exchanged zeolite-Y and the zeolite framework stabilized ruthenium(0) nanoclusters showed that the sodium cation site distribution in the zeolite is essentially restored upon reduction of ruthenium(III) by sodium borohydride. The cation sites left by $Ru^{3+}$ upon reduction are reoccupied by $Na^+$ cations coming from sodium borohydride. Hence, the host framework retains its integrity including the cation sites

104

population after the generation of ruthenium(0) nanoclusters within the supercages of zeolite-Y.

- Zeolite framework stabilized ruthenium(0) nanoclusters formed in-situ during the hydrolysis of sodium borohydride provide a record TTO of 103200 mol $H_2$ / mol Ru and TOF up to 33000 mol $H_2$ / mol Ru · h in this reaction at room temperature. Recall that the prior best catalyst has a TTO of 5170 [98].

- Importantly, the zeolite framework stabilized ruthenium(0) nanoclusters have also outstanding catalytic activity in the range of 34-64 mL $H_2$ / min, even at low catalyst concentrations (0.50-1.50 mM Ru, respectively) and room temperature in the hydrolysis of sodium borohydride in basic medium (5 wt %).

- Working in basic solution expectedly causes a decrease in the catalytic activity and lifetime of the zeolite framework stabilized ruthenium(0) nanoclusters. However, they show still unprecedented catalytic lifetime providing a TTO of 27200 mol $H_2$ / mol Ru and TOF up to 4000 mol $H_2$/mol Ru · h in the hydrolysis of sodium borohydride in basic medium (5 % wt NaOH solution) at room temperature.

- The kinetic studies of the zeolite framework stabilized ruthenium(0) nanoclusters catalyzed hydrolysis of sodium borohydride perfomed separately in aqueous and basic (5 wt % NaOH) solution (Eq. 8) reveal the following rate law for this catalytic reaction in both medium;

$$NaBH_4 + 2H_2O \xrightarrow[\text{at RT in } H_2O \text{ or 5 \% wt NaOH solution}]{\text{intrazeolite ruthenium(0) nanoclusters}} NaBO_2 + 4H_2 \qquad (8)$$
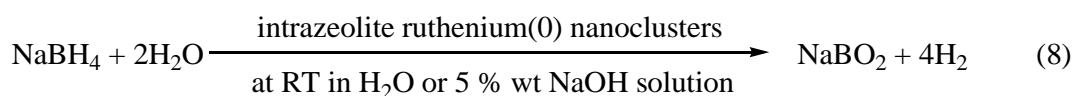
$$-\frac{4d[\text{NaBH}_4]}{dt} = \frac{d[\text{H}_2]}{dt} = k[\text{Ru}][\text{NaBH}_4]^{\alpha} \quad (9)$$

$$\alpha = 0 \text{ for } [\text{NaBH}_4] < 0.6\,\text{M} \qquad\qquad (10)$$

$$\alpha \neq 0 \text{ for } [\text{NaBH}_4] > 0.6\,\text{M} \qquad\qquad (11)$$

- The activation energies for the zeolite framework stabilized ruthenium(0) nanoclusters catalyzed hydrolysis of sodium borohydride in aqueous and basic medium were found to be $49 \pm 2$ kJ/mol and $34.9 \pm 2$ kJ/mol, respectively and both of them are lower than those found under the same conditions for the hydrolysis of sodium borohydride catalyzed by bulk ruthenium; 56 kJ/mol in aqueous medium [99] and 47 kJ/mol in basic medium [107].

- The activation enthalpy ($\Delta H^{\#}$) and activation entropy ($\Delta S^{\#}$) of zeolite framework stabilized ruthenium(0) nanoclusters catalyzed hydrolysis of sodium borohydride were found to be $\Delta H^{\#} = 48 \pm 2$ kJ/mol (in aqueous medium) and $32 \pm 2$ kJ/mol (in basic solution); and the activation entropy, $\Delta S^{\#} = -82 \pm 4$ J/K·mol (in aqueous medium) and $139 \pm 4$ J/K·mol (in basic solution). These values imply on an associative mechanism for the zeolite framework stabilized ruthenium(0) nanoclusters catalyzed hydrolysis of sodium borohydride in both aqueous and basic medium.

- Testing the reusability of zeolite framework stabilized ruthenium(0) nanoclusters in the hydrolysis of sodium borohydride shows that the complete release of hydrogen is achieved in both aqueous and basic media even in successive runs performed by redispersing the zeolite framework stabilized ruthenium(0) nanoclusters isolated after the previous run. Thus, the zeolite framework stabilized ruthenium(0) nanoclusters are isolable, bottleable, and redipersible. When redispersed they retain 76 % or 61 % of their initial catalytic activity in

aqueous and basic solution, respectively, at the fifth run with a complete release of hydrogen.

- The isolated and vacuum dried samples of zeolite framework stabilized ruthenium(0) nanoclusters are also found to be highly active catalyst in the hydrogenation of cyclohexene, benzene, toluene and *o*-xylene in cyclohexane, they provide TOF values of 6150, 5660, 3200, and 1550 mol $H_2$/mol Ru·h, respectively under mild conditions (at $22.0 \pm 0.1$ °C, and $40 \pm 1$ psig of initial $H_2$ pressure).

- More importantly, they are the lowest temperature, most active, highest selective at high conversion (100 % selectivity with complete conversion) and longest lifetime catalyst yet reported for the hydrogenation of neat benzene to cyclohexane. They provide a record TTON of 2420 and TOF of 1040 mol benzene/mol Ru·h in this ubiquitous chemical transformation (*see* Table 1 *vide supra*).

- Moreover, the ruthenium(0) nanoclusters exhibit high durability throughout their catalytic use in the hydrogenation reaction against agglomeration and leaching. This significant property makes them reusable catalyst in the hydrogenation of olefins and arenes without appreciable loss of their inherent activity. Expectedly, the complete hydrogenation of neat benzene is achieved even in successive runs performed by redispersing zeolite framework stabilized ruthenium(0) nanoclusters isolated after the previous run. When redispersed they retain 82 % of their initial catalytic activity at the fifth run with a complete hydrogenation of benzene into cyclohexane.

- It is also noteworthy that XRD and TEM analyses of the zeolite framework stabilized ruthenium(0) nanoclusters recovered at the end of the fifth run of benzene hydrogenation reveal (*i*) no loss in the crystallinity of the host material, (*ii*) no sintering or migration of ruthenium(0) nanoclusters stabilized by zeolite framework throughout their catalytic cycles.

-

- The kinetic studies for the zeolite framework stabilized ruthenium(0) nanoclusters catalyzed hydrogenation of neat benzene depending on temperature and ruthenium concentration show that (*i*) zeolite framework stabilized ruthenium(0) nanoclusters can achieve the complete hydrogenation of benzene to cyclohexane even at low temperature (15.0 ± 0.1 °C) low Ru amount (0.002 mmol Ru), (*ii*) the catalytic hydrogenation of neat benzene (Eq. 12) proceeds in first order with respect to ruthenium concentration (Eq. 13),
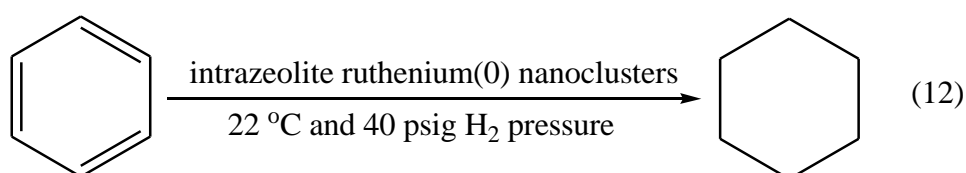


$$-\frac{3d\,[\text{Benzene}]}{dt} = -\frac{d\,[\text{H}_2]}{dt} = k\,[\text{Ru}] \quad (13)$$

(*iii*) zeolite framework stabilized ruthenium(0) nanoclusters provides very low activation energy (32 ± 1 kJ/mol) with respect to the majority of heterogeneous catalyst tested in the hydrogenation of neat benzene, (*iv*) the determined activation parameters (activation enthalpy, $\Delta H^{\#} = 32 \pm 2$ kJ/mol; and activation entropy, $\Delta S^{\#} = -139 \pm 4$ J/K· mol) are indicative of the associative mechanism in the transition state for the zeolite framework stabilized ruthenium(0) nanoclusters catalyzed hydrogenation of neat benzene.

- Furthermore, zeolite framework stabilized ruthenium(0) nanoclusters catalyzed hydrogenation of neat benzene system is "relatively green" in its environmental impact in that it satisfies 7 of the 12 proposed principles of green chemistry [148] including that (*i*) it is 100% selective thus minimizing the byproducts or waste, (*ii*) it maximizes the incorporation of all reactants into the products, (*iii*) it is solventless (i.e., uses neat benzene as the substrate/solvent), (*iv*) it needs relatively low energy requirements due to its low temperature of 22.0 ± 0.1 °C

and low pressure of ≤ 3 atm, (*v*) it is catalytic not stoichiometric, (*vi*) it does not use any blocking, protecting/deprotecting group, (*vii*) real-time monitoring is easy by following the $H_2$ pressure loss or $^1$H NMR, for example.

- The slow hydrogenation rate observed in the zeolite framework stabilized ruthenium(0) nanoclusters catalyzed hydrogenation of mesitylene (TOF = 135 mol $H_2$/mol *total* Ru•h)  implies that some ruthenium(0) nanoclusters locate on the surface of zeolite-Y as the kinetic diameter of mesitylene is larger than the supercage aperture of zeolite-Y and its hydrogenation can not be catalyzed if all ruthenium(0) nanoclusters located inside the cages of zeolite-Y.

- To investigate the distribution of ruthenium(0) nanoclusters on the external surface or within the cages of zeolite-Y a series of poisoning experiments in the zeolite framework stabilized ruthenium(0) nanoclusters catalyzed hydrogenation of neat benzene were performed by using two different phosphine ligands as poison;  tricyclohexylphosphine ($P(C_6H_{11})_3$), and 4-ethyl-2,6,7-trioxa-1-phosphabicyclo[2.2.2]octane ($PC_6H_{11}O_3$),  having kinetic diameters of  10.9 Å and 4.6 Å, respectively. The result of these experiments showed that 31 % of catalytically active ruthenium(0) nanoclusters are on the external surface, which most probably migrated to the external surface during the drying process (performed at $10^{-3}$ torr) of zeolite framework stabilized ruthenium(0) nanoclusters, whereas 69 % of them locate inside the zeolite-Y.

- The superb catalytic activity and the outstandingly long lifetime of zeolite framework stabilized ruthenium(0) nanoclusters catalyst in both aqueous and organic medium result from (*i*) small size of the nanoclusters within the zeolite cages, (*ii*) the fact that nanoclusters are partially free, since they interact only on one side with internal surface of zeolite. The fact that the channels of Zeolite-Y remain open is a propensity of the catalytic reactions that do not produce any substance.The high catalytic activity, easy preparation, isolability, bottleability, and reusability of zeolite framework stabilized ruthenium(0) nanoclusters raise the prospect of using this type of simply prepared catalytic material for possible industrial applications as well as in small scale organic synthesis.

# REFERENCES

[1]     Pool, R., *Science*, **1990**, 248, 1186.

[2]     Aiken III J.D., Lin, Y., Finke R.G., *J. Mol. Catal. A,* **1996,** 114, 29.

[3]     Feldheim, D. R., Foss Jr, C. A. (Eds.), *Metal Nanoparticles: Synthesis, Characterization, and Applications*, Marcel Dekker, NewYork, **2002**.

[4]     Schmid, G. (Ed), *Clusters and Colloids: From Theory to Applications*, VCH Publishers, New York, **1994.**

[5]     Jongh, L.J.(Ed), *Physics and Chemistry of Metal Cluster Compounds*, Kluwer Publishers, Dordrect, **1994.**

[6]     Simon, U., Schön, G., Schmid, G., *Angew Chem. Int. Ed. Eng*., **1990**, 248, 1186.

[7]     Glanz, J., *Science*, **1995**, 269, 1363.

[8]     Antonietti, M.; Göltner, C.;  *Angew Chem. Int. Ed. Eng.*, **1997**, 36, 910.

[9]     Elghanian, R.; Storhoff, J.J.; Mucic, R.C.; Setinger, R.L.; Mirkin, C.A.; *Science*, **1997**, 277, 1078.

[10]    Colvin, V.L., Schlamp, M.C., Alivisatos, A.P., *Nature*, **1994**, 370, 354.

[11]    Sonti, S.V., Bose, A., *J. Colloid Int. Sci*., **1995**, 170, 575.

[12]    Vossmeyer, T., Delenno, E., Heath, J.R., *Angew. Chem., Int. Ed. Eng*., **1997**, 36, 1080.

[13]    (a) Schmid, G., Maihack, V., Lantermann, F., Pechel, S., *J. Chem. Soc. Dalton Trans.*, **1996**, 199, 589. (b) Lin, Y., Finke, R. G., *J. Am. Chem. Soc.*, **1994**, 116, 8335. (c) Bönneman, H.; Braun, G.A., *Angew Chem. Int. Ed. Eng.*, **1996**, 35, 1992. (d) Lewis, L.N.; Lewis, N., *J. Am. Chem. Soc.*, **1986**, 108, 7228. (e) Wilcoxon, J.P.; Martinho, T.; Klavetter, E.; Sylwester, A.P., *Nanophase Mater.* **1994**, 771. (f) Na, Y.; Park, S.; Bong, S.H.; *J. Am. Chem. Soc.*, **2004**, 126, 250. (g) Pelzer, K.; Vidoni, O.; Phillot, K.; Chaudret, B.; Colliére, V., *Adv. Func. Mater.*, **2003**, 12, 118. (h) Hostetler, M.; Wingate, J.; Zong, C.; Evans, N.; Murray, R., *Langmuir*, **1998**, 14, 17-30 (ı) Pelzer, K.; Phillot, K.; Chaudret, B., *Z. Anorg. Allg. Chem.*, **2003,** 629, 1217.

[14]    Schmid, G., *Chem. Rev.*, **1992**, 92, 1709.

[15]    (a) Schmid, G., Bäumle, M., Geerkens, M., Heim, I., Osemann, C., Sawitowski, T., *Chem. Soc. Rev.*, **1999**, 128, 79.

[16]    Verwey, E. J. W., Overbeek, J. T. G., *Theory of the Stability of Lyophobic Colloids*, Dover Publications: Mineola, New York, **1999**.

[17]    Ninham, B. W., *Adv. Coll. Int. Sci.*, **1999**, 83,

[18]    Ott, L. S., Hornstein, B. J., Finke, R. G., *Langmuir*, **2006**, 22, 9357.

[19]    Zahmakiran, M., Özkar, S., *Inorg. Chem.*, **2009**, 48, 8955.

[20]    Leger, B., Denicourt-Lowicki, A., Roucoux, A., Olivier-Barbique, H., *Adv. Synth. Catal.*, **2008**, 350, 153.

[21]    Bidan, O., Phillippot, K., Amiens, C., Chaudret, B., Balmes, O., Balm, O. J., Senocq, F., Casanove, M. J., *Angew. Chem. Int. Ed.*, **1999**, 38, 3736.

[22]    Willner, I., Mandler, D., *J. Am. Chem. Soc.*, **1989**, 111, 1330

[23]     Bönneman, H., Richards, R. M., *Eur. J. Inorg. Chem.*, **2001**, 10, 2445

[24]    (a) Tano, T., Esumi, K., Meguro K., *J. Colloid Interface Sci.*, **1989**, 133, 530. (b) Esumi, K., Tano, T., Meguro, K., *Langmuir*, **1989**, 5, 268. (c) Dhas, N. A., Suslick, K. S., *J. Am. Chem. Soc.*, **2005**, 127, 2368. (d) Suslick, K A., Choe, S.-B., Cichowias, A. A., Grinstaff, M. W., *Nature*, **1991**, 353, 414.

[25]    Duteil, A., Queau, R., Chaudret, B., Mazel, R., Roucau, C., Bradley, J. S., *Chem. Mater.*, **1993**, 5, 341

[26]    Klabunde, K. J., Habdas, J., Cardenas-Trivino, G., *Chem. Mater.*, **1989**, 1, 481.

[27]    (a) Reetz, M. T., Helbig, W., Quaiser, S. A., *In Active Metals:Preparation, Characterization, Applications*, VCH: New York, **1996**. (b) Reetz, M. T., Helbig, W., *J. Am. Chem. Soc.*, **1994**, 116, 7401.

[28]    Smith, G. V., Notheisz, F., *Heterogeneous Catalysis in Organic Chemistry*; Academic Press, San Diego, **1999**.

[29]    Gates, B. C., *Catalytic Chemistry*; Academic Press: New York,**1992**.

[30]    Thomas, J. M., Thomas, W. J., *Principles and Practice of Heterogeneous Catalysis*, VCH, New-York, **1997**.

[31]    Anthonsen, T., *Reactions Catalyzed by Enzymes In Applied Biocatalysis*, 2. Harwood Academic Publishers, UK, **1999**.

[32]    Grassian, V. H., *J. Phys. Chem. C*, **2008**, *112,* 18303.

[33]    Richards, R. M., *Surface and Nanomolecular Catalysis*, Taylor & Francis, **2006**, Boca Raton.

[34]    Klabunde, K. J., Stark, J., Koper, C., Park, D., *J. Phys. Chem.*, **1996**, 100, 12142.

[35]    Schmid, G., *Endeavour*, **1990**, 14, 172.

[36]    Van Den Berg, J. P., Lucien, J. P., Germaine, G., Thielemans, G. L. B., *Fuel Processing Technology.* **1993**, *35*, 119.

[37]    Corma, A., Martínez, A., Martínez-Soria, V., *Journal of Catalysis*, **2001**, *200*, 259.

[38]    Bönnemann, G. A., Braun, G. A., *Angew. Chem. Int. Ed.*, **1996**, 35,.1992.

[39]    Lewis, L. N., Lewis, N., *J. Am. Chem. Soc.*, 108, **1986**, 7228–7231

[40]    Schmidt, T. J., Noeske, M., Gasteiger, H.A., Behm, R. J., Britz, P., Brijoux, W., Bönnemann, H., *Langmuir*, 13, **1997**, 2591.

[41]    Reetz, M.T., Quaiser, S.A., Merk, C., *Chem. Ber.*, **1996**, 129, 741.

[42]    Reetz, M. T., Breinbauer, R., Wanninger, K., *Tetra. Lett.*, **1996**, 37, 4499.

[43]    Reetz, M.T., Lohmer, G., *J. Chem. Soc. Chem. Comm.*, **1996**, 1921.

[44]    Reetz, M.T., Breinbauer, R., Wedemann, P., Binger, P., *Tetrahedron*, **1998**, 54, 1233.

[45]    Cronstedt, A. F., *Akad. Handl. Stockholm*, **1756**, 18, 120.

[46]    Baerlocher, C. H., Meier, W. M., Olson, D. H., *Atlas of Zeolite Framework Types*, 5th revised edition, Elsevier, Amsterdam, **2001**.

[47]    Kern, D., Schall, N., Schmidt, W., Schmoll, R., Schürtz, J., Winnacker-Küchler,S., *Chemische Technik, Prozesse und Produkte*, Vol. 3, Wiley-VCH., Siliciumverbindungen, **2005**.

[48]    Bhatia, S. *Zeolite Catalysis: Principles and Applications*, CRC Press, Florida, **1989**.

[49]    Özkar, S., Finke, R. G., *J. Am. Chem. Soc.*, 2002, 124, 5796.

[50]  Özkar, S., Finke, R. G., *Langmuir*, **2003**, 19, 6247.

[51]  (a) Kawi, S., Chang, J. R., Gates, B. C., *J. Am. Chem. Soc.* **1993**, 115, 4830. (b) Zhang, W., Shi, J., Wang, L., Yang, D., *Chem. Mater.* **2000**, 12, 1408. (c) Grubert, G., Stockenhuber, M., Tkachenko, O. P., Wark, M., *Chem. Mater.* **2002**, 14, 2458. (d) Zhang, L. X., Shi, J. L., Yu, J., Hua, Z. L., Zhao, X. G., Ruan, M. L., *Adv. Mater.* **2002**, 14, 1510. (e) Yang, C., Liu, P., Ho, Y., Chiu, C., Chao, K., *Chem. Mater.* **2003**, 15, 275. (f) Knya, Z., Puntes, V. F., Kiricsi, I., Zhu, J., Ager, J. W., Ko, M. K., Frei, H., Alivisatos, P., Somorjai, G. A., *Chem. Mater.* **2003**, 15, 1242.

[52]  Tosheva, L., Valtchev, V. P., *Chem. Mater*., **2005**, 17, 2494.

[53]  (a) Tzou, M., S., Teo, B. K., Sachtler, W. M. H., *J. Catal.*, **1988**, 113, 220. (b) Homeyer, S. T., Sachtler, W. M. H., *J. Catal.*, **1989**, 117, 91. (c) Homeyer, S. T., Sachtler, W. M. H., *J. Catal.*, **1989**, 118, 266. (d) Feeley, J. S., Sachtler, W. M. H., *J. Catal.*, **1991**, 131, 573. (e) Zhang, Z., Zhang, Y. D., Hines, W. A., Budnick, J. I., Sachtler, W. M. H., *J. Am. Chem. Soc.* **1992**, 114, 4834.

[54]  Ryoo, R., Cho, S. J., Pak, C. H., Kim, J. G., Ihm, S. K., Lee, J. Y., *J. Am. Chem. Soc.* **1992**, 114, 76.

[55]  de Graaf, J., van Dillen, A. J., de Jong, K. P., Koningsberger, D. C., *J. Catal*., **2001**, 203, 307.

[56]   Ryoo, R., Jung, S.M., Cho, S.J., Shul, Y.G., *J. Phys. Chem.*, **1992**, 96, 9922.

[57]  Apple, T., Shoemaker, R., *J. Phys. Chem.*, **1987**, 91, 4024

[58]  *Basic Research Needs For the Hydrogen Economy, Report of the Basic Energy Sciences Workshop on Hydrogen Production, Storage and Use*, , **2003**, Office of Science, U.S. Department of Energy: Washington, DC, www.sc.doe.gov/bes/hydrogen.pdf (12/04/2010)(b) Turner, J., Sverdrup, G., Mann, K., Maness, P. G., Kroposki, B., Ghirardi, M., Evans, R. J., Blake, D.,

*Int. J. Energy Res*., **2007**, 32, 379. (c) *IAC Report. Lighting the Way towards a Sustainable Energy Future*, Interacademy Council, Amsterdam, **2007**.

[59]   Grochala, W., Edwards, P. P., *Chem. Rev*. **2004**, 104, 1283.

[60]   *Annual Energy Outlook 2005 with Projections to 2025*, Energy Information Administration: Washington, DC, **2005**, [www.eia.doe.gov/oiaf/aeo/pdf/0383(2005).pdf](www.eia.doe.gov/oiaf/aeo/pdf/0383(2005).pdf) (12/04/2010).

[61]   Wee, J. H., Lee, K-Y., Kim, S. H., *Fuel Process. Technol.* **2006**, 87, 811

[62]   Amendola, S. C., Janjua, J. M., Spencer, N. C., Kelly, M. T., Petillo, P. J., Sharp-Goldman, S. L., Binder, M., *Int. J. Hydogen Energy*,  **2000**, 25, 969.

[63]   (a) Schlesinger, H. I., Brown, H. C., Finholt, A. E., Gilbreath, J. R., Hoekstra, H. R., Hyde, E. K., *J. Am. Chem. Soc.*, **1953**, 75, 215. (b) Davis, R. E., Swain, C. G., *J. Am. Chem. Soc.* **1960**, 82, 5950. (c) Levy, A., Brown, J. B., Lyons, C. J., *Ind. Eng. Chem.*, **1960**, 52, 211. (d) Brown, H. C., Brown, C. A,. *J. Am. Chem. Soc.* **1962**, 84, 1493. (e) Mesmer, R. E., Jolly, W. L., *Inorg. Chem.* **1962**, 1, 608. (f) Gardiner, J. A., Collatt, J. W., *J. Am. Chem. Soc.*, **1964**, 86, 3165. (g) Gardiner, J. A., Collatt, J. W., J. Am. Chem. Soc., **1965**, 87, 1692. (h) Sen, B., Kaufman, C. M., *J. Chem. Soc., Dalton Trans.* **1985**, 307, 64. (i) Kojima, Y., Kawai, Y., Suzuki, K. I., Fukumoto, K., Sasaki, M., Yamamato, T., Hayashi, H., *Int. J. Hydrogen Energy*, **2002**, 27, 1029. (j) Hanxi, Y., Hua, D., Xinping, A., Chuansin, C., *Int. J. Hydrogen Energy*, **2003**, 28, 1095. (k) Lee, J. Y., Kim, J. H., Han, S. C., Kim, H. S., Song, M. S., *Int. J. Hydrogen Energy* **2004**, 29, 263. (l) Wu, C., Wu, F., Bai, Y., Yi, B., Zhang, H., *Mater. Lett*. **2005**, 59, 1748. (m) Kim, J. H., Kim, K. T., Kang, Y. M., Kim, S. K., Song, M. S., Lee, Y. J., Lee, J. Y., *J. Alloys Compd.*, **2004**, 379, 222. (n) Yang, T. H., Krisshan, P., Lee, W. Y., Kim, C. S., *J. Power Sources*, **2005**, 143, 17. (o) Cho, K. W., Kwon, H. S., *Catal. Today*, **2007**,120, 298. (p) Zhang, H., Ye, W., Xu, D., Ma, L., Yi, B., *J. Power Sources*, **2007**, 164, 544.

(r) Patel, N., Guella, G., Kale, A., Miotello, A., Patton, B., Zanchetta, C., Mirenghi, L., Rotolo, P., *App Cat. A*, **2007**, 323, 18. (s) Keceli, E., ¨Özkar, S., *J. Mol. Catal. A*, **2008**, 286, 87. (t) Alonso, R. P., Sicurelli, A., Callone, E., Carturan, G., Raj, R., *J. Power Sources*, **2007**, 165, 315.

[64]    Larock, R. C., *Comprehensive Organic Transformations*, Willey-VCH, New-York, **1999**.

[65]    Augustine, R. L., *Heterogeneous Catalysis for the Synthetic Chemistry*, Marcel Dekker, New York, **1996**.

[66]    A SciFinder literature search confirms that ca. 95% of the reports of benzene hydrogenation catalysis employ high temperature and/or high pressure with only 5% (90 of >1900) hits refining according to the terms "benzene hydrogenation at room temperature".  Seventeen of the 95 hits report the complete (100%) hydrogenation of benzene without side products at room temperature and they were tabulated in Table 2.

[67]    (a) Schulz, J., Patin, H., Rouchoux, A., *Chem. Comm.*, **1999**, 535. (b) Schulz, J., Patin, H., Rouchoux, A., *Chem. Eur. Jour.*, **2000**, 6, 618. (c) Schulz, J., Patin, H.,  Rouchoux,  A., *Adv. Synth. Catal.*, **2003**, 345, 222.

[68]    Mevellec, V., Ramirez, E., Phillippot, K., Chaudret, B., Rouchoux, A., *Adv. Synth. Cat.*, **2004**, 346, 72.

[69]    Nowicki, A., Zhong, Y., Leger, B., Rolland, J. P.,  Bricout, H., Monflier, E., Rouchoux, A., *Chem. Comm.*, **2006**, 296.

[70]    Rouchoux, A., Phillippot, K., Payen, E., Granger, P., Dujardin, C., Nowicki, A., Mevellec, V., *New J. Chem.*, **2006**, 30, 1214.

[71]    Seeberger, M. H., Jones, R. A., *J. Chem. Soc. Chem. Comm.*, **1985**, 6, 373.

[72]    Park, I. S., Kwon, M. S., Kim, N., Lee, J. S., Kang, K. Y., Park, J., *Chem. Comm.*, **2005**, 5667.

[73]    Zhang, J., Xie, Z., Liu, Z., Wu, W., Han, B., Huang, J., Jiang, T., *Catalysis Letters* **2005**, 103, 59.

[74]    Nicholas, J. P., Ahn, H., Marks, T. J., *J. Am. Chem. Soc.*, **2003**, 125, 4325.

[75]    Hubert, C., Denicourt-Nowicki, A., Guégan, J.-P., Roucoux, A., *Dalton Trans.* **2009**, 7356.

[76]    Pan, H. B., Wai, C. M., *J. Phys. Chem. C*, **2009**, 113, 19782.

[77]    Breck, D.W *Zeolite Molecular Sieves* Krieger Malabal, FL. **1984**

[78]    Guella, G., Zanchetta, C., Patton, B., Miotello, A., *J. Phys. Chem. B*, **2006**, 110, 17024.

[79]    Hutchison, J. E., Woehrle, G. H., Özkar, S., Finke, R. G., *Turkish J. Chem.*, **2006**, 30, 1.

[80]    (a) Wagner, C., Riggs, W. M., Davis, L. E., Moulder, J. F., Muilenberg, G. E., *Handbook of X-ray Photoelectron Spectroscopy*; Physical Electronic Division, Perkin-Elmer, **1979**, Vol 55, p 344. (b) Park, K. W., Choi, J. H., Kwon, B. K., Lee, S. A., Sung, Y. E., Ha, H. Y., Hong, S. A., Kim, H., Lee, S. A., Sung, Y. A., Ha, H. Y., Hong, S. A., Kim, H., Wieckowski, A., *J. Phys. Chem. B*, **2002**, 106, 1869. (c) Nyholm, R., Maartensson, N., *Solid State Phys.*, **1980**, 13, L279; (d) Chakroune, N., Viau, G., Ammar, S., Poul, L., Veautier, D., Chehimi, M. M., Mangeney, C., Villain, C., Fievet, F., *Langmuir*, **2005**, 21, 6788.

[81]    Jiang, Y-X.,Weng, W-Z., Si, D., Sun, S-G., *J. Phys. Chem. B*, **2005**, 109, 7637.

[82]   Guczi, L., Bazin, D., *Appl. Catal., A* ,**1999**, 188, 163.

[83]   Fukuoko, A., Higashimoto, N., Sakamoto, Y., Inagaki, S., Fukushima, Y., Ichikawa, M., *Top. Catal*., **2002**, 18, 73.

[84]   Okitsu, K., Yue, A., Tanabe, S., Matsumoto, H., *Bull. Chem. Soc. Jpn.*, **2002**, 75, 449.

[85]   Korotcov, A. V., Huang , Y. S., Tiong , K. K., Tsai, D. S., *Journal of Raman Spectroscopy*, 2007, **38**, 737.

[86]   Triggs, P., Lévy, F., *Phys. Status Solidi B*, **2006**, 129, 363.

[87]   Taqui-Khan, M. M., Siddiqui, M. R., Amjad-Hussain, H., Moiz M. A., *Inorg. Chem.*, **1986**, 25, 2765.

[88]   Miyazaki, A, Balint, I., Aika, K., Nakano, Y., *J. Catal.*, **2001**, 204, 71.

[89]   Storck, S., Bretinger, H., Maier, W. F., *Appl. Catal. A*, **1998**, 174, 137 .

[90]   Mikhail, R. S. H., Brunauer, S., Bodor, E. E., *J. Colloid Interface Sci.*, **1968**, 26, 45.

[91]   Barrett, E. P., Joyner, L. G., Halenda, P. P., *J. Am. Chem. Soc.*, **1951**, 73, 373.

[92]   Wark, M., Kessler, H., Schulz-Ekloff, G., *Microporous Mater.*,**1997**, 8, 241.

[93]   Baker, M. D., Godber, J., Ozin, G. A., *J. Am. Chem. Soc.*, **1985**, 107, 3033

[94]   Özkar, S., McMurray, L., Holmes, A. J., Kuperman, A., Ozin, G. A., *J. Phys. Chem.*, **1991**, 95, 9448.

[95]   (a) Jelinek, R., Özkar, S., Ozin, G. A., *J. Am. Chem. Soc.*, **1992**, 114, 4907. (b) Jelinek, R., Özkar, S., Ozin, G. A.,  *J. Phys. Chem.*, **1992**, 96, 5949. (c) Jelinek, R., Özkar, S., Pastore, H. O., Malek, A., Ozin, G. A., *J. Am. Chem.*

*Soc.*, **1993**, 1145, 563. (d) Ozin, G. A., Özkar, S., Macdonald, P., *J. Phys. Chem.*, **1990**, 94, 6939.

[96]   Laidler, K. J., *Chemical Kinetics*; Third Ed.; Benjamin-Cummings, **1997**.

[97]   (a) Evans, M.G., Polanyi M., *Trans. Faraday Soc.*, **1935**, 31, 875. (b) Eyring, H., *J. Chem. Phys.*, **1935**, 3, 107. (c) Eyring, H., Polanyi M., *Z. Phys. Chem. Abt. B*, **1931**, 12, 279.

[98]   Zahmakiran, M., Özkar, S., *J. Mol. Catal. A*, **2006**, 258, 95.

[99]   Amendola, S. C., Janjua, J. M., Spencer, N. C., Kelly, M. T., Petillo, P. J., Sharp-Goldman, S. L., Binder, M., *Int. J. Hydrogen Energy* , **2000**, 25, 969.

[100]  Kaufman, C. M., Sen, B., *J. Chem. Soc. Dalton. Trans.*, **1985**, 83, 307.

[101]  Davis, R. E., Swain, C. G.,  *J. Am. Chem. Soc.*, **1960**, 82, 5950.

[102]  Jaska, C. A., Clark, T. J., Clendenning, S. B., Grozea, D., Turak, A., Lu, Z-H., Manners, I., *J. Am. Chem. Soc.*, **2005**, 127, 5116.

[103]  Clark, T. J., Whittell, G. R., Manners, I., *Inorg. Chem.*, **2007**, 46, 7522.

[104]  Schreiner, P., Schaefer, H., Schleyer, P. V., *J. Chem. Phys.*, **1994**, 101, 7625.

[105]  Mesmer, R. E., Jolly, W. L., *Inorg. Chem.*, **1962**, 1, 608.

[106]  (a) Chatenet, M., Micoud, F., Roche, I., Chainet, E., *Electrochim. Acta*, **2006**, 51, 5459. (b) Guella, G., Zanchetta, C., Patton, B., Miotello, A., *J. Phys. Chem. B*, **2006**, 110, 17024. (c) Zhang, H., Yi, B., Wu, C., *Catal. Today*, **2004**, 93, 477. (d) Ingersoll, J. C., Mani, N., Thenmozhiyal, J. C., Muthaiah, A., *J. Power Sources*, **2007**, 173, 450.(e) Walter, J. C., Zurawski, A., Montgomery, D., Thomburg, M., Pevankar, S., *J Power Sources*, **2008**, 179, 335.

[107] Amendola, S. C., Janjua, J. M., Spencer, N. C., Kelly, M. T., Petillo, P. J., Sharp-Goldman, S. L., Binder, M., *J. Power Sources*, **2000**, 85, 186.

[108] Ingersoll, J. C., Mani, N., Thenmozhiyal, J. C., Muthaiah, A., *J. Power Sources*, **2007**, 173, 450.

[109] Dai, H. B., Liang, Y., Wang, P., Chang, H. M. *J. Power Sources,* **2008**, 177, 17.

[110] Hanxi, Y., Hua, D., Xinping, A., Chuansin, C., *Int. J. Hydrogen Energy*, **2003**, 28, 1095.

[111] Lee, J., Kong, K. Y., Jung, C. R., Cho, E., Yoon, S. P., Han, J., Lee, T.-G., Nam, S. W., *Catal. Today*, **2007**, 120, 305.

[112] Demirci, U. B., Garin, F., *J. Mol. Catal. A Chem.*, **2008**, 279, 57.

[113] Zhao, J., Ma, H., Chen, J., *Int. J. Hydrogen Energy*, 2007, 32, 4711.

[114] Patel, N., Patton, B., Zanchetta, C., Fernandes, R., Guella, G., Kale, A.,. Miotello, A., *Int. J. Hydrogen Energy*, **2008**, 33, 287.

[115] Zhang, Q., Wu, Y., Sun, X., Ortega, J., *Ind. Eng. Chem. Res.*, **2007**, 46, 1120.

[116] Mitov, M., Rashkov, R., Atanassov, N., Zielonka, A., *J. Mater. Sci.*, **2007**, 42, 3367.

[117] Zhang, Z. S., Delgass, W. N., Fisher, T. S., Gore, J. P., *J. Power Sources*, **2007**, 164, 772.

[118] Alonso, R. P., Sicurelli, A., Callone, E., Carturan, G., Raj, R., *J. Power Sources*, **2007**, 165, 315.

[119] Dai, A. B., Liang, Y., Wang, P., Yao, X. D., Rufford, T., Lu, M., Cheng, H. M., *Int. J. Hydrogen Energy*, **2008**, 33, 4405.

[120] Hsueh, C. L., Chen, C. Y., Ku, J. R., Tsai, S. F., Hsu, Y. Y., Tsau, F. H., Jeng, M. S., *J. Power Sources*, **2008**, 177, 485.

[121] Zahmakiran, M., Özkar, S., *Langmuir*, **2009**, 25, 2667.

[122] Aiken, J. D., Finke, R. G., *J. Am. Chem. Soc.*, **1998**, 120, 9545.

[123] (a) March, J., *Advanced Organic Chemistry: Reactions, Mechanisms, and Structure*, fourth edition, Wiley-Interscience, New York, **1992**. (b) Fonseca, G. S., Silveira, E. T., Gelesky, M. A., Dupont, J., *Adv. Synth. Catal.*, **2005**, 347, 847. (c) Bahaman, M. V., Vannice, M. A., *J. Catal.*, **1991**, 127, 251.

[124] Bratlie, K., Lee, H., Konvopoulos, K., Yong, P., Samorjai, G. A., *Nano Lett.*, **2007**, 7, 3097.

[125] Lewoandowska, A., Monteverdi, S., Bettahar, M., Ziolek, M., *J. Mol. Cat: A Chem.*, **2002**, 188, 85.

[126] Jen, P. H., Hsu, Y. H., Lin, S. D., *Catalysis Today*, **2007**, 123, 133.

[127] Chou, P., Vannice, M. A., *J. Catalysis*, **1987**, 107, 140 and the references cited in this article.

[128] Januszklewicz, K.R., Alper, H., *Organometallics*, **1983**, 2, 1055.

[129] Seeberger, M.H., Jones, R.A., *J. Chem. Soc. Chem. Comm.*, **1985**, 6, 373.

[130] Duan, Z., Sylwester, A.P., Hampden-Smith, M.J., *Chem. Mater.*, **1992**, 4, 1146.

[131] Schulz, J., Patin, H., Roucoux, A., *Chem. Comm.*, **1999**, 535.

[132] Schulz, J., Patin, H., Roucoux, A., *Chem. Eur. Jour.*, **2000**, 6, 618.

[133] Schulz, J., Patin, H., Rouchoux, A., *Adv. Synth. Catal.*, **2003**, 345, 222.

[134] Nicholas, J. P., Ahn, H., Marks, T. J., *J. Am. Chem. Soc.*, **2003**, 125, 4325.

[135] Mevellec, V., Ramirez, E., Phillippot, K., Chaudret, B., Roucoux, A., *Adv. Synth. Cat.*, **2004**, 346, 72.

[136] Park, I. S., Kwon, M. S., Kim, N., Lee, J. S., Kang, K.Y., Park, J., *Chem. Comm.*, **2005**, 5667.

[137] Zhang, J., Xie, Z., Liu, Z., Wu, W., Han, B., Huang, J., Jiang, T., *Catalysis Letters*, **2005**, 103, 59.

[138] Roucoux, A., Phillippot, K., Payen, E., Granger, P., Dujardin, C., Nowicki, A., Mevellec, V., *New J. Chem.*, **2006**, 1214, 30.

[139] Nowicki, A., Zhong, Y., Leger, B., Rolland, J. P., Bricout, H., Monflier, E., Roucoux, A., *Chem. Comm.* **2006**, 296.

[140] Nowrick, A., Le Boulaire, V., Roucoux, A., *Adv. Synt. Catal.*, **2007**, 349, 2326.

[141] Park, I. S., Kwon, M. S., Lee, J. S., Kang, K. Y., Park, J., *Adv. Synth. Catal.*, **2007**, 349, 2039.

[142] Zahmakiran, M., Özkar, S., *Langmuir*, **2008**, 24.7065.

[143] Hubert, C., Denicourt-Nowicki, A., Guégan, J.-P., Roucoux, A., *Dalton Trans.*, **2009**, 7356.

[144] Pan, H.-B., Wai, C. M., *J. Phys. Chem. C*, **2009**, 113, 19782.

[145] Li, X., Ozin, G. A., Ozkar, S., *J. Phys. Chem.*, **1991**, 95, 4463.

[146] Lin, Y., Finke, R. G., *Inorg. Chem.*, **1994**, 33, 4891.

[147] Hornstein, B. J., Aiken, J. D., Finke, R. G., *Inorg. Chem.*, **2002**, 41, 1625.

[148]   Poliakoff, M., Fitzpatrick, J. M., Farren, T. R., Anastas, P. T., *Science* **2002**, 297, 807
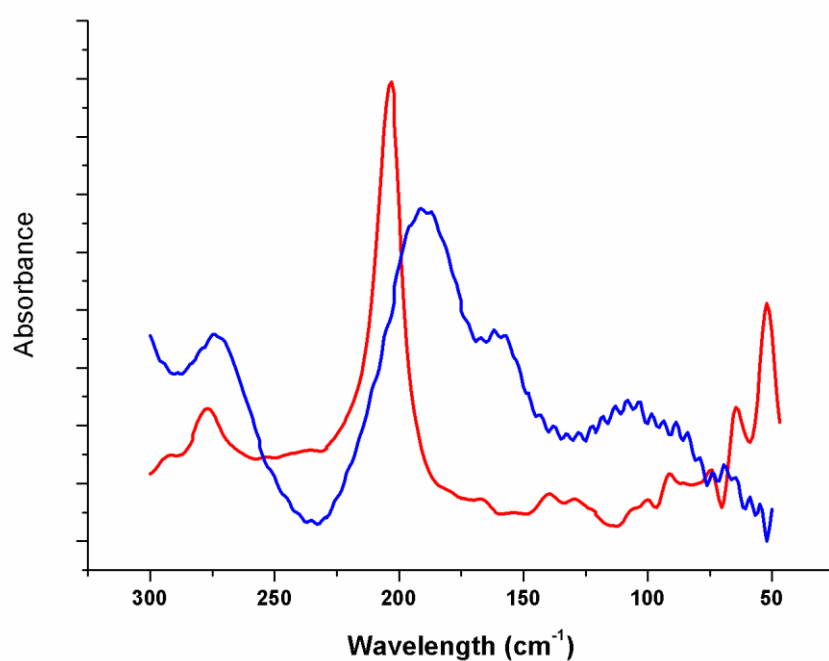
FIGURES



**Figure 70.** The far-IR spectra of vacuum thermally dehydrated ($10^{-7}$ Torr, 550 $^{o}$C); $Ru^{3+}$-exchanged Zeolite-Y sample (red) with a nominal composition of $Ru_{5.8}Na_{48.6}Y$ and zeolite framework stabilized ruthenium(0) nanoclusters (blue) ($Ru(0)/Na_{54}Y$) prepared by the borohydride reduction of $Ru_{5.8}Na_{48.6}Y$.
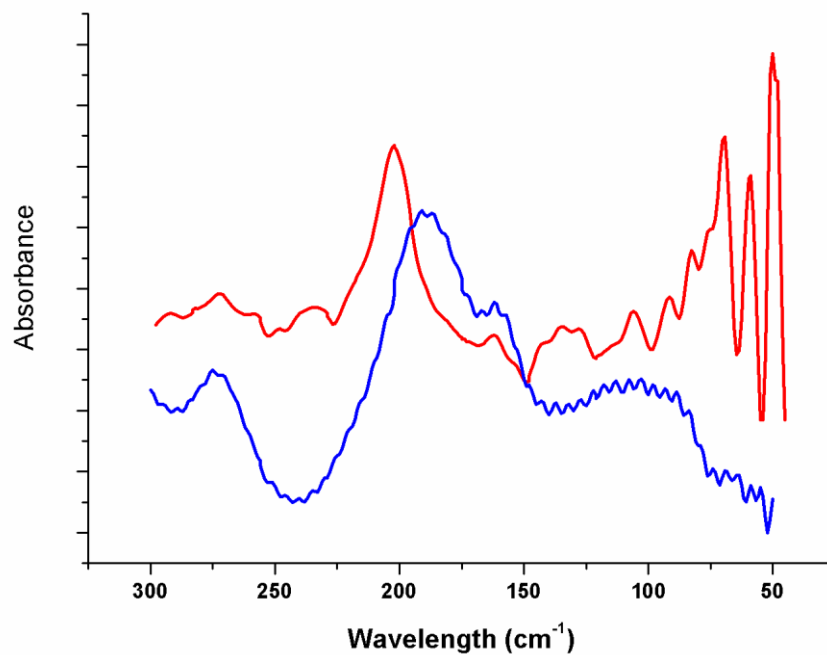
**Figure 71.** The far-IR spectra of vacuum thermally dehydrated ($10^{-7}$ Torr, 550 $^o$C); $Ru^{3+}$-exchanged Zeolite-Y sample (red) with a nominal composition of $Ru_{7.9}Na_{32.3}Y$ and zeolite framework stabilized ruthenium(0) nanoclusters (blue) ($Ru(0)/Na_{52}Y$) prepared by the borohydride reduction of $Ru_{7.9}Na_{32.3}Y$.
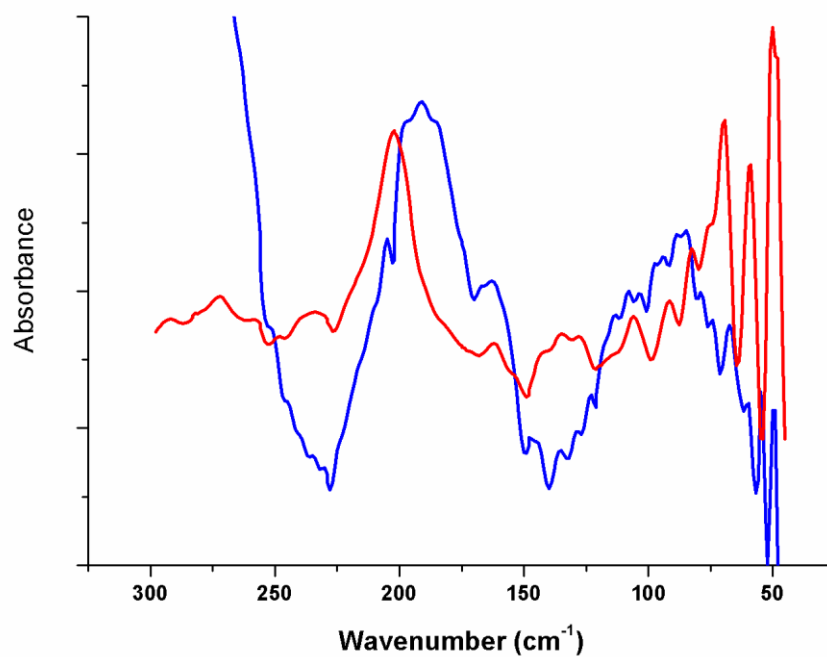
**Figure 72.** The far-IR spectra of vacuum thermally dehydrated ($10^{-7}$ Torr, 550 $^{\circ}$C); $Ru^{3+}$-exchanged Zeolite-Y sample (red) with a nominal composition of $Ru_{11.6}Na_{21.2}Y$ and zeolite framework stabilized ruthenium(0) nanoclusters (blue) ($Ru(0)/Na_{49}Y$) prepared by the borohydride reduction of $Ru_{11.6}Na_{21.2}Y$.

**Figure 73.** The far-IR spectra of vacuum thermally dehydrated ($10^{-7}$ Torr, 550 $^{\circ}$C); $Ru^{3+}$-exchanged Zeolite-Y sample (red) with a nominal composition of $Ru_{14.9}Na_{11.3}Y$ and zeolite framework stabilized ruthenium(0) nanoclusters (blue) $(Ru(0)/Na_{44}Y)$ prepared by the borohydride reduction of $Ru_{14.9}Na_{11.3}Y$.
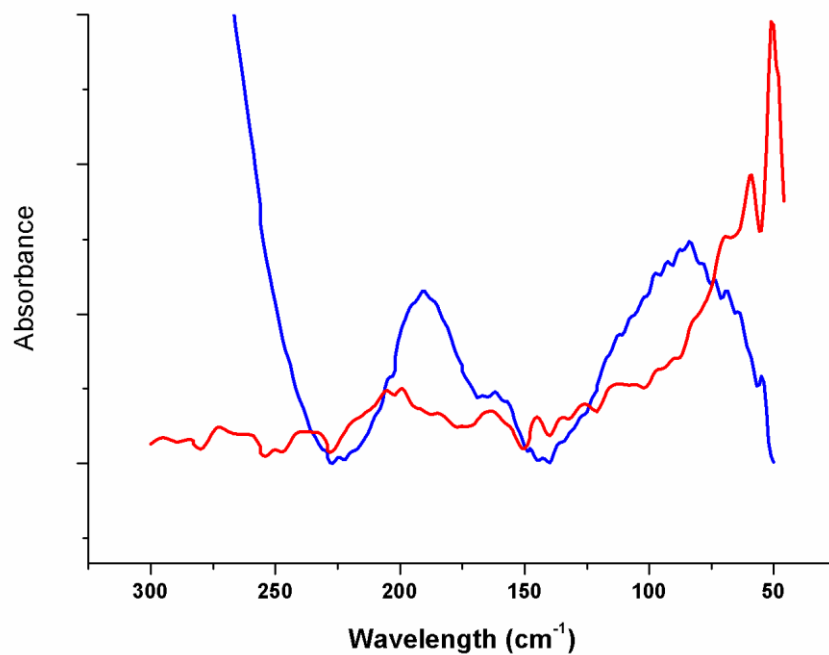
127
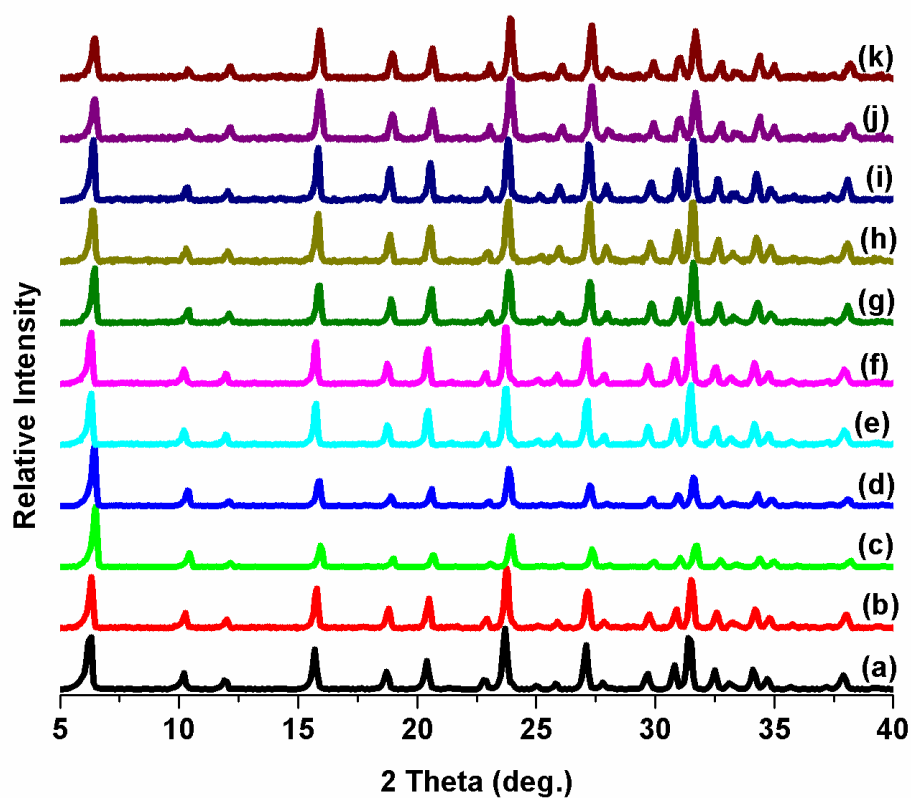
**Figure 74.** The powder XRD patterns of (a) zeolite-Y ($Na_{56}Y$), $Ru^{3+}$-exchanged zeolite-Y with a nominal compositions of (b) $Ru_{3.2}Na_{46.4}Y$, (c) $Ru_{5.8}Na_{48.6}Y$, (d) $Ru_{7.9}Na_{32.3}Y$, (e) $Ru_{11.6}Na_{21.2}Y$, (f) $Ru_{14.9}Na_{11.3}Y$ and zeolite framework stabilized ruthenium(0) nanoclusters prepared by $NaBH_4$ reduction of (g) $Ru_{3.2}Na_{46.4}Y$, (h) $Ru_{5.8}Na_{48.6}Y$, (i) $Ru_{7.9}Na_{32.3}Y$, (j) $Ru_{11.6}Na_{21.2}Y$, and (k)$Ru_{14.9}Na_{11.3}Y$.
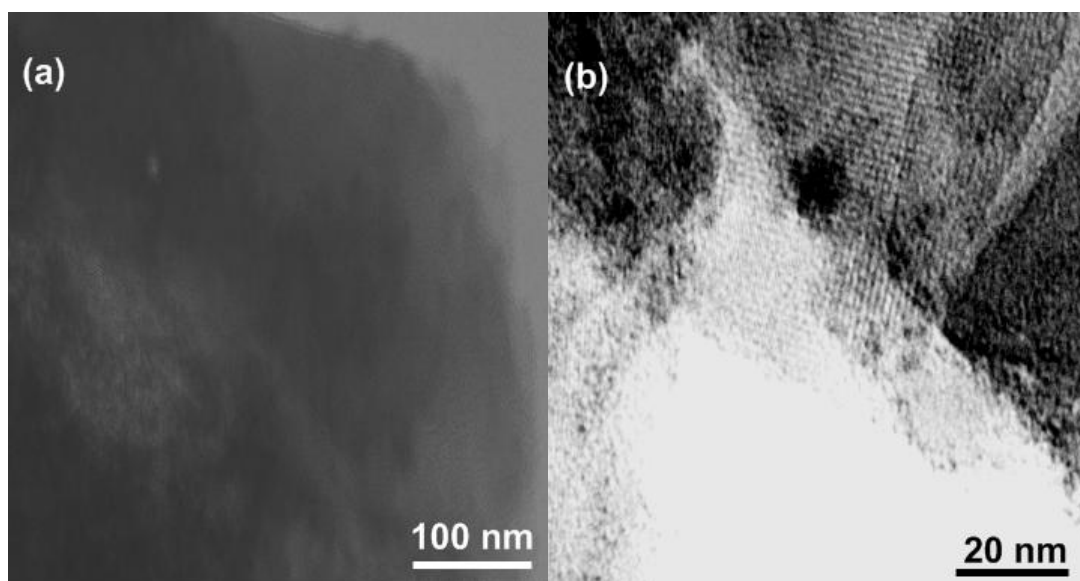
**Figure 75.** (a) Low resolution, (b) high resolution  TEM images of zeolite framework stabilized ruthenium(0) nanoclusters harvested after their fifth reuse from the hydrolysis of sodium borohydride in the basic medium (5 % wt NaOH solution), showing that no bulk ruthenium was formed from the possible migration followed by agglomeration of ruthenium(0) nanoclusters.

**Figure 76.** XRD patterns of zeolite-Y, zeolite framework stabilized ruthenium(0) nanoclusters (ZFS-Ru(0)) fresh and harvested after their fifth reuse in the hydrolysis of sodium borohydride in the basic medium (5 % wt NaOH solution).
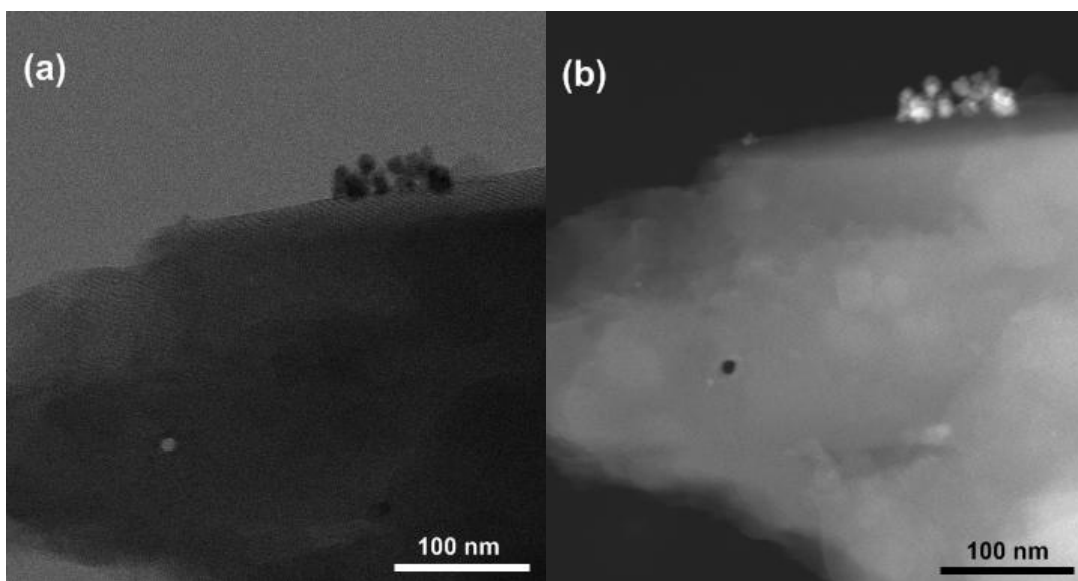
**Figure 77.** (a) Low resolution TEM and corresponding zero contrast TEM images of zeolite framework stabilized ruthenium(0) nanoclusters harvested after their fifth reuse from the hydrogenation of neat benzene, showing that slight agglomeration of zeolite surface supported ruthenium(0) nanoclusters.
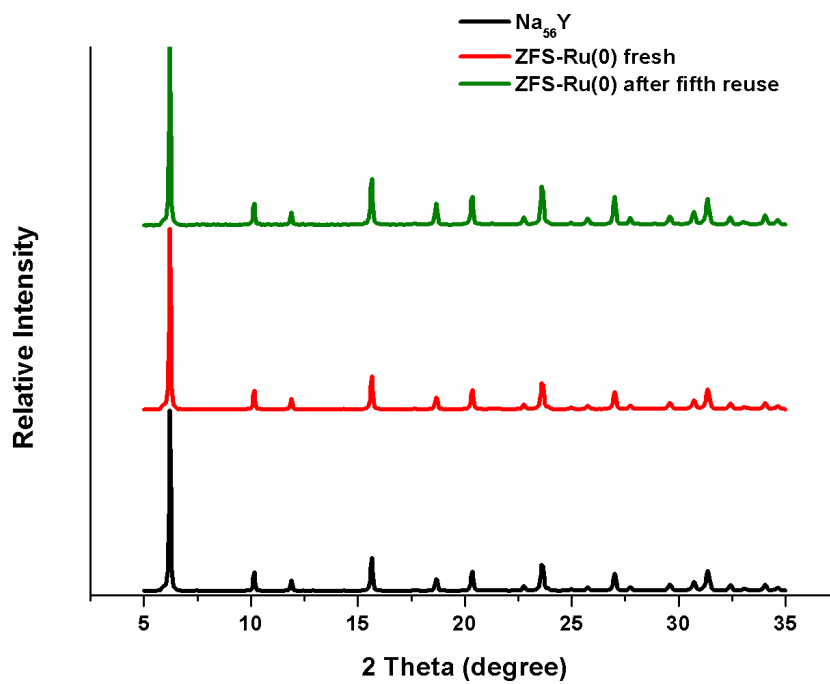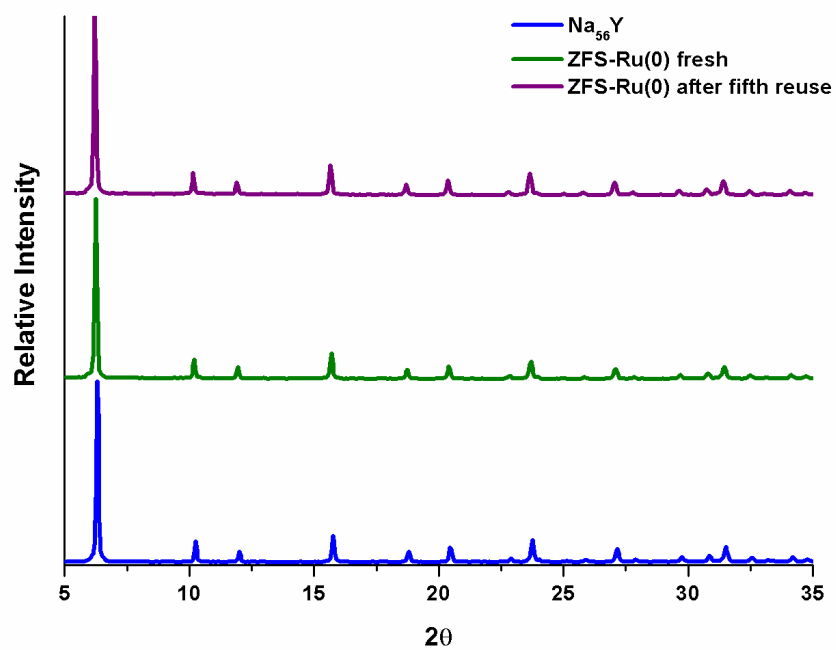
**Figure 78.** XRD patterns of zeolite-Y, zeolite framework stabilized ruthenium(0) nanoclusters (ZFS-Ru(0)) fresh and harvested after their fifth reuse in the hydrogenation of neat benzene.

<div align="center">**CURRICULUM VITAE**</div>

## Personal Information

Surname, Name: Zahmakıran, Mehmet

Nationality: Turkish (TC)

Date and Place of Birth: 24 February 1979, Antalya

Marial Status: Single

Phone: 90 3122105135

Fax: 90 3122103200

e-mail: zmehmet@metu.edu.tr

## Education

| | | |
|---|---|---|
| BS | Abant Izzet Baysal University, Department of Chemistry | 2002 |
| MS | Middle East Technical University, Department of Chemistry | 2005 |
| PhD | Middle East Technical University, Department of Chemistry | 2010 |

## Work Experience

Research Asistant; Middle East Technical University, Department of Chemistry (2002-Present)

## Foreign Languages

Advanced English

# Publications

**(1)** Zahmakıran M., Tonbul Y., Özkar S. **"**Ruthenium(0) Nanoclusters Supported on Hydroxyapatite: Simply Prepared, Highly Active and Reusable Catalyst in the Hydrogenation of Aromatics Under Mild Conditions with a Record Catalytic Lifetime in the Solvent-Free Hydrogenation of Benzene" submitted to Chem. Comm., 2010.

**(2)** Bayram E., Zahmakıran M., Özkar S., Finke R. G. "In-situ formed Ir(0)/Dry-HCl as "Semi-Naked Nanocluster Catalyst" for the Complete Hydrogenation of Neat Benzene at Room Temperature and Mild Pressures" submitted to Langmuir, 2010.

**(3)** Zahmakıran M., Tonbul Y., Özkar S. "Ruthenium(0) Nanoclusters Stabilized by Nanozeolite Framework; Isolable, Reusable, and Green Catalyst for the Hydrogenation of Neat Aromatics under Mild Conditions with the Unprecedented Catalytic Activity and Lifetime" J. Am. Chem. Soc., article in press, 2010.

**(4)** Zahmakıran M., Akbayrak S., Kodaira T., Özkar S. **"**Osmium(0) nanoparticles-Doped Zeolite; Highly Active and Reusable Catalyst for the Aerobic Oxidation of Alcohols" Dalton Trans., article in press, 2010.

**(5)** Zahmakıran M., Kodaira T., Özkar S. **"**Ruthenium(0) Nanoclusters Stabilized by Zeolite Framework as Superb Catalyst for the Hydrogenation of Neat Benzene Under Mild Conditions: Additional Studies Including Cation Site Occupancy, Catalytic Activity, Lifetime, Reusability and Poisoning" App. Cat. B; Env., 96 (3-4), 533-540, (2010).

**(6)** Zahmakıran M., Tristany M., Fajerwerg K., Philippot K., Özkar S., Chaudret B., Aminopropyltriethoxysilane Stabilized Ruthenium(0) Nanoclusters as an Isolable and Reusable Heterogeneous Catalyst for the Dehyrogenation of Dimethylamine-Borane" Chem. Comm., 46, 2938-2942, (2010).

**(7)** Zahmakıran M., Özkar S., "Preparation and Characterization of Zeolite Framework Stabilized Gold(0) Nanoclusters: Highly Active, Selective and

Reusable Catalyst in Aerobic Oxidation of Benzyl Alcohol" Mater. Chem. Phys., 121 (1-2), 259, (2010).

**(8)** Çalışkan S., Zahmakıran M., Özkar S., "Zeolite Confined Rhodium(0) Nanoclusters as Highly Active, Reusable, and Long-Lived Catalyst in the Methanolysis of Ammonia-Borane" App. Cat. B: Env., 93 (3-4), 387, (2010).

**(9)** Zahmakıran M., Durap F., Özkar S., "Zeolite Confined Copper(0) Nanoclusters as Cost Effective and Reusable Catalyst in Hydrogen Generation from the Hydrolysis of Ammonia-Borane" Int. J. Hyd. Energy, 35 (1), 187, (2010).

**(10)** Durap F., Zahmakıran M., Özkar S., "Water Dispersible Rhodium(0) Nanoclusters Catalyst with Unprecedented Catalytic Lifetime in the Hydrolytic Dehydrogenation of Ammonia-Borane" App. Cat. A: Gen., 369 (1-2), 53, (2009).

**(11)** Zahmakıran M., Özkar S. "Dimethylammonium Hexanoate Stabilized Rhodium(0) Nanoclusters Identified as True Heterogeneous Catalysts with the Highest Observed Activity in the Dehydrogenation of Dimethylamine−Borane" Inorg. Chem., 48, 8955, (2009).

**(12)** Zahmakıran M., Özkar S. "Zeolite Confined Nanostructured Dinuclear Ruthenium Clusters: Preparation, Characterization and Catalytic Properties in the Aerobic Oxidation of Alcohols under Mild Conditions" J. Mater. Chem., 19, 7112, (2009).

**(13)** Durap F., Zahmakıran M., Özkar S., "Water Soluble Laurate-Stabilized Ruthenium(0) Nanoclusters Catalyst for Hydrogen Generation from the Hydrolysis of Ammonia-Borane: High Activity and Long Lifetime" Int. J. Hyd. Energy, 34 (17), 7223, (2009).

**(14)** Zahmakıran M., Özkar S., "Zeolite Framework Stabilized Rhodium(0) Nanoclusters Catalyst for the Hydrolysis of Ammonia-Borane in Air: Outstanding Catalytic Activity, Reusability and Lifetime" App. Cat. B: Env., 89 (1-2), 104, (2009).

**(15)** Zahmakıran M., Özkar S., "Zeolite-Confined Ruthenium(0) Nanoclusters Catalyst: Record Catalytic Activity, Reusability, and Lifetime in Hydrogen

Generation from the Hydrolysis of Sodium Borohydride" Langmuir, 25, 2667, (2009).

**(16)** Zahmakıran M., Özkar S., "Preparation and Characterization of Zeolite Framework Stabilized Cuprous Oxide Nanoparticles" Mater. Lett., 63 (12), 1033, (2009).

**(17)** Zahmakıran M., Kodaira T., Toru S., Özkar S. "A Novel Simple Organic Free Preparation and Characterization of Water Dispersible Photoluminescent $Cu_2O$ Nanocubes" Mater. Lett. 63 (3-4), 400, (2009).

**(18)** Zahmakıran M., Özkar S., "Intrazeolite Ruthenium(0) Nanoclusters; a Superb Catalyst for the Hydrogenation of Benzene and the Hydrolysis of Sodium Borohydride" Langmuir, 24, 7065, (2008).

**(19)** Zahmakıran M., Özkar S., "Water Dispersible Acetate Stabilized Ruthenium(0) Nanoclusters as Catalyst for the Hydrolysis of Sodium Borohydride" J. Mol. Cat. A: Chem., 258 (1-2), 95, (2006).

**(20)** Zahmakıran M., Özkar S., "Hydrogen Generation from the Hydrolysis of Sodium Borohydride by using Ru(0) Nanoclusters as Catalyst" J. Alloy. Comp., 404, 728, (2005).